Transient Analysis of DC Distribution Grids

Dimitrios Petropoulos

Technische Universiteit Delft

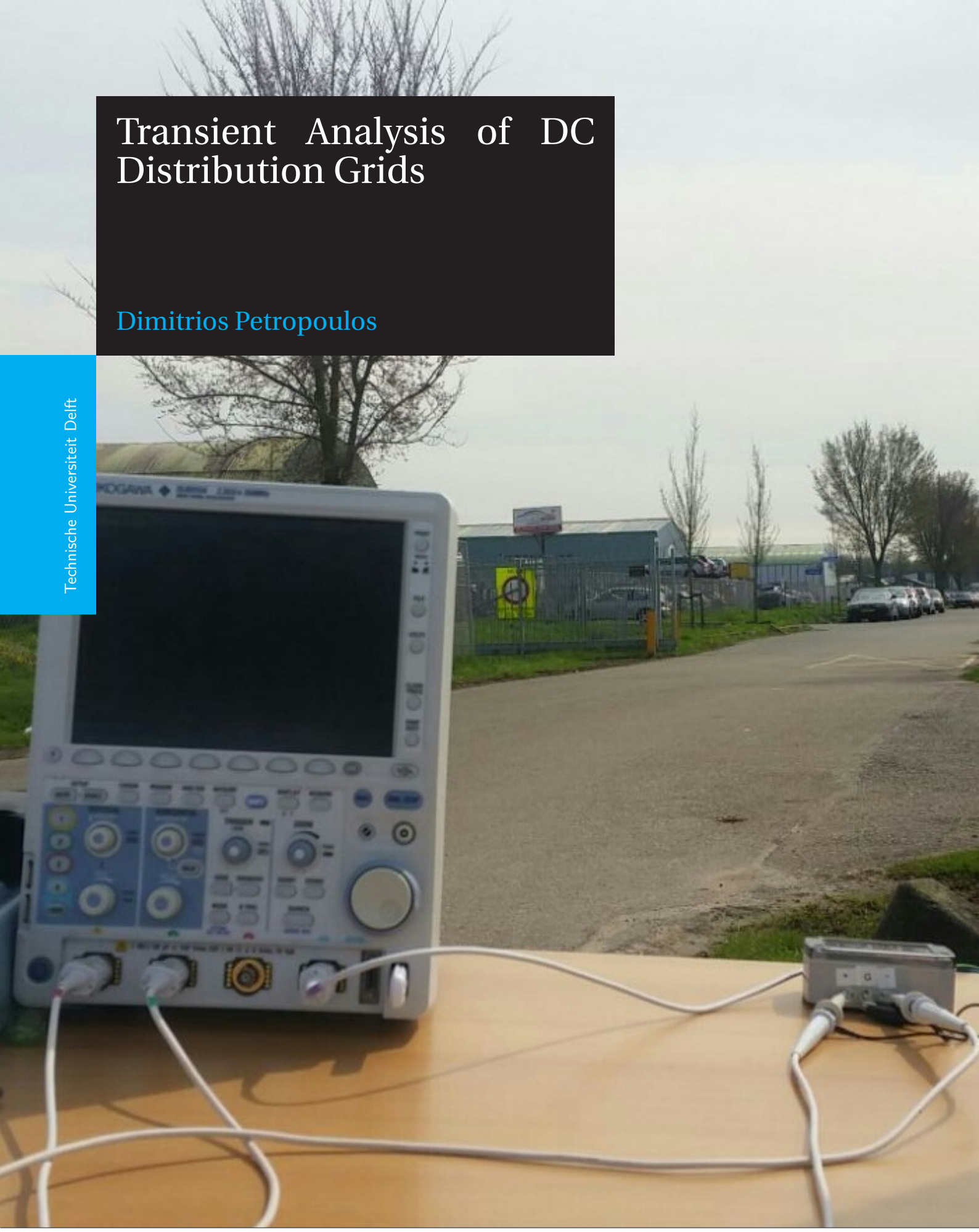

TU Delft Delft University of Technology

Challenge the future

TRANSIENT ANALYSIS OF DC DISTRIBUTION GRIDS

by

Dimitrios Petropoulos

in partial fulfillment of the requirements for the degree of

Master of Science

in Electrical Sustainable Energy

at the Delft University of Technology,

to be defended publicly on Thursday September 15, 2016 at 01:00 PM.

Supervisor:	Dr. ir. L.M. Ramirez Elizondo	
Thesis committee:	Dr. Ir. M. Popov,	TU Delft
	Prof. dr. P. Bauer,	TU Delft
	Dr. ir. L.M. Ramirez Elizondo,	TU Delft

This thesis is confidential and cannot be made public until September 1st 2017.

An electronic version of this thesis is available at http://repository.tudelft.nl/.

TU Delft Delft University of Technology

ABSTRACT

The latest developments in power electronics along with the increased generation from Renewable Energy Sources (RES), the new prosumers who both generate and consume electricity and the rapid adoption of DC loads in the household are forcing us to rethink the manner with which power is distributed and consumed. The proposal to make DC technology an integral part of the distribution network seems to have more merit. This change would lead to energy savings in power conversion and enable the creation of meshed DC grids, highly controllable and flexible networks which will be able to facilitate the more sustainable energy future towards which we strive. To build such a system, however, a different approach than the one used in AC systems is needed, due to the peculiarities of DC technology. In our research for the best possible way to protect these systems, it is imperative to constantly test the protection circuit not only as a standalone, but also incorporate it in the systems that will be built and test them together. In other words, transient analysis of the systems with the proposed protection included is an integral part in gauging the impact of the latter on the former during operation, and therefore in assessing and improving the protection for this specific application.

This thesis presents such a transient analysis of various configurations of DC distribution systems. A combination of theoretical and practical methods were used to investigate the behavior of the systems' variables after the occurrence of faults and current interruption. A number of networks of varying complexity were built with detailed cable models using the EMTP/ATP software package in order to simulate a multitude of faults and assess each network's response at various positions and most crucially, the effectiveness of the protection scheme in reducing the impact of the transients after the fault. The travel speed of the transients was also investigated. At the same time, a set of measurements was conducted on a DC street lighting network to study the transient behavior of a real system. A separate model was built to resemble the measured system, in order to compare between the simulations and the measurements. The evaluation of the measurement and simulation results led to conclusions that will contribute to the creation of better, safer and more versatile DC distribution grids. The comparison showed that the models used can approach the behavior of the real system to a reasonable degree. The other simulations indicated that the transient impact is significantly smaller in locations far from the fault, but continued operation of the healthy pole cannot be guaranteed, especially after earth faults.

Dimitrios Petropoulos
Delft, September 2016

ACKNOWLEDGEMENTS

I would first like to thank my thesis supervisor, Assistant Professor Laura Ramirez Elizondo, who trusted me with this for always guiding me and steering me in the right direction whenever necessary. Further, I would also like to thank PhD candidate Laurens Mackay, who was there with me all the way, for helping me with the lab work and everything else regarding the thesis. Additionally, I would like to express my gratitude to Associate Professor Marjan Popov, whose door was always open for me, for the valuable guidance in key parts of the thesis. I would also like to acknowledge Professor Pavol Bauer, who guides all of us as the Head of the DCE& S group, and provided us all with inspiration and motivation to do our best. Furthermore, I am grateful to everyone else who helped me in one way or another, namely Tsegay Hailu, Venugopal Prasanth, Nils van der Blij, Joris Koeners, Bart Roodenburg and Harrie Olsthoorn.

Finally, I wish to thank the people closer to me who supported me throughout my studies; my parents, my sister and my grandparents for their patience and understanding. I especially want to thank my grandfather, who has been a great influence and source of support to me. I couldn't forget to thank my beloved Athena. Without her unconditional support and belief in me I would not be where I am today.

CONTENTS

List of Figures

List of Tables

1

INTRODUCTION

1.1. A STEP TOWARDS A PROMISING FUTURE

The emergence of renewable energy generation and the significant development of the distributed generation sector in the past decades are a direct result of the ever increasing population of our planet, as well as the growing power needs of an individual in the developed countries. Electricity has always been an important driving factor of society and industry. Even today more and more aspects of our lives depend on a reliable power grid that can provide us with good quality power in the form that is needed.

Another significant point is the fact that we have already reached the expected lifetime of a great number of the grid's most vital components, which means that any replacement taking place in the very near future would facilitate a possible move to a different technology for at least a part of the grid. It becomes clear, then, that we are at a crossroads; we either keep using the same radial, unidirectional configuration for the grid, with the usual centralized production units or we make use of the latest developments in power electronics that allow us to build a more flexible, controllable and adjustable delivery system to cover our power needs.

In truth, however, the choice has been made for the most part. We are already moving towards a more sustainable future due to the environmental concerns. Distributed generation (DG) is certainly not a new concept, and it has been a part of the medium voltage grid for a while, but only in the past decade or so has it seen a widespread adoption in the low voltage levels, mostly in the form of photovoltaic panels or small wind generators. It falls to distributed generation to help us reach the goals we set for ourselves for 2020, in order to reduce the impact of our energy systems on the environment. The only factor that is against these newer technologies is the increased costs to install and integrate them to the existing power system, but these costs have already been reduced significantly, due to the widespread adoption of these technologies. In many countries, parity has already been reached [1] .

The introduction of these small but numerous power sources has a profound effect on the grid, as they may cause frequency fluctuations and voltage disturbances, thus posing a serious challenge to both transmission and distribution grid operators. If the element of bidirectional power flow introduced by distributed generation is taken into account, it is evident that important changes are needed so as not only to secure electricity supply, but also to finally take steps towards a future where humanity can fulfill their needs without destroying the environment.

1.2. AC VERSUS DC

A commercial war broke out in the late 19^{th} century between Edison's Electric Light Company and Westinghouse's Electric Company regarding the choice between *DC* and *AC* for the emerging power distribution systems. The two companies were developing their respective applications of each technology around the same time. The turning point was the introduction of the transformer by Westinghouse in 1886 to step up voltage and transport electricity over longer distances with higher efficiency and lower costs. Edison's existing prototypes could not compete with that, so he resorted to propaganda, trying to convince the public that his

competitor's technology was dangerous to people and could cause death by electrocution. The propaganda included public torture of animals with AC power to discredit his competitors and prove his point. However, despite Edison's best efforts, alternating current was adopted over the direct current technology, which was abandoned by the 1920s. Edison left his company, which was merged with Thomson-Houston and included AC technology in their patents. This company is now known as General Electric.

There were several technical reasons for the prevalence of AC over DC technology. Chief among those is the fact that DC had no equivalent component to the transformer at the time, which means that generation, transmission and distribution had to be at the same voltage level which was already defined by the (low) voltage of the customers' lamps. This would require large wires to transport the needed amount of current, resulting in significant costs. Losses would also be an issue, forcing generation to be as close as possible to the loads. In comparison, AC possessed the technology required to raise the voltage level after generation, so that power could be transported at lower currents, minimizing conductor dimensions and thus costs and losses. This would lead to the centralization of generation, allowing for fewer, larger centralized and more efficient power plants. Alternating current (AC) technology has been dominant in power systems ever since. It has served the existing grid satisfactorily, as the components perform quite reliably and have a sufficiently long expected lifetime.

1.3. THE REEMERGENCE OF DC AS A VIABLE ALTERNATIVE

Although the dominance of AC technology is undisputed, the recent developments in both power generation and consumption, along with the sustainability goals we have set for ourselves, force us to rethink our strategy. An important reason to question the AC technology is because of the challenges introduced by distributed generation, but there are many others, such as the rapid increase of DC electronic loads in domestic environments, or the inherent DC output of many RES and energy storage systems like batteries. While it is true that AC technology has indeed evolved during the past century, producing more efficient and cost-effective components, the potential of DC technology is still largely untapped.

The evolution of home computers in the past 3 decades has tipped the scales significantly. As the silicon industry exploded, an increasing number of electronic devices compete for a spot in our everyday lives. These rapid advancements in the field of semiconductors 'bled out' to other industries that stood to benefit from these impressive and unprecedented achievements. One of the industries that benefited was the power sector. As the electronics industry is one of the highest in the world by revenue, even more developments are expected. This means we can also expect smaller, more efficient power electronic components to emerge as a result.

1.4. DC MICROGRID: ADVANTAGES AND DISADVANTAGES

Based on the above arguments, the next logical step would be to gradually introduce small scale low voltage distribution systems, which would seamlessly connect the DC sources and loads, without an intermediate AC stage in between. The existing AC loads can be serviced by a DC/AC inverter. Although remarkable progress has been made on AC microgrids, there are a number of benefits to adopting a DC microgrid configuration:

- Avoid the expensive option of expanding the existing centralized power generation to accommodate the increasing amount of power demand [2].
- Since both sources and loads operate in DC, there are fewer stages of power conversion needed in the distribution level, which means reduced costs and losses, as well as fewer power electronic components required [3].
- In case of a fault on the utility side, the DC side will not be directly impacted, because the AC/DC inverter controls the voltage on that side through the stored energy on the DC capacitor.
- The efficiency of the DC system itself can be higher than the AC one, assuming that losses in semiconductors components are reduced by half, as stated in Nilsson and Sannino [4]. This is also demonstrated in Pratt *et al.* [5], where power delivery efficiency in a 400 V DC distribution system was found to be 7% better in terms of power savings than an equivalent 480 V AC system.

- A DC system can deliver at least $\sqrt{2}$ times more power than an AC system of the same (rms) value, using the existing cables. This is due to the fact that AC delivers power based on its rms value, while for DC things are more straightforward. It has even been suggested [6] that a 1.5 kV unipolar system is theoretically able to transfer up to 16 times more power compared to traditional 400 V AC distribution. However, in order to use the existing cables of AC, an appropriate voltage level should be chosen, as argued by Sannino *et al.* [7]. In the same paper, that voltage is found to be 326 V.

- An LVDC distribution network would at first seem more complicated, but in truth it could result in a simpler control system, as there is no reactive power and therefore no need for separate frequency and voltage regulation. All the system parameters can be controlled through the voltage. The absence of the unavoidable reactive power flow is also one of the major reasons contributing to a DC system's higher power delivery potential.

- The frequent problem of harmonics is also eliminated in DC, as well as any concerns regarding synchronizing any connected device with the utility grid. Instead of the usual 4 requirements (voltage, frequency, phase and phase sequence) that a component should fulfill, connection here is much simpler.

- A DC system can be more versatile in its operation than an equivalent AC system. By utilizing power electronic components, it is possible to shape the power more easily according to our needs. In comparison, the conventional AC system has limited flexibility when it comes to processing power.

DC microgrids are a new technology, which appears to be an amalgam of the traditional DC applications and the existing AC microgrids. As a result, there is no infrastructure in low and middle voltage yet, and existing small systems are either autonomous or plugged in to the AC utility.

According to the above, there is definitely a case for the introduction of DC technology to the distribution level. Nevertheless, the introduction of every new technology in the industry has always been faced with obstacles and challenges regarding its practical implementations, and this is most definitely the case with DC. The most prominent are the following:

- The standardization of voltage levels is a prerequisite to move forward with the actual implementation of DC on a distribution level. Having a set voltage level means that installation cost will inevitably drop, as the equipment needed will be standard and not custom made for each application. The need for standards is highlighted in many publications [3], [8]. As noted in Mackay *et al.* [9], the standard voltage level for for generic devices will be in the 350-400 V range, which is close to what is being used today in AC/DC links.

- A DC distribution system is more complex than an AC one, making its operation more diffficult. More specifically, smart communication between units and coordinated control techniques are needed [10] to achieve correct current and voltage regulation.

- Protection and safety are major concerns for the new LVDC applications. Detecting, locating and clearing a fault should be fast to ensure the proper protection of the system, as mentioned in a multitude of papers (Baran and Mahajan [11], Park *et al.* [12] and others). Appropriate grounding for each system case is imperative to make it safe for people. In difficult grounding conditions, high earth voltages can appear in an LVDC system, leading to potential hazard for the public [13]. Hence grounding and protection configurations have to adapt to the characteristics of an LVDC system.

- Power electronic components introduce problems themselves, such as being able to cause switch faults. A challenge for existing converters, for example, is increasing their fault current capability [13].

- Fault detection and isolation becomes more challenging in the case of multiterminal dc grids [11], where the faulted section needs to be isolated. The need for selectivity is at odds with the need for speedy interruption of the fault current.

- The lifetime of power electronic units is another issue, as it may even be a quarter of the lifetime of traditional AC components, so around 15-20 years, at least according to Salonen *et al.* [13]. The short lifetime forces us to spend more on maintenance and replacement of these converters. The costs tie in with other, non-technical challenges of DC microgrids, such as pricing.

Out of all the above issues, the protection of LVDC systems is quite possibly the most prominent one, presenting challenges that have not been conclusively solved as of yet. In order to move forward with DC distribution, the breaking of the dc arc, the type of protective equipment and the lack of standard rules and experience need to be addressed.

1.5. RESEARCH QUESTIONS

The research questions this thesis will focus on are:

1. *What are the fault after effects and how can they be handled?*
   (a) What happens to the system variables (bus voltage, line current, etc.) right after a short circuit occurs?
   (b) What is the cause of the over-voltages and under-voltages that appear after the fault and after tripping?
   (c) How can we limit the transients caused by the interruption of the fault current to minimize the negative impact on the system?
   (d) What happens if the protection is not operating as intended and trips when there is no fault or does not trip when there is one?
2. *Do the after effects change in more complex, large, bipolar systems, and how fast do transients travel across those large systems?*
   (a) How does the above change with the implementation of a bipolar LVDC microgrid? Which additional parameters should be considered in this case?
   (b) How fast does the fault (or any signal for that matter) propagate through the system?
3. *Does the comparison with real measurements validate the constructed models?*
   (a) How do the simulation results compare to measurements from an actual DC system, such as the street lighting system constructed by the company Direct Current BV?

1.6. MAIN GOAL AND OBJECTIVES

The overall objective of the thesis will be to perform short circuit simulations and fault analysis in LVDC distribution system models and identify the various side effects that are caused by the protection that clears these faults. A subsequent goal is finding ways to minimize the impact of those effects in order to ensure that the system is protected adequately in case of a fault without inadvertently impacting the existing equipment. More specifically, the goal is to give a satisfying answer to the above research questions, which include running simulations and tests for over-voltages, propagation speed etc. as detailed already. Different configurations of a DC microgrid with varying complexity will be built in order to answer the research questions. To achieve this, the models that will be used for the simulations will be as realistic as possible, so that the conclusions drawn from this research can contribute to the future of DC systems in the industry.

2

Literature Review

In this literature review, some basic differentiating factors between HVDC and LVDC are discussed, then an introduction to DC protection follows. Analysis of the stages of a short circuit fault in a DC system is next, as it is important to be aware of how the components of the system affect the transients. The propagation of faults as surges in the system is also explored, as it is an important step in defining the needed protection conditions. Finally, the work of various research groups in DC protection and fault analysis is discussed and their results presented in a succinct manner.

2.1. DC Technologies

The increasing efficiency and compactness of modern power electronics devices, along with the steady decrease of their prices, has made the use of DC in power systems a viable choice in recent years. In both documentation and actual applications, DC technologies can be classified in two distinct categories:

- High Voltage DC
- Low Voltage DC

Due to the different philosophy between the two applications, it is useful to briefly discuss the two technologies.

2.1.1. HVDC

The first actual DC distribution system was implemented in 1954 by the Soviet Union. Since then, there have been more than a hundred HVDC projects worldwide. The European projects can be seen from Figure 2.1, where red colored lines indicate the existing installations, the green ones are under construction and the blue ones are proposed.

HVDC technology first began by utilizing Current Source Converters (CSC), the traditional, thyristor based converters which were essentially DC current sources. In the past two decades, Voltage Source Converters (VSCs) have been adopted,composing advanced power electronics switches, such as IGBTs, MOSFETs, etc. which could now handle higher power levels. The newer type of converters can offer a number of advantages [15], such as independent active and reactive power control on the AC side, black start capability and high dynamic performance.

HVDC transmission systems are especially suitable for longer distances, where the gains from loss reduction (no capacitor charging in DC) overtake the higher installation costs in comparison to HVAC. As the cost of power electronics is decreasing, HVDC transmission is expected to be cost-effective for smaller distances as well.

The different configurations that have been used are, among others, unipolar with earth (1 conductor), unipolar with metallic return (2 conductors), or bipolar (two conductors with +/- voltage each and usually a

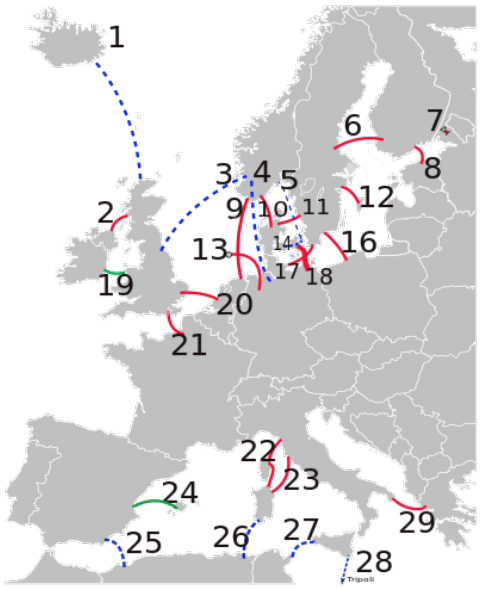

Figure 2.1: Existing and future HVDC projects in Europe[14]

third one as a middle).

An important note regarding HVDC is that, because of their purpose as transmission systems, there was no need (at least at first) to create multiterminal systems, which means that almost all of them are point-to-point connections. This has important ramifications regarding the protection schemes and devices of these systems, something that will be discussed later.

2.1.2. LVDC

Low Voltage in DC is not (yet) strictly defined, but regarded to be up to 1.5 kV [16]. It refers to applications regarding distribution level systems, and has several benefits in comparison to the 400 V AC distribution, including higher transmission capacity and higher thermal limits for current.

However, due to the very recent interest in the field of LVDC, there are no definite standards so far, which is a challenge in itself. Previous experience with DC systems in the telecom and transportation sector is valuable in this new field. Some elements of the HVDC technology can be used here with some alterations. Like in HVDC, the use of voltage source converters is widespread in the distribution level too.

A simplified example of an LVDC system can be seen in Figure 2.2. This distribution system interfaces with the existing AC higher voltage level with AC/DC converters. The same are used to connect with the AC loads of residences. It is important to note that there is no distinction between inverter and rectifier operation here. While the AC load converter may indeed only work as a rectifier, the component between the DC microgrid and the AC grid will definitely need to have bidirectional power flow capability, due to production from the DC level. The same goes for the converters connecting wind turbines or AC storage devices, such as flywheels. For this level of flexibility, VS converters are the most appropriate, as mentioned in Nilsson and Sannino [4].

One of the main advantages of DC microgrids becomes apparent in this figure. The latest technological developments suggest that DC loads will soon command a significant percentage of power consumption. Applications such as the new USB-C cable, which can deliver up to 100 W in DC power [18] and blurs the line between power plug and data cable, point to this direction. A higher share of DC loads means that more DC-DC choppers will be used, instead of the bigger and more expensive AC/DC converters that would be used for AC loads. A buck converter which utilizes only one switch, will most definitely be smaller and cheaper than a 3 phase IGBT converter.

The different configurations for LVDC are similar to the existing ones for high voltage, with the bipolar configuration being dominant in applications because of the higher total power capability and the ability

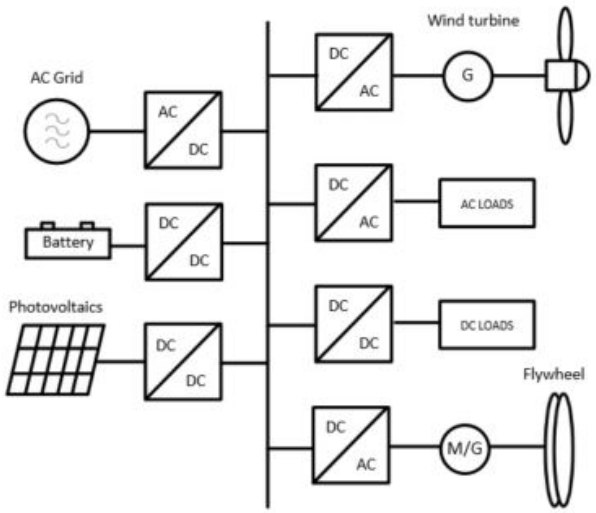

Figure 2.2: LVDC system diagram[17]

for loads to connect to the system in different ways (across positive pole-middle, positive pole-negative pole and negative pole-middle) according to their power needs. However, as a distribution grid, the system is expected to connect more than two nodes together, which implies that a multiterminal/meshed configuration is necessary, in contrast with the simple link between two terminals in the HVDC case.

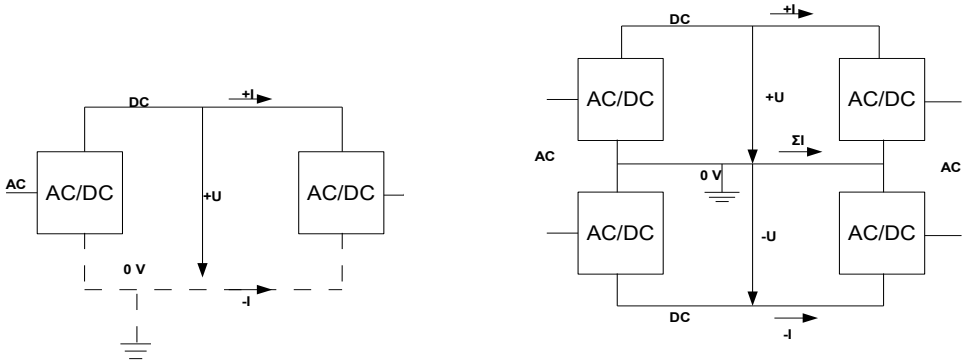

(a) A unipolar system

(b) A bipolar system

Figure 2.3: The two possible configurations of an LVDC connection

The unipolar circuit may or may not include a second conductor for the current to return. If one conductor is used, the current returns through the earth, in which case corrosion of the dc electrode that injects the current through the earth can happen. Safety and interference concerns may prevent the injection of dc current to the ground. Because of that, a return conductor is utilized in most cases of a unipolar system.

The unipolar circuit is ideal for applications on a small scale grid, such as a nanogrid, where power de-

mand is small and can be provided by the low voltage level. However, power demand increases in a microgrid that approaches distribution size, necessitating the use of a bipolar circuit. As can be seen, such a system can double the effective system voltage while using conductors of the same size as the ones in the unipolar system. That is because the potential of each conductor does not change, it's just the voltage level between the conductors that is higher. In this way, the voltage in the positive and negative pole is symmetrical and centered around zero. In order for the voltage to be indeed centered around zero and not 'float', a third middle conductor is introduced, with a grounding point close to the converter. In this way, the desired system voltage is achieved. Nevertheless, this solidly grounded neutral conductor does bring some complications. Ground faults in particular should be cleared as fast and efficiently as possible [19], as current loops with the earth can be formed, compromising the protection system and endangering people.

2.2. INTRODUCTION TO DC PROTECTION

2.2.1. DESIGN CHARACTERISTICS FOR PROTECTION

The term *protection* in power systems can be very general, as it encompasses the protection of the system itself against unwanted effects that may result to damage of precious and costly components, as well as the protection of people that may come in contact with an exposed conductor. An important difference between the two is the fact that the components are usually affected by extreme conditions and high values of current and voltage, while humans are much more sensitive to small currents, with a momentary direct current of just 300 to 500 mA being able to inflict fatal damage, according to El-Masry [20, p. 2319]. This thesis will focus on the large scale faults.

The protection of a system in general is characterized by the following design principles:

- *Reliability*, to ensure that the protection system operates as intended.
- *Performance*, to ensure continuity of service to the customers after a fault occurs.
- *Speed*, so that the fault is removed as fast as possible from the system.
- *Economics*, which have to do with costs of installation and maintenance.
- *Simplicity*, which is an indication of its complexity (or lack thereof), including number of parts, protection zones and more.

Added on top of the above, the sensitivity and selectivity of protection are also crucial aspects that can make or break the system. By making sure that the protection scheme is sensitive, it is ensured that only fault currents will be identified as such and consequently trigger the appropriate actions, while regular loading of the system is not interrupted by the protection devices. Meanwhile, selectivity should ideally enable the system to isolate the faulted part of the system. The disconnected area needs to be as small as possible, to minimize the number of affected customers. As we will see, however, achieving selectivity is not an easy matter, especially in DC grids.

In a nutshell, the primary objective of a protection system [3] is to detect and isolate faults within a set time frame, in order to minimize the propagation of disturbances to the rest of the power system.

2.2.2. PROTECTION CHALLENGES

The protection of a DC microgrid constitutes one of the greatest challenges for its proper function, as we already established in Section 1.4. Despite the undoubted benefits of LVDC, the implementation of this innovative and beneficial technology arguably makes the task of designing a protection system much more complex.

The lack of zero crossings in the DC current waveform makes the use of conventional AC circuit breakers impractical. Since the latter are able to interrupt the circuit when currents are close to zero, the arc that is produced from the tripping is easily quenched. In the case of DC, the breakers would have to be oversized to be able to stop the current during normal operation. This arc does not only compromise the safety of the system, it also causes erosion of the circuit breaker's contacts, leading to short component lifetime and high maintenance costs [21].

Therefore, it becomes clear that the existing protection devices are not ideal for DC systems. The first solution to that was to shut down the whole system at the converter level in case of a fault, but then there is absolutely no selectivity achieved, as all loads are disconnected. Another reason that makes the use of AC breakers in a DC system impractical is the fact that they operate very slowly compared to the rising slope of a DC fault current. By the time the breaker's contacts separate, the current will have reached high values, rendering the resulting arc very hard to stop.

It should be stressed that power electronic components are the most troublesome regarding protection. Flexible in their operation as they may be, converters have poor overcurrent capabilities compared to their AC counterparts. IGBT manufacturers tend to place their overcurrent capability around two to three times their nominal current, with only a few milliseconds of allowed overcurrent duration[22]. This is very small compared to the 400 ms, the minimum short circuit current supply time, which means that the protection has to operate close to the nominal current of the IGBTs, as they cannot withstand the overcurrent for such a long time. Their overcurrent capability is thus unused, due to the inadequate speed of the protection.

Another important point to be made is the fact that a system on a distribution level is expected to have a more complex structure than a transmission system. This has two implications:

- The more complex structure will inevitably introduce new types of faults with different transient characteristics, which will most definitely have an impact on protection strategies, as the protection techniques are based on the form of the transients to operate in the best way.
- The existing protection for HVDC transmission bypasses the DC protection problem by relying on opening the circuit on the AC side of the converter in case of a DC fault, which effectively disconnects the whole DC link. This works if this link is used to connect autonomous (AC) systems that operate perfectly fine on their own, and just use the DC link to supplement power in case of a fault, but if the DC system is a microgrid connecting customers, this strategy will not work. We have not yet reached the point where a LVDC microgrid can sustain itself purely on its own with distributed generation. Until then, selectivity is a necessary and inseparable part of protection in LVDC, which leads to developing new means of protecting this kind of system closer to the fault.

2.3. DC FAULT ANALYSIS

Fault analysis in DC microgrids is a relatively new subject. However, there have been some research publications that have studied the effects of these faults. One of those, Ouroua *et al.* [23], where an MVDC/LVDC architecture with AC and DC loads is subjected to various faults. From the simulation results, useful conclusions and suggestions can be made regarding the proper manner of protecting DC microgrids. Fault analysis and modeling are therefore important in addressing the protection requirements. Another paper [24], which looks into an LVDC/MVDC system with marine loads, has shown that such a network can be severely affected even by a fault with a duration of 0.05 s, highlighting in this way the need for fast and correct detection and isolation of the faults.

2.3.1. FAULT CATEGORIES

In order to analyze the fault transients in a short circuit, it is necessary to highlight the various faults that can happen in a standard bipolar DC circuit:

1. Short circuits.
   (a) Between positive and negative pole.
   (b) Between positive and middle (or negative and middle, in case of a symmetrically loaded system).
2. Ground faults.
   (a) Positive (or negative in case of symmetry) pole to earth.
   (b) middle conductor to earth.
3. Overcurrents, which can happen also in case of overloading, for example.

4. Overvoltages, which can occur for example a converter is brought back online after a fault.

All the above faults can occur with a high or low fault impedance, but some are more likely than others. Specifically, short circuits tend to have a low fault impedance, which results in higher fault currents. Ground faults, on the other hand, can be characterized as either high or low impedance. Of course, fault impedance also depends on many other parameters, such as fault location, cable arrangement etcetera. From the above, the thesis focuses on the faults that cause high overcurrents. Those will definitely be the short circuits, along with some cases of pole to ground bolted (or low resistance) faults. Identifying all possible faults and calculating the fault current for every given location is the first step to understanding how the system should be protected, leading to development of a scheme that adequately protects the microgrid.

2.3.2. THEORETICAL ANALYSIS OF FAULTS

The 61660 standard from IEC [25] describes the method for calculating the short circuit current contribution of DC fault sources, namely batteries, converters, motors and capacitors. A more detailed look at these currents is in Figure 2.4:

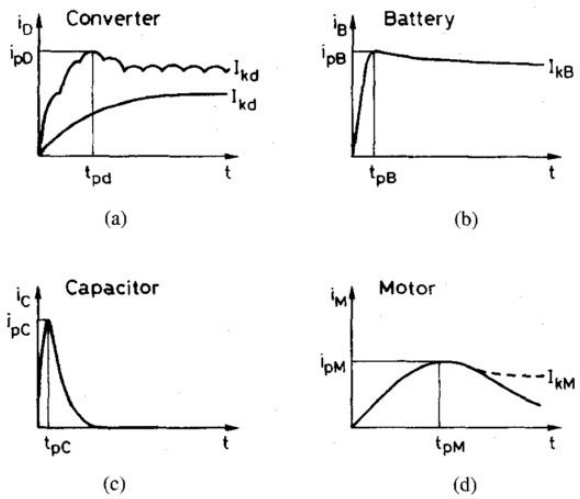

Figure 2.4: Short circuit current sources [26]: (a) Converter with and without smoothing reactor. (b) Battery. (c) Capacitor. (d) Motor with and without inertia mass.

The superposition principle is applied to the individual current from each source, in order to obtain the waveform of the total current. However, this depends on the system topology, like the distance of each source from the fault. For this reason, the standard instead proposes an approximation function to depict the current. That function is described by the following equations:

$$i_1(t) = \mathrm{i_P} * \frac{(1 - e^{-t}/\tau_1)}{(1 - e^{-\mathrm{t_p}}/\tau_1)},\ 0 \le t \le \mathrm{t_p} \tag{2.1}$$

$$i_2(t) = \mathrm{i_p} * [(1 - \alpha) * e^{-(t - \mathrm{t_p})/\tau_2} + \alpha],\ \mathrm{t_p} \le t \le \mathrm{T_k} \tag{2.2}$$

,where:

$$\alpha = \frac{\mathrm{I_k}}{\mathrm{i_p}} \tag{2.3}$$

The above equations suggest a waveform of two different sections; this can be confirmed by plotting the function, like in Figure 2.5. It is obvious that i_p is the peak short circuit current, τ_p is the time it takes for the current to reach this peak value, I_k is the steady state fault current after the transient stage and τ_1 and τ_2 are the rise and decay time constant, respectively, defined by the tangents of the two distinct curves at their starting point. The short circuit is assumed to be cleared at time T_k after its occurrence.

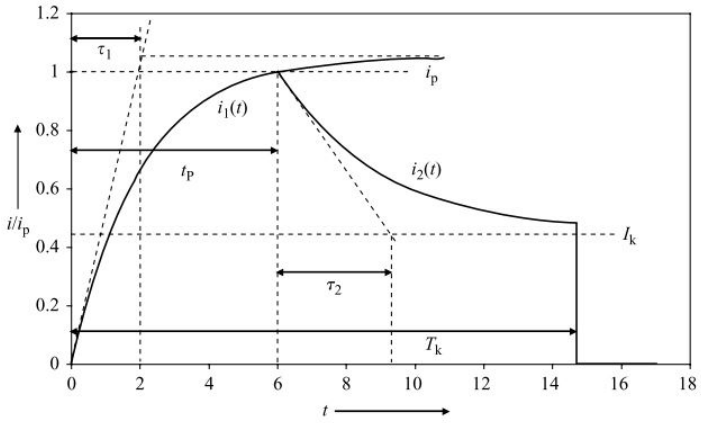

Figure 2.5: Short circuit current approximation function [26]

When calculating the maximum and minimum current, it is valid to assume that the effect of the fault impedance and the loads of the system are negligible. However, these do need to be factored in in order to have a detailed analysis, as the fault impedance can have a significant effect on the fault, The capacitors in the input of DC loads, meanwhile will discharge and therefore have a small contribution to the fault current.

The IEC standard then goes on to derive equations for the peak (i_p) and the quasi-steady state current (I_k), using coefficients which depend on the R/X ratio of the dc system. It should be noted however, that the standard is clearly focusing on 'DC auxiliary installations in power plants and substations'. Furthermore, as correctly pointed out in Berizzi *et al.* [26], the standard is not concerned with other DC systems, such as traction power or power distribution systems. Indeed, in such a system, the ratio of resistance to inductance will be significantly different, being out of the range of values included in the standard. The conclusion is that the standard cannot be used for a detailed analysis on anything but DC auxiliary power generation. Extrapolation of the existing graphs to obtain an approximation of the needed coefficients is the only way to utilize the standard in a meaningful manner for DC microgrids. The fact that the standard cannot be used for distribution networks has been shown in research [27], proving that the DC transient phenomena are underestimated in the case of DC microgrids when using the IEC61-660. Nevertheless, that is the only standard available that is concerned with short circuit currents and faults in DC, which highlights the need for more up-to-date official documentation facilitating and streamlining the fault analysis in DC grids, as already mentioned in Section 2.1.

2.3.3. DC FAULT STAGES

Since a standard method to predict a fault current is not yet available, the next best thing is to analyze the different stages of a fault occurring in specific configurations and obtain some vital information regarding the protection of the system. The motive for such an analysis is given by previous research [28], where it has been established that the transient phenomena of a DC fault are much different than the one in AC. For example, the DC distribution system has a fault ride through capability not seen in AC, due to the charging and discharging characteristics of the capacitor in the DC/DC converter. The peculiarities of a DC system can be better understood when the contribution of each of the system's component to the fault is clear.

The Figures 2.6 and 2.7 show a simple model of a VSC and cable which are short circuited on the DC side, and the corresponding equivalent circuits formed at each stage of the fault.

1. *Capacitor discharge* is the first stage, which is a natural response of the component to the voltage drop. As shown in Fig. 2.7 (a), a second-order RLC circuit is formed, causing oscillations, the frequency of which depends on the components of the circuit. The time at which the capacitor voltage drops to zero also depends on the initial conditions for the cable current and capacitor voltage. The current is given by the equation:

$$i_{\text{cable}} = -\frac{I_0 \omega_0}{\omega} e^{-\delta t} \sin(\omega t - \beta) + \frac{V_0}{\omega L} e^{-\delta t} sin\omega t \tag{2.4}$$

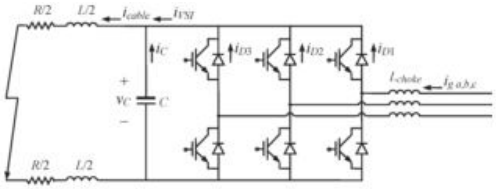

Figure 2.6: VSC with cable short circuit [29]

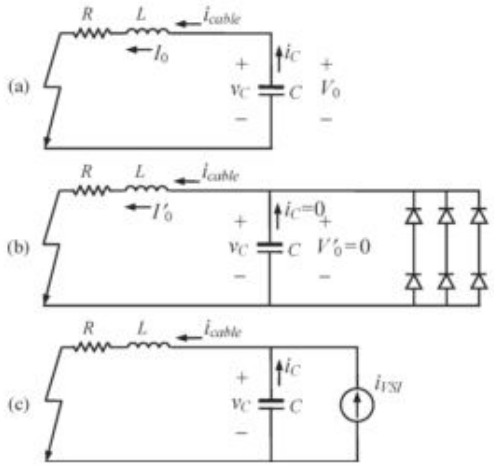

Figure 2.7: Equivalent circuit for each of the stages: (a) 1-Capacitor discharge. (b) 2-diode freewheel. (c) 3-grid current feeding [29]

, with

$$\delta = \mathrm{R}/2\mathrm{L}, \quad \omega^2 = (1/LC - (R/2L))^2, \quad \omega_0 = \sqrt{\delta^2 + \omega^2} \quad \text{and } \beta = \arctan(\omega/\delta)$$

A remarkable characteristic of this stage is that it remains largely the same. Grounding practice, fault resistance or bipolar/unipolar configuration seem to have no significant effect to the first 5 ms of the transient. The characteristic spike always appears at the start of the fault [30].

2. *Diode freewheel*: After the capacitor has fully discharged, the diodes start supplying the fault with current, as it naturally commutates to them from the capacitor. The equivalent circuit is first-order, and the cable current is decaying exponentially.

$$i_{\text{cable}} = \mathrm{I}_0^{'} e^{-(\mathrm{R}/\mathrm{L})t} \tag{2.5}$$

This is the most dangerous stage, component-wise, because the high uncontrolled current from the capacitor discharge is flowing through the diodes, possibly damaging them.

3. *Grid-side current feeding*, which occurs when the VSC IGBTs are blocked, and constitutes a forced current response, unlike the two previous stages. Due to the high current, the converter switches to constant current mode, to prevent damage. That gives the equivalent circuit of 2.7(c), and the circuit reaches in this way a steady state.

It is important to state that, depending on the value of the fault resistance, $\mathrm{R_f}$, it is possible for the capacitor voltage to not drop low enough for the antiparallel diodes to conduct (if $\mathrm{R_f}$ is high). The second stage is consequently skipped completely, with the grid feeding stage taking its place. It is obvious then, that high impedance faults (mainly ground faults) have a significantly lower chance of damaging the converter. As this thesis will not be focusing on high impedance ground faults, however, the above stages will be representative of this research.

2.3.4. FAULT PROPAGATION AND CONTRIBUTION OF DIFFERENT COMPONENTS

To further understand the far-reaching effects that a fault can have on the whole system, it is important to investigate the propagation of the surges caused by the short circuit across the circuit, and what effect those traveling waves can have on the protection system and the components. There is very little documentation regarding this topic on DC grids, with one notable example; a recent article from Bucher and Franck [31], in which the development of fault currents in a DC CB during a (low resistance) ground fault is investigated. In order to come to a conclusion regarding protection requirements, the article carefully examines the individual contributions of components to the fault current. Even though an HVDC cable and breaker are used, there

is no reason that the findings from this research would not apply to LVDC. These transients should not be fundamentally affected by the voltage level.

The system presented in Fig. 2.8 is studied, and the resulting currents from each component are in Fig. 2.9.

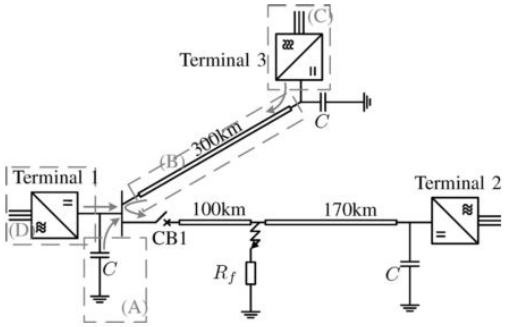

Figure 2.8: Network studied to determine various fault current feeding sources:(A) dc capacitor, (B) adjacent feeder cable along with Terminal 3 capacitor, (C) ac contribution of Terminal 3, (D) ac contribution at Terminal 1 [31].

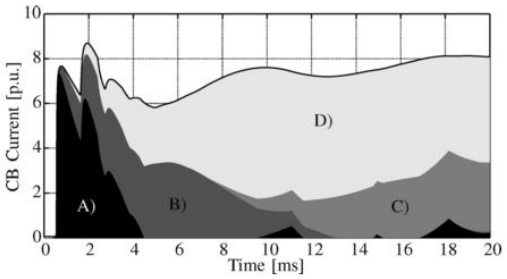

Figure 2.9: Contribution of each component to the fault current [31].

There are no less than 4 different sources for the fault to draw current from, even in this relatively simple configuration. Figure 2.9 provides a wealth of information. First, we notice the current arriving with a small delay at Terminal 1. As expected, the first peak is contributed to the capacitor at that terminal.

As soon as the fault occurs, negative voltage surges start traveling from the fault location towards both sides. The peak of the voltage surge depends on the fault resistance. As it travels toward terminal 1, the surge discharges the cable distributed capacitance, essentially drawing current to the fault. When the surge arrives at terminal 1 with a traveling time τ, it is partially reflected back as a positive surge due to the terminal capacitor, which creates a negative reflection coefficient. The now positive surge travels towards the fault again, gets reflected with opposite polarity again and travels towards terminal 1. This results in multiple smaller (due to attenuation) peaks in the fault current instead of just one. The negative surge that reached the terminal is transmitted to the feeder connecting the two terminals. There is a subsequent discharge of the feeder's capacitance and the capacitor at terminal 3, which is visualized as a second peak for the fault current. The larger distance to terminal 3 from the fault causes a bigger delay.

After the initial stage, the capacitance current drops and the ac infeed from the terminals dominates. It should be made clear that the discharging of the terminal capacitors and the AC contribution from the same terminal can start as soon as the voltage wave reaches that specific terminal, provided that the voltage drop in the surge is enough to make the converter diodes conduct (as explained in the previous subsection). If the surge itself does not reduce the voltage enough, the subsequent drop due to the capacitor discharging makes the diode conduct.

Another important observation that can be made from Figure 2.9 is that every component starts contributing at a time that depends on its distance from the fault. In other words, the further away a contributing component is, the more time it takes for its contributing current to reach the fault, as the AC infeed from terminal 3 appears last. Of course, the nature of the component and the specific fault conditions also play a role, as the current from the feeder and terminal 3 capacitor rises before the ac infeed from terminal 1.

The paper further discusses the influence of varying the fault resistance, capacitor size, feeder length, short circuit capability of AC grid and DC pole reactor on the fault current. What stands out from those is the remark that the time to peak current in the circuit breaker can vary, and depends on which discharge current peak is larger. This in turn depends on the fault resistance. The discharge current from the first capacitor does not drop to zero immediately after the first peak (first negative voltage surge), which means that there is enough time for the *second* negative voltage surge (reflected from the fault point) to reach the capacitor before the first discharge has stopped. The two discharges are superposed and, depending on the magnitude of the second negative voltage surge, they can surpass the peak of the first discharge. However, the magnitude

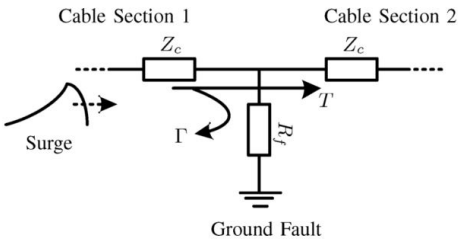

Figure 2.10: Reflection and transmission of traveling waves at fault point [26]

of the reflected surge from the fault depends on the reflection coefficient at the fault point, which is given by the following equation, if Figure 2.10 is also taken into account.

$$\Gamma = -\frac{1}{1+2\frac{R_f}{Z_c}} \tag{2.6}$$

This equation shows that a low R_f means a reflection coefficient of almost -1, which is practically full inverted reflection. A higher fault resistance would push the coefficient towards zero, which means a smaller reflected voltage surge. So the takeaway is that R_f has a significant impact on the peak of the fault current. The size of the capacitors also plays a role, as a larger capacitor will take longer to discharge, therefore adding a larger value to the second surge compared to a smaller one.

The publication concludes by suggesting ways to mitigate the first from the discharges. These include using smaller capacitors, limit the number of feeders connected to a bus to limit current contributions, and increasing the pole reactor size to limit the rate of rise of the fault current.

All the above serves to show that fault analysis and wave propagation are very closely related, and should be investigated in tandem to arrive to requirements for the protection system. It is hard to have a clear understanding of what exactly is happening with fault propagation. In a larger system, where contributing components are many more, such an analysis becomes very complex. One positive note is the fact that, in terms of fault propagation and surges, a DC system does not differ significantly from an AC one, because these surges are so short in time that both systems could be considered DC for that duration. As a consequence, it is realistic to rely on existing experience on fault propagation from AC applications, something that is not possible with the protection itself.

2.4. PROTECTION SCHEMES

2.4.1. PROTECTION DEVICES

In order to meet the safety requirements and solve the above problems in DC microgrids, a number of protection strategies have been proposed in an outburst of publications in recent years.Before presenting them, the commercially available protection devices should first be accounted for:

1. AC devices
   (a) AC circuit breakers, which disconnect the converter and the DC system completely and are thus suitable mostly in back to back or point to point transmission systems.
   (b) Fuses, which have already been proven to not be a good solution for DC systems and VS converters[32].
2. DC protection devices
   (a) Solid state circuit breakers (SSCB), along with an anti-parallel diode. Once a system is detected, the corresponding insulated-gate bipolar transistor (IGBT) receives a gate signal to turn off, and opens faster than the AC circuit breaker. It also enables a bipolar system to operate in mono-polar mode, as it does not disconnect the whole converter. On the other hand, it is unfortunately a unidirectional device on its own. While it can successfully protect from faults on the DC side, in

case of a fault on the converter the fault current would flow through the parallel diode as seen in Figure 2.11. This means that, in case of such a fault, the SSCB must rely on the blocking of the converter's components, What's more, fast DC switches that physically interrupt the circuit after the current is stopped are also needed, since a visible contact gap is required for protective devices.

It should be noted that gate turn-off thyristors (GTOs) and insulated-gate commutated thyristors (IGCTs) may also be used instead of IGBTs in an SSCB, with the first two also demonstrating lower on losses than the IGBT [21].

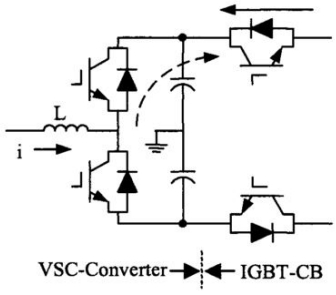

Figure 2.11: IGBT circuit breaker[33]

(b) ETO (Emitter turn off) devices. These are embedded in the converter, placed in antiparallel configuration, and handle both switching and protection, as seen in [11]. In the event of a fault, the devices can supply the fault with current, unlike the antiparallel diodes. In this way, the problem of the VSC during DC faults, as explained in Subsection 2.3.3, is eliminated. Once the fault is identified as permanent, the devices turn off.

(c) Capacitor DC circuit breakers (CDCCB), introduced in [32] and also mentioned in [34], are what the name implies. They are very fast devices with a 10 μs operation time. As already mentioned in 2.3.3, the converter capacitor discharges extremely fast at the beginning of the fault. This breaker is fast enough to disconnect the capacitor before it discharges Being in series with the converter capacitor, this breaker disconnects the capacitor fast enough to prevent it from discharging into the fault and protecting it from the stress associated with such a large current spike. Another added benefit is a shorter charging time when the converter is brought back online after the fault is cleared.

The advantages of multiple level converters has been well documented [35]. An interesting protection mechanism can be found in the newer Multi Modular Converters (MMC), as argued in Ding *et al.* [36]. Two protective IGBT switches are included in each submodule of the converter, as seen in Figure 2.12.

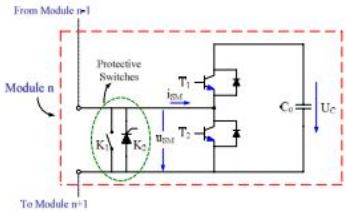

Figure 2.12: MMC submodule configuration [36]

The first of those, K_1, acts as a high speed- bypass switch. This means that it can close in redundant submodules so that they output zero voltage and therefore do not contribute to the converter operation. K_1 is also useful in case of a faulted submodule, in which case the switch closes, the submodule is shorted out and another one is brought into operation by having its bypass switch open. In this way the uninterrupted operation of the converter is guaranteed in case of faults in submodules.

The second IGBT switch is used in the event of a DC short circuit. After the IGBTs of the converter turn off due to the high current, the diodes will conduct. Assuming that actual protection devices are AC circuit breakers, the diodes will not be able to withstand this large current surge. For this reason, K_2 is closed, so that most of the high fault current flows through that thyristor, bypassing the diode. This 'press-pack' thyristor can withstand surge currents, and damage to the converter is avoided.

Finally, a newer development in protective devices should be mentioned. That is the z-source DC circuit breaker,mentioned in multiple publications, but most notably in [37] and [38]. The circuit of the device can be seen in Figure 2.13:

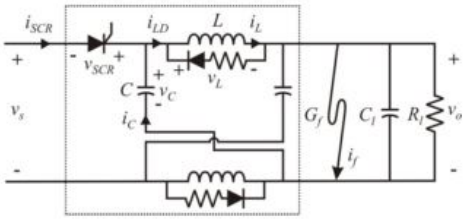

Figure 2.13: Z-source circuit breaker [37]

In case a fault occurs, none of the two capacitors in the circuit are directly shorted, as there are inductors in between. If there is a short at the load, its capacitor will discharge, but a part of the fault current will come from the other two capacitors. Because inductors keep their current constant, the fault current through the capacitors will increase until it reaches the current of the inductor. The current through the SCR device goes to zero then and it switches off (natural commutation). In this way, the source is disconnected from the fault. The remaining circuit is essentially a resonant circuit, and the oscillations will continue until the inductor voltage attempts to go below zero, where the parallel diode will turn on, dissipating the remaining energy in the resistor. It is clear that the fault current is cleared in an effective manner here, as seen in Figure 2.14. The output voltage drops to zero microseconds after the SCR current is extinguished, and the fault current follows, acquiring a smaller value until it is fully dissipated. As a result, the Z-circuit breaker appears to respond to faults and instantly disconnects the source to avoid further current contribution to the fault. An important design aspect is to have appropriate values for the inductor and capacitor components to ensure that the resonance allows enough time for the SCR to complete its reverse recovery process. This way, the SCR can completely switch off before it is forward biased due to the oscillation.

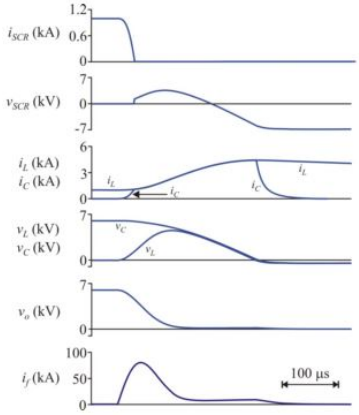

Figure 2.14: Fault analysis of a Z-source circuit breaker [37]

2.4.2. PROTECTION TOPOLOGIES

With the help of the above circuit components, there has been a significant number of proposals regarding the successful protection of a DC microgrid. A few of those involve the use of Intelligent Electronic Devices (IEDs) in conjunction with protective devices to form a protection scheme, while others still support the traditional overcurrent protection methods.

TRADITIONAL OVERCURRENT PROTECTION

One of the publications [11] argues for the use of ETO-based CDCCBs to prevent the capacitors from discharging. Specifically, the current sensing ability of the ETO, which triggers a hard turn-off when the current crosses a certain threshold. In order to stop the converter from also discharging current during the fault, it is further proposed that the antiparallel diodes be replaced with turnoff devices. A relay is used for detection, monitoring both the DC current and voltage for added security. When the two typical conditions for a fault occur (voltage drop below 80% and overcurrent) occur, a signal is sent to the converter to interrupt the current. After that, the paper discusses the coordination between the various protection devices. However, a

proper microgrid scheme is not presented, and it is recognized that locating the fault to minimize the impact is one of the biggest challenges.

Another paper [33] is approaching the protection problem in much the same way. Although the focus is on HVDC, there is nothing that could not be reasonably applied to distribution level. The use of the unidirectional IGBT-CBs discussed in 2.4.1 is suggested, along with the blocking capability of the converter's IGBTs, while fast DC switches for separation are also included. As the closest pair of CB and converter shut down first, the other pairs will follow, because the drawn current through them will increase. In this way, the DC network is isolated.

A different proposition can be found in the paper of Tang and Ooi [39]. The protection devices are mainly AC circuit breakers, the ones already installed on the AC side of the converters. Fast DC switches are also utilized on the DC side. During a fault, the IGBTs of the converter block while large DC currents flow through the diodes. The fault current is extinguished from the AC side by the AC CBs, and fault isolation follows by utilizing the DC switches in what is called the 'handshaking' method, explained below.

IEDs, Communication and Differential Protection

Many publications, especially the more recent ones, have begun utilizing more sophisticated schemes, which include communication between protective devices to solve the challenges faced in a DC microgrid.

For example, the scheme in [40] is more communication-based, with a combination of circuit breakers, relays and multiple IEDs for monitoring DC fault currents and voltages. Both SSCBs and AC CBs are used, the former to interrupt DC faults and the latter to protect against converter faults and faults on the DC point of common coupling (PCC). In case of a DC fault, the rapid decrease of the voltage along with the changes in the currents are the trigger for detecting and locating the fault. In order to achieve selectivity, the direction of the measured currents is used. Several faults are simulated at different locations in a last mile LVDC system. Quick detection and interruption are achieved due to the fast communication method, with a 'significantly limited fault level and supported ride-through capability' as a result.

A similar approach is presented in two complementary papers ([12], [41], where a ring bus system is studied.The loop is broken down in several zones of protection, defined by overlapping nodes and links. Each node contains three circuit breakers and there are two of them in each link (line), one at each end. This can be seen in Figure 2.15.

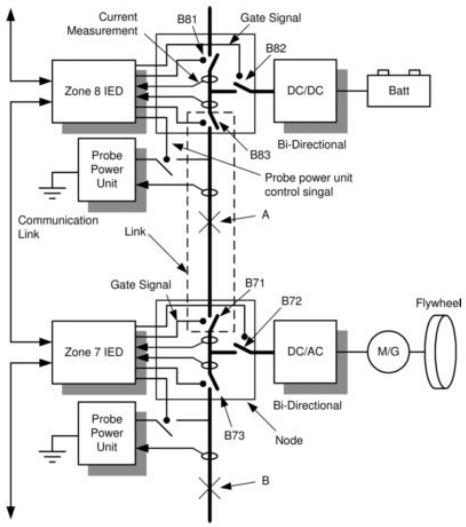

Figure 2.15: Ring bus DC microgrid system [12]

Each zone has an IED, which monitors and controls the local breakers in the node and links. Communication is used once again to coordinate the protection elements in case of a fault. IEDs also monitor their zone for breaker failures, making sure that all CBs operate as intended, while another mode takes care of reclosing and restoring the system.

IEDs are also used for fault discrimination in [40], where they exchange signals only when the fault thresholds (undervoltage and overcurrent) are crossed. Current magnitudes and directions are measured, and a signal is sent to the appropriate relay for selective tripping.

Another publication [42] argues for the use of unit protection in more complex DC microgrids to achieve better fault discrimination. This necessitates the use of additional communication and relay technology. The shortcomings of non-unit (overcurrent) protections are discussed and presented. Current differential protection, which is one form of unit protection is examined, along with challenges and proposed solutions. Finally, the paper recognizes the significant cost of unit protection, as well as the increased complexity it would entail. The resulting suggestion is that the protection scheme has to be optimized so that fault discrimination can be achieved in an economic way.

A more recent publication [43] also discusses differential protection, albeit in a more practical manner. It is pointed out (again) that this method is a lot less sensitive to varying fault levels and impedances than the simpler non-unit methods, but the operation time frame is still a challenge, as it can be up to 2 cycles in AC systems. The paper then goes on to quantify the response time of a differential protection system in a DC network. For the considered simple system, the allowed processing time for the differential device is found to be 1.5 ms which is much shorter than that of typical differential protection. Furthermore, a solution is proposed to this problem, namely the use of a central processor to compare all the measurements, utilizing calculations that take advantage of the nature of DC (only magnitude and polarity are needed) to make computation time shorter. This largely succeeds, as results show. The protection operating time can be as low as a few μs, 'although that is application-specific'. In any case, operation time takes no longer than a few tens of μs, which is considered adequate and a significant decrease over the response time of conventional differential protection.

Another possible solution is presented in the article by Nuutinen *et al.* [22]. This publication is based on the argument that protection is closely connected with the control scheme of the system. For this reason, a control scheme is developed where, the voltage of the converter is controlled during normal operation. As soon as a fault system is detected, the fault current is controlled in order to have a more direct effect on the current itself without having the possible parameter sensitivity that occurs when trying to control the fault current indirectly through the voltage. The control scheme dynamically switches between the two modes of operation. By controlling the fault current, it can be limited to a predetermined value which can be withstood by the IGBTs of the converter for a given time. This control scheme is used in conjunction with a Controlled CB. If the fault current has been flowing for a specific amount of time, an external signal is sent to the CB to trip it.

This method has some significant advantages. By not allowing the current to reach high fault values, it is possible to use lower-rated IGBTs, as they would not have to withstand such high currents. Saturation of the inductive components is also avoided. Another advantage that is not explicitly mentioned is the fact that this method gives a larger time window for the protection to operate, which is not the case for other schemes, where the protection has a very small margin to operate before the uncontrolled current rises to very high values. This is very important, mostly because sending an external signal to a CB for tripping definitely takes more time than just using its embedded overcurrent function. However, that delay is not a problem here due to the limited short circuit current control scheme.

FAULT LOCATION

Along with the interruption of the faulted circuit, it is very important to locate the precise area of the fault so that only that part is isolated and the rest of the system can operate as usual. It is one of the challenges faced when designing a protection system, because service with no (or very brief) interruptions to customers is essential. Some of the publications concerning protection schemes that were presented above also discuss fault location and the subsequent reclosing. The most interesting approaches are summarized here.

In [33], the faulted line is located by comparing the line currents. Due to their proximity to the fault, the currents will have the largest initial change and also the longest rise time interval, according to the author.

Another article [39] presents what is called the 'handshaking' method, which is applied after the fault has been cleared. The principle of this method is based on the idea that every converter will choose to open only

one of the DC switches from the lines connecting to it. The criterion of this selection is the line with the highest *positive* current, which is defined as current *leaving* the VSC node.

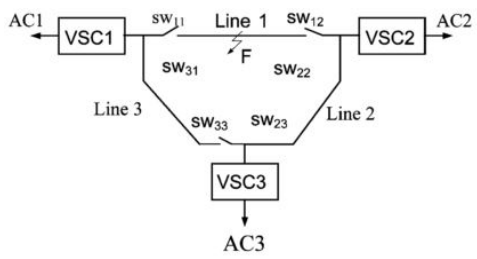

Figure 2.16: Handshake method [39]

From the example of Figure 2.16 it can be seen that the faulted line will have both its ends disconnected ,as both VSCs will contribute positive current in that line. Unfaulted lines, meanwhile, will only have one end open, because the fault current will enter from one side and leave through the other. In this way, it is certain that the fault, wherever it may be, has been isolated. Because of that, the AC CBs close, charging the DC capacitors. A DC switch will reclose only when the voltage on its one side is close to the voltage on the other side, after the capacitors have been recharged. This ensures that only healthy lines are brought back online.

The name of the method is due to the fact that two healthy hands (voltages) recognize each other, leading to a 'handshake' which allows for reclosing of the DC switch. The handshaking method is further validated by simulations. It makes clearing and isolating DC faults possible without the use of expensive DC circuit breakers. It should also be noted that no communication is used for this method, only voltage and current measurements.

A mix of AC and DC CBs is even suggested as an alternative, where the solid state CBs on the DC side can separate the system after a fault in two or more independent subsystems, so that the healthy parts can continue operating, while the faulted one can further isolate the fault with the aforementioned handshake method.

The paper by Park *et al.* [12] also deals with fault location, proposing an interesting solution. A probe power unit is placed near every node in the loop bus, forming an RLC circuit with the line impedance, after the protection isolates the faulted part. The oscillating current can then be measured with the probe. The response obtained is a damped oscillating signal. The envelope of that signal (or the attenuation factor, equivalently) gives an indication of the line impedance that is a part of the sub-circuit, making the distance between the fault and the probe known. This method is unique in that it does not require reclosing of the main circuit breakers to locate the fault. On the other hand, more equipment is needed in this case compared to the handshaking method.

According to the case study in the publication of Salomonsson *et al.* [44] a combination of the slope of the converter current and the capacitor voltage during the fault can be used to successfully distinguish between different faults. This way, we can determine the fault location and achieve selectivity in isolating the appropriate part of the system while minimizing the impact to the customers. This cannot be so easily achieved only with the current, which effectively means that careful monitoring of the capacitor voltage is a crucial part of designing the protection scheme for an LVDC system.

It is also suggested in Vanteddu *et al.* [45] that the slopes of the converter current and voltage can be successfully used for protection and fault isolation. The authors believe that monitoring the two slopes can help the protection devices react faster, whether they are hybrid or molded case circuit breakers. Coordination can be achieved by monitoring the different slope values that each different fault causes, based on the different fault conditions presented in the paper.

2.4.3. GROUNDING

Grounding is one of the more complex issues in power systems. It is very strongly connected to the protection scheme, and the technique used has a profound effect on the operation of the system. Grounding is used for ground fault detection and equipment and personnel safety [25]. A system can be ungrounded, low resistance grounded or high resistance grounded. A lower ground resistance would cause higher fault currents, making them easier to detect but harder to interrupt. The opposite is true for high resistance grounding. There is a further division of grounding schemes depending on the point of connection, and whether the protective earth (PE) or neutral (N) conductors are connected to ground at any point. Ultimately, a grounding scheme

should fit the system it is designed for. It is easy to understand that the complexity of grounding practices combined with the relative inexperience of the industry in the field of meshed DC grids can be quite the challenge for designing an adequate protection system. However, grounding practices are not a part of this thesis, and it will be assumed that simple low resistance/solid grounding is applied.

2.4.4. CONCLUSION

One conclusion from the above is that traditional protection methods (such as with relays) seem to be able to achieve satisfactory protection in some cases, but that requires careful coordination of the protection devices. Modern methods with communication, on the other hand, manage to effectively protect the grid but add another layer of complexity (and cost) to the whole system. Meanwhile, there are concerns regarding the delay required by the communication, which has a severe impact on the speed of the protection system, as seen in the lengthy publication of Li *et al.* [46], where communication delays are thoroughly investigated. According to that, this delay can be assessed and quantified *a priori* with simulations. Alternatively, it is possible to limit the current to an acceptable level to compensate for the protection delay. Therefore, it seems possible for systems heavily relying on communication to overcome the obstacles and achieve fast reaction times. Regarding fault location, the takeaway is that, unless the protection uses communication, interruption of service to healthy parts of the grid even for a brief amount of time is unavoidable.

2.5. SUMMARY

The above literature review contains the basic characteristics of DC microgrids, the faults that can occur and finally the various protection schemes that can be found in literature for dealing with faults effectively. This section will summarize all the techniques mentioned above in a table, highlighting the contribution of each article to a specific part of the protection strategy. The intended contribution of this thesis is also included.

Table 2.1: Summary of the contributions of the thesis and the referenced publications

	Protection schemes		Protective devices	Fault Location	Fault analysis	Wave propagation
	Communication	Traditional				
[32]		✓	✓			
[21]	✓	✓	✓		✓	
[11]		✓	✓			
[34]		✓	✓	✓		
[36]			✓			
[37, 38]			✓		✓	
[33]		✓	✓	✓		
[39]		✓		✓		
[40]	✓			✓	✓	
[12]	✓			✓	✓	
[41]	✓				✓	
[42]	✓				✓	
[43]	✓				✓	
[22]		✓			✓	
[44]		✓			✓	
[45]		✓			✓	
Thesis				✓	✓	✓

It should be noted that the publications on fault location in the above table are the ones included in the corresponding part 2.4.2. The coordination of protective equipment for fault location and isolation is discussed in most of the papers presenting a protection scheme, but as it is not the driving point of the publication, they are not included.

3

TRANSIENT SIMULATIONS

This chapter is meant to serve as a preamble to the simulations and the software used in this thesis. First, the software that was chosen will be introduced and briefly described, and then the specific components used in building the models will be shown.

3.1. CHOICE OF SOFTWARE

At the beginning of this thesis, a choice had to be made regarding the software that would be suited for transient simulations. That software was chosen to be ATP-EMTP. The Alternative Transients Program is one of the most widely used software packages for digital simulation of electromagnetic transient phenomena in electric power systems. It contains realistic models of most power system components, such as rotating machines, transformers, surge arresters, transmission lines, cables and more.

ATP also has a simple and clean user interface, with a report log that makes it easier to detect the position and nature of errors. Furthermore, it is capable of simulating transients in control systems (TACS), and even has its own simulation language (MODELS). The main reason for choosing this specific software was its ability to realistically represent the behavior of a real transmission line or cable. Matlab/Simulink was considered at first, due to its flexibility and all-around competence with various tasks. However, the accuracy of modeled components is very important in transient phenomena, and thus ATP was ultimately chosen.

Another characteristic of ATP that should be mentioned is the calculation method used for predicting variables of interest in electric power networks. ATP uses the trapezoidal rule of numerical integration to solve the differential equations in the time domain. The method divides a function $f(x)$ in sections [a,b] and approximates the region under the graph of the function in [a,b]. A trapezoid is formed, and its area is calculated by the following equation:

$$\int_a^b f(x) \approx (b-a) * \frac{f(a)+f(b)}{2} \tag{3.1}$$

The trapezoidal rule is generally considered to be one of the faster integration methods, and is also known to be quite accurate when applied to periodic functions, which makes it ideal for use in power systems.

More information about ATP and also a short manual for new users can be found in Appendix B.

3.2. BUILDING THE MODELS

Before discussing the simulations and the results (which will be thoroughly presented in Chapter 4, an explanation of the model building process should come first. Let's take a very simple system, like the one in Figure 3.1.

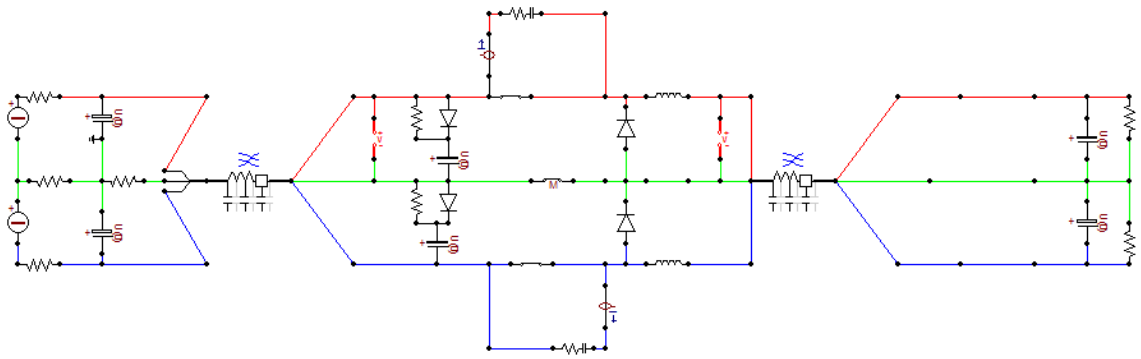

Figure 3.1: Basic bipolar DC system built in ATP

3.2.1. SOURCE, LOAD AND PROTECTION CIRCUIT

The above bipolar circuit contains a DC source with capacitors at its output (voltage characteristic). The loads are made up of resistors and capacitors and are connected to each pole. With the assumption that every load is a house, an average power consumption of 2 kW at 350 V is reasonable. This leads to the following calculations for the current and load:

$$I_{load} = \frac{P}{V} = \frac{2000W}{700V} \approx 2.86\,A \tag{3.2}$$

$$R_{load} = \frac{V^2}{P} = \frac{700^2}{2000} \approx 245\,\Omega \tag{3.3}$$

Which means a load of 123 Ω per pole. The capacitors are sized in a way that makes sense for the DC load. As a rule of thumb, the RC sub-circuit should take approximately 10 ms to discharge from 400 to 300 V. From the basic RC decay equation:

$$V(t) = V_0 * e^{-t/R_{load} * C_{load}} \tag{3.4}$$

With

$$V_0 = 400\,V, \qquad R_{load} = 61\Omega, \qquad t = 0.01\,s \qquad V(0.01) = 300\,V$$

We solve for C_{load}:

$$C_{load} = \frac{-0.01}{61 * \ln(300/400)} \approx 570\,\mu F$$

The rest of the example system is made out of the protection circuit and the cable elements.

The protection circuit consists of a MOSFET switch along with its RC snubber in parallel, an RCD damper/voltage clamp, and a diode with an inductor on the load side. Normally, when the switch is turned off, the current is interrupted immediately and as a result, a large voltage difference appears across the contacts of the switch. The snubber absorbs a part of this energy as the capacitor is getting charged. The purpose of the clamp is

to minimize the overvoltage on the source side, so the impact on the rest of the system (which is still functioning) is minimal. The inductor serves to limit the fast rise of the current on the fault side. The maximum current rate of change that is acceptable without destroying components is 4 MA/s , and the limit of acceptable overvoltage is roughly 50 Volts above normal operation, so 400 V. This results in an inductor of:

$$L = \frac{\mathrm{U}}{di/dt} = \frac{400}{4 * 10^6} = 100\ \mu\mathrm{H}$$

Based on that, a rough approximation for the dimensions of the clamp capacitor was made. A similar inductor further up the system would have stored energy equal to $\frac{1}{2*L*I^2}$. After the switch close to the fault turns off, this steady state energy (minus losses of the cable in between, which are neglected here) will need to be stored in the clamp capacitor. With an inductor of 100 μH, a steady state current of roughly 40 A and a maximum overvoltage of 50 V, according to the energy conservation rule:

$$\frac{1}{2}\mathrm{LI}^2 = \frac{1}{2}C\mathrm{V}^2 \tag{3.5}$$

And the desired capacitance would be:

$$C = \mathrm{L} * \frac{\mathrm{I}^2}{\mathrm{V}^2} = 4\ \mu\mathrm{F}$$

It should be noted that the above calculation is done with a certain level of approximation; the result was tested in simulations and a value that was closer to the desired results was chosen, that capacitance is in the range of $6-8$ μF.

Also, the steady state current considered here is an approximation of the maximum current that could be flowing in a distribution grid. The same protection circuit used for a load (house) that draws around 7 A peak would understandably produce much lower overvoltages.

The behavior of this protection circuit is further analyzed in Subsection 4.3.1, where its transient response is illustrated.

3.2.2. CABLE COMPONENT

The first step to creating an accurate cable model is to obtain all the relevant component parameters from the manufacturer. The cable that was used in the street lighting system (Chapter 5) will be considered for the models as well. It is a halogen-free, braided 0.6-1 kV power cable, with XLPE insulation, commonly used in AC. The specific model contains 4 conductors (3+1 protective earth) of 4 mm^2 area each, mad eof solid copper (models with a cross section area above 6 mm^2 are made of Litz wire). The specifications of the particular cable are presented in Table 3.1:

Resistance(Ω/km)	Self-inductance (mH/km)	Capacitance (nF/km)	Permitted current (A)
4,61	0,36	172	37

Table 3.1: Cable electrical characteristics, as found in [47]

Given the above parameters, it is possible to use some elements from the ATP library. When choosing among them, it is important to consider the use of the model and its intended purpose. Since this thesis concerns a transient analysis, it is clear that the simplest lumped cable/line elements (pi model, for example) will not do. That is because a cable (or a transmission line) is so much more than just a single pi shaped RLC circuit. Its electrical characteristics (R, L and C) are spread along its length, which in turn means that a distributed element will give us a much more accurate idea of the response. The downside to that is, of course, higher overall model complexity, meaning longer running time. In a steady state study (and in larger systems) it would make sense to simplify the cable by using the common pi-model. But in a transient analysis, where precision is the goal and simulation time is also in the range of a few milliseconds, the distributed model is the way to go.

The first models included the distributed one phase elements (one for each of the 3 current currying conductors). This meant that a difference in response due to the distributed nature was observed. On the other hand, characteristics such as mutual inductance and capacitance were not taken into account, since the element is 1-phase and there is no interaction between each phase. Even if the manufacturer's inductance and capacitance values accounted for the effect between conductors, one could argue that the current ATP element was still not good enough, as the interference between the conductors is not physically modeled. In any case, it becomes clear that the 1-phase is not sufficient.

In order to use a more sophisticated model, it was important to ascertain if mutual inductance and capacitance were taken into consideration in the above values. The manufacturer provided some insight in the calculation process of the inductance, and it seemed that mutual inductance was indeed accounted for in one value that encompasses everything, called 'operating inductance'. However, it seemed prudent to do an independent calculation to verify that this is the case. For this, relevant documentation was consulted, such as [48],[49].

According to the above documentation, the formula for calculating the inductance will only be simple in symmetrical arrangements, where the combination of each conductor is equal. Because of that, a simplification was made to consider a cable containing 3 conductors instead of 4, placed in an equilateral triangle, as seen in Figure 3.2. The simpler formula is a result of the equal distance of each conductor from another. By omitting the only non current carrying conductor (PE), we can use a much simpler formula to calculate the inductance, while only slightly deviating from the actual value due to the simplification.

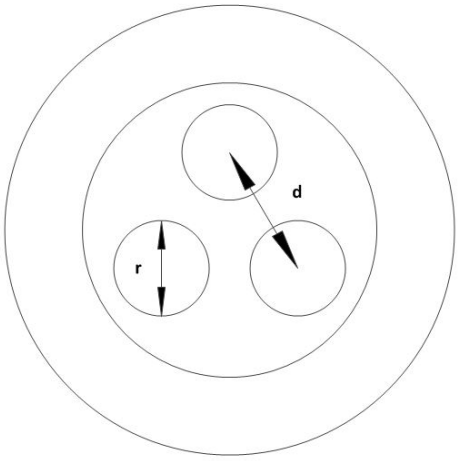

Figure 3.2: Cable cross section

The inductance is mainly affected by two factors, shown in Figure 3.2. Those are the radius r of each conductor and the distance d. The inductance formula that applies the most to the above configuration is the following:

$$\mathrm{L} = \frac{\mu_0}{2 * \pi} * \ln\left(\frac{GMD}{GMR}\right) \tag{3.6}$$

Assuming symmetry and identical, equidistant solid inductors, then the GMR (geometric mean radius) is equal to the effective radius of the conductors, while the GMD (geometric mean distance) is the distance between their centers.

The radius can be calculated by the given conductor area, $\mathrm{r} = \sqrt{\frac{4}{\pi}} = 1.12$ mm and $\mathrm{GMR} = \mathrm{r}' = 0.779 * \mathrm{r}$. The distance between conductors is not known, but a reasonable approximation would be $\mathrm{d} \approx 3 * \mathrm{r}$. Using these values, (3.6) gives the inductance per conductor:

$$\mathrm{L} = 0.2 * \ln\left(\frac{5.25}{0.779 * 1.75}\right) \approx 0.359\,\mathrm{mH/km}$$

The result is very close to the one given by the manufacturer. However, it should be noted that the inductance formula (3.6) (which was most likely used by the manufacturer as well) is mainly used for the calculation of inductance in a transmission line. In the case of lines, the radius of the conductors is negligible compared to the distance between them, which is certainly not a safe simplification to make in a cable. Furthermore, it is very likely that the actual inductance can be somewhat different than the one calculated due to the smaller distance and thus more flux linkage between the conductors. The result from the above calculation confirms that the given number includes the effect of mutual inductance, but the effect of the conductors' close proximity on this value should be taken into account.

Having established that the mutual effect is included in the supplied datasheet, a choice should be made for the ATP element that would best fit the model. Regarding multi-phase distributed cable/line elements, ATP provides two different choices. The first one is in the form of a custom block called LCC, where the user can choose between cable/line, different known models for each, and input the geometric characteristics so ATP builds the component according to that. It would be ideal to use this custom block, however it appears that this element does not accurately portray the characteristics of the cable, and it has been a known issue within the user group of ATP. This leaves only the other two options available.

The second one is the Bergeron constant parameter (frequency independent) model, which represents the L and C elements of a pi-section in a distributed manner. The user can choose between transposed (Clarke) and untransposed (KCLee). Unfortunately, the KCLee one uses a modal transformation matrix with complex elements. This phasor representation means that a steady state frequency must be chosen, which is a problem for the DC system in this case. Because of that, the Clarke transposed model was chosen, which uses the following simple transformation matrix:

$$T = \sqrt{\frac{2}{3}} * \begin{bmatrix} 1 & -\frac{1}{2} & -\frac{1}{2} \\ 0 & \frac{\sqrt{3}}{2} & -\frac{\sqrt{3}}{2} \\ \frac{1}{\sqrt{2}} & \frac{1}{\sqrt{2}} & \frac{1}{\sqrt{2}} \end{bmatrix}$$

The above is also known as the power invariant $\alpha\beta$ transform, which we know does not rotate the reference frame and thus contains no phasors in the transformation. In a balanced system, the sum of phase voltages or currents is always zero, which means the third equation of the transformation matrix can be eliminated to give the simplified form:

$$T = \sqrt{\frac{2}{3}} * \begin{bmatrix} 1 & -\frac{1}{2} & -\frac{1}{2} \\ 0 & \frac{\sqrt{3}}{2} & -\frac{\sqrt{3}}{2} \end{bmatrix}$$

The model requires the data for resistance, capacitance and inductance (or alternatively resistance, impedance and propagation speed) for the two sequences 1 and 0. The 1 sequence components for R,L and C are considered to be equal to the operating value given, so we just need to calculate the zero sequence.

From [50], the following is true for the sequence components of this cable configuration:

$$L_0 = 3 * L_1 = 3 * L = 1.08\ \mu H/m \tag{3.7}$$

where L is the given operating inductance, and is assumed equal to the positive sequence inductance.

The relationship between the operating capacitance C_b (which is given) and the capacitance of each conductor to earth C_E and to another conductor C_g is:

$$C_b = C_E + 3 * C_g \tag{3.8}$$

But:

$$C_E \approx 0.6 * C_b = 0.1032\ nF/m \tag{3.9}$$

The only thing that remains is to find a relationship between C_E and C_0. The zero sequence component can be found by shorting all the conductors at one end of the cable to ground and connecting a known voltage

source V_0 at the other. If each conductor draws current I_0 from the source then the zero sequence impedance of the cable is $Z_0 = \frac{V_0}{3 * I_0}$. Figure 3.3 shows the equivalent circuit.

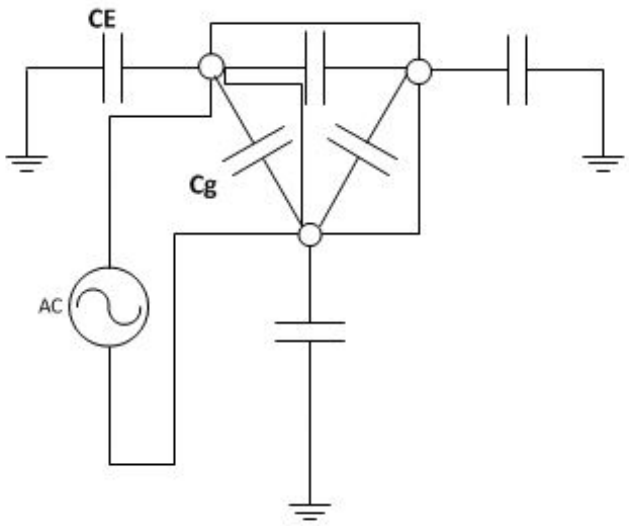

Figure 3.3: Equivalent circuit for zero component capacitance

Since the capacitance between the conductors is shorted, only C_E remains in the calculation. In fact, it is easy to see now that the zero sequence capacitance is $C_0 = 3 * C_E = 0.3096\,\text{nF/m}$.

As for R_0, according again to [49] it is

$$R_0 = R_1 + 3 * R_{\text{neutral}}$$

We consider the neutral to be the PE conductor here, since there is no sheath, so we get

$$R_0 = 4 * R_1 = 0.01844\,\Omega/\text{m}$$

Using the formulas for impedance and speed:

$$Z = \sqrt{\frac{L}{C}}, \qquad Z_1 = 45.7496\,\Omega, \qquad Z_0 = 59.0624 \tag{3.10}$$

$$v = \frac{1}{\sqrt{L * C}}, \qquad v_1 = 1.2708 * 10^8\,\text{m/s}, \qquad v_0 = 0.54687 * 10^8\,\text{m/s} \tag{3.11}$$

This is all the data that the Bergeron Clarke model requires.

A final note regarding the settings; when the timestep of the simulation is equal or greater than the travel time of a pulse along the shortest piece of cable, the program halts the simulation with an error. For this reason, it is important to always set a timestep that is at least half the travel time along the shortest cable of each system.

4

SIMULATION RESULTS

4.1. INTRODUCTION

In this Chapter, the models that were created in the way described in Chapter 3 will be presented, together with the results from the corresponding simulations.

Before the actual simulation results, a lab experiment regarding the propagation of pulses along the cables will be discussed. This will help put the following simulation results that focus on propagation in context, as the speed measured in the experiment will be compared to the speed in the models.

On the simulation side, a fairly simple system is used at first to show the basic response of the components that were used to the faults and the subsequent current interruption from the protection. Following that, a system with several branching lines is next, where more emphasis is placed on the effect of a fault on one load to the rest of the loads and the rest of the healthy system. The third system that is shown is an approximation of a street with several houses as loads. Faults are simulated in different locations and their impact is discussed. The final system is a ring structure, with faults typically occurring at one side of the ring, and the effect spreading through both sides to the rest of the system.

4.2. PROPAGATION EXPERIMENT

When investigating the propagation speed of pulses along cables, it makes sense to have something practical to compare the simulation results to. Moreover, the propagation speed can be tested with a very simple setup, such as the on in Fig. 4.1:

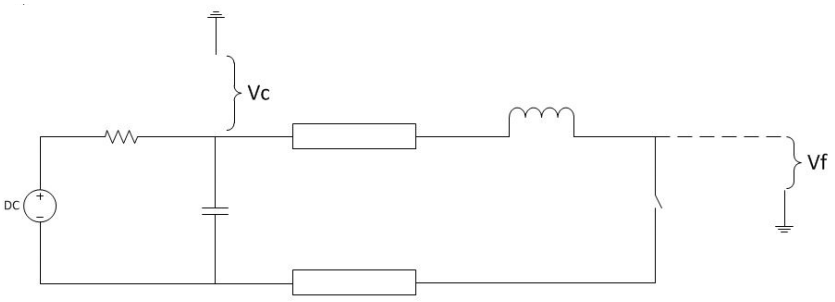

Figure 4.1: Propagation experiment setup

The setup comprises a DC power supply connected to 4 meters of cable. By shorting the end of the cable while measuring at both ends, it should be simple to observe the time delay in the response of the

two voltages. We are measuring the potential of the output capacitor and the potential at the corresponding end of the cable to ground. However, after the first test, it became clear that the voltage response at the output of the power supply was too slow to accurately measure the delay, on account of the output capacitor limiting the voltage rate of change at that point. For this reason, an inductor was inserted at the power supply output. Right after the cable is shorted, resonance commences and the voltage responds much faster. The inductor was carefully chosen to avoid a voltage that would be too high for the measuring equipment, with the same principle as in 3.2.1. Specifically, for a voltage up to 400 V and the absolute maximum limit of current rate of change of 4 MA/s the inductor specified above would result in a voltage of: $U_L = L * \frac{di}{dt} = 100\ \mu H * 4\ MA/s = 400\ V$, while the probe can measure up to 600 V.

The oscilloscope measurement can be seen in Figure 4.2. The delay in voltage response between the two ends of the cable is approximately 20 ns. This is in accordance with the observation by [31], where a 0.5 ms delay was measured for 100 km. Such a delay corresponds to a propagation speed of:

$$v = \frac{x}{t} = \frac{4}{20 * 10^{-9}} = 2 * 10^8\ m/s$$

which is 66% of the speed of light.

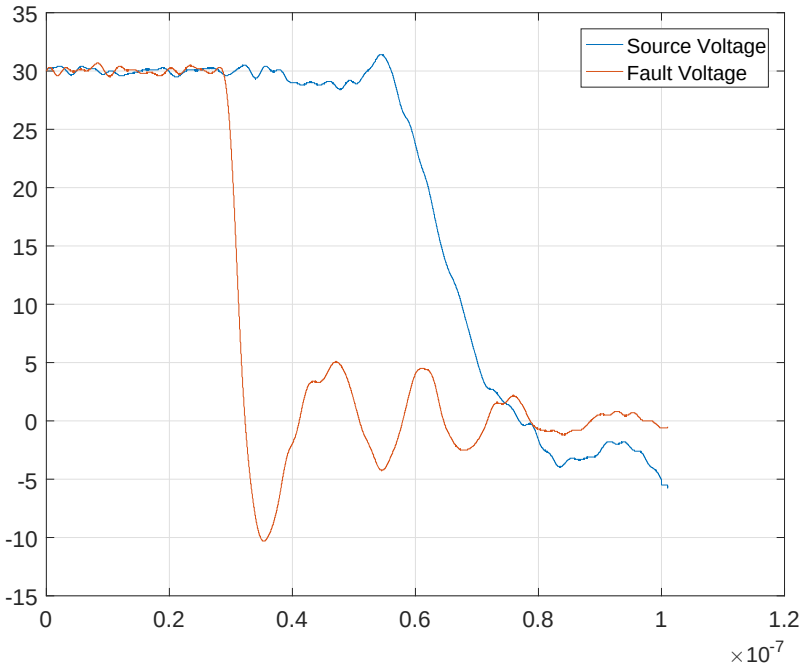

Figure 4.2: Propagation delay

The purpose of the inductor was to decouple the end of the cable with the source output capacitor, so that the voltage response would be more prominent. A different inductor would thus only affect the oscillation frequency in theory. The inductor as a lumped component has a zero travel time for the voltage pulse. It is therefore unlikely that any change in the inductor would significantly impact the delay measured here.

4.3. ATP SIMULATIONS

This section presents the various models that were briefly discussed in 4.1, along with the corresponding measurement results.

4.3.1. SIMPLE LINE MODEL

The first model to be presented is the one shown in Figure 4.3.

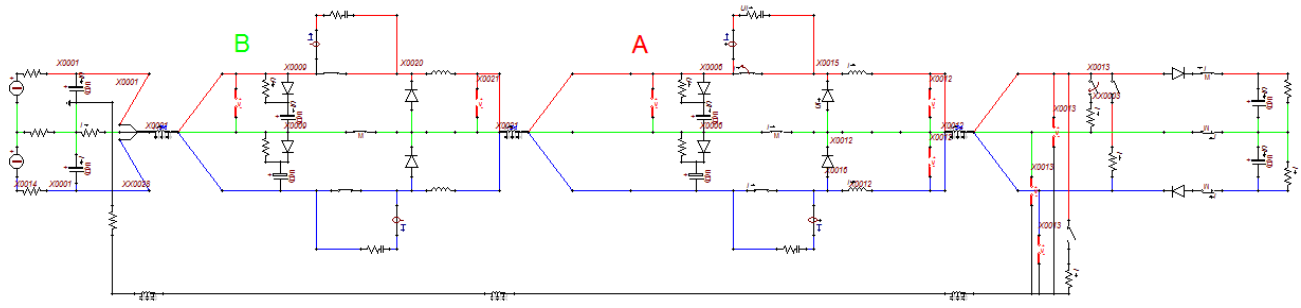

Figure 4.3: Simple line model

The DC source is on the left, with its protection circuit right next to it (B). After some length of cable follows the protection circuit of the load with the load itself. Note that the extra conductor in black is the fourth conductor of the cable, the protective earth(PE). The loads in DC are not grounded as the ones in AC, because any stray current will be unidirectional, and according to existing studies[51], direct stray currents cause more than 100 times the damage that equivalent alternating currents would cause. Since the loads are not connected to ground, the protective earth conductor in these simulations is used only to simulate earth faults.

The first thing to focus on in this simple circuit is the operation of the protection circuit, the components of which were initially discussed in 3.2.1. The simulations in this example will highlight the behavior and importance of this circuit.

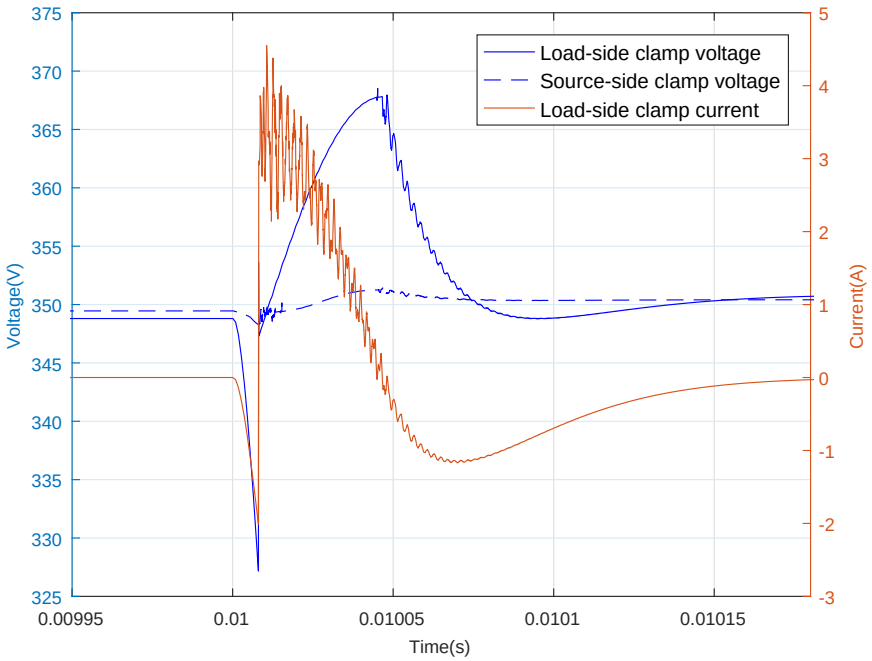

Figure 4.4: Clamp voltage and Current during bolted short circuit

Figure 4.4 shows the voltage and current of the load-side clamp (point A) , as well as the voltage of the source-side clamp (point B) during a bolted short circuit between the positive and neutral conductor close to the load at 0.010 s. Immediately after the fault, the capacitor at point A starts feeding current into the fault (voltage drop), and the protection circuit close to the fault interrupts the current, at which point the same capacitor stops discharging. However, the current flowing in the rest of the system cannot immediately

stop flowing due to inductance. That explains the clamp current inrush right after the circuit is interrupted. During this stage, the clamp capacitor at A is charged by the source through the diode, as is evident by the rise in the voltage. In this way, the clamp absorbs the residual energy in the healthy part of the system.

The capacitor will now have to discharge, since its voltage is higher than the system nominal 350 V. The discharging is done through the clamp resistor, where part of the stored energy is dissipated. For that reason we are not seeing a smooth voltage during the discharge phase. The rest of the energy is returned to the system. During the discharge process, the capacitor voltage drops and the current is of course negative. The dotted plot indicates the voltage at the source-side clamp, and is included to show the effect that the fault and the protection have on the rest of the system with the current configuration.

It is also important to note that the overvoltage observed at the clamp is depending on the inductance before it. This inductance is the sum of the cable inductance and the previous clamp's inductor, which is much larger than the cable inductance. As a result, the clamp can be designed with a specific maximum allowed overvoltage in mind based on just the value of that inductor (100 μH), since the cable would have to be impractically long to have an appreciable impact on the clamp overvoltage.

Another important characteristic to be investigated is the ability of the system to maintain operation of one pole in case of a fault. It makes sense that after a fault between the two poles (positive and negative) that cannot happen, since the protection will definitely interrupt the current on both poles. What is not certain is what happens in the case of a pole-to-neutral and a pole-to-ground fault. One could think that these would produce similar results, since the neutral conductor is essentially grounded on its source side, but the results are very different. Figures 4.5 and 4.6 show the currents in each conductor for the pole-to-neutral and pole-to-ground fault respectively, in case only the protection of the affected pole turns off.

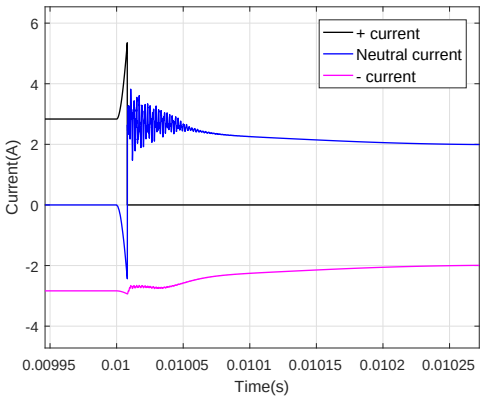

Figure 4.5: Currents in case of + to Neutral fault

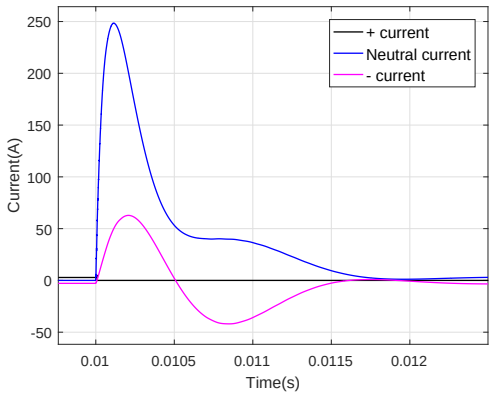

Figure 4.6: Currents in case of + to earth(PE) fault

In the case of the + to Neutral fault, the + current starts rapidly increasing, but is soon interrupted, by the top MOSFET. Despite that, some very high currents in the range of kA can flow on the load side, since the load capacitor is practically shorted. The closer to the load such a fault occurs, the higher the discharge current can get. This may not affect the rest of the system, since the interruption has already occurred, but it is a very real danger for typical capacitive DC loads.

The current of the - conductor is affected, but not in a way that would cause the protection on the bottom to interrupt; that is, the current does not reach extreme values and its rate of change is high only when it briefly drops after the top protection opens. Given that the protection will trip only when the rate of change has a positive high value, it is safe to assume that the negative pole will continue normal operation, with current supplied through the middle (neutral) conductor.

The same cannot be said for the earth fault case, where very large currents are observed on the neutral and negative conductors on the healthy part of the system after the fault. The positive pole current is of course interrupted, but it is clear that this is not enough to stop the fault current. Even after the + conductor is disconnected, the top load capacitor continues to be effectively shorted between ground and neutral. Since the PE is connected at the source grounding, a loop is made through which the top capacitor discharges. The bottom capacitor, on the other hand, retains more or less the same level of charge, as can be seen by its

current waveform, and could theoretically continue to operate as normal, were it not for the extremely high currents. Interestingly, this analysis leads to the conclusion that even if the bottom MOSFET were to turn off, there would be nothing to stop the middle conductor from discharging the top capacitor through the earth loop. Proposed solutions for this will be discussed later in this chapter.

Referring back to Figure 4.3, the loop formed because of the earth fault will channel current back to the grounding point of the source. The current will split. Most of it will flow through the neutral conductor, but a significant amount will flow through the two source output capacitors. Due to the + conductor being interrupted, the part of the fault current flowing in that pole will end up charging the clamp capacitor close to the load.

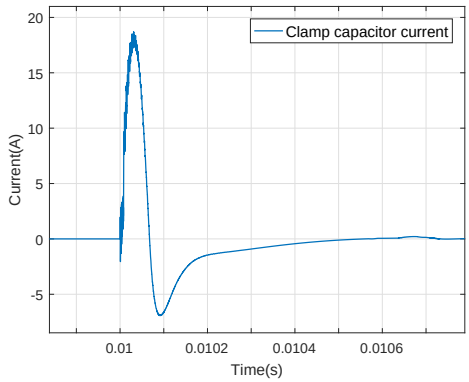

Figure 4.7: Current through the load side clamp capacitor (Point A)

Figure 4.7 shows this current, and a quick calculation can confirm the above hypothesis. The dominant frequency of the displayed current is determined by the LC filter that is formed by the top source output capacitor (220 µF) in series with the inductor of the source side protection (100 µ H) and the load side clamp capacitor (4 µF). The cable and inductance is considered insignificant for this calculation. The two capacitors in series will produce a capacitance that is very close to 4 µF, so an approximation of the resonant frequency of the circuit that is formed is given by the equation:

$$2 * \pi * f_{\text{res}} = \frac{1}{\sqrt{L * C}} \tag{4.1}$$

Solving for the frequency yields:

$$f_{\text{res}} = \frac{1}{2 * \pi * \sqrt{0.1 * 10^{-3} * 4 * 6 * 10^{-6}}} \approx 7.9\,\text{kHz}$$

which is close to the observed frequency of the current, since its half cycle lasts around 0.65 ms, which corresponds to a frequency of 7.7 kHz.

Based on the above we can safely assume that, in case of a + to neutral fault, the other pole can keep operating as usual. An earth fault, on the other hand, will have a big impact even on the healthy part of the system, the severity of which is determined by the fault impedance.

Since a bolted fault is the worst case scenario, higher impedance faults will produce even smaller current surges. In the case of the pole fault, the faulted part of the system is truly isolated and because the fault current is stopped very fast, the effect on the rest of the system is expected to be roughly the same. In contrast to that, an earth fault with varying impedance is expected to produce markedly different results with respect to the voltages in the healthy part of the system.

Figure 4.8 shows the voltages (between + and neutral) at the two points A and B for + to N bolted and 100 Ω faults and Figure 4.9 shows the same voltages at A and B for bolted and 1kΩ earth faults. The previous expectations are confirmed, and it is very clear that a varying fault impedance will produce very similar results for pole fault (left) after the fault has been cleared, because the fault impedance is isolated from the rest of the system. The drop in voltage is naturally much more pronounced in the bolted case, due to the higher fault current. This current is also the reason for the higher overvoltage of the capacitors in both points A and B, as they are forced to charge to higher levels to absorb the stored energy. Again, the impact to the rest of the system (point B) is barely noticeable.

In stark contrast to that, a varying earth fault impedance makes a big difference, since it still affects the system even after the top switch interrupts the circuit as already shown above. In the bolted fault case, the overvoltage at point A is exceeding the allowed levels (roughly 50-100 V above steady state voltage) due to the circulating current observed. The peculiar small increase of voltage in point B even after peak voltage has been reached is caused by the same effect.

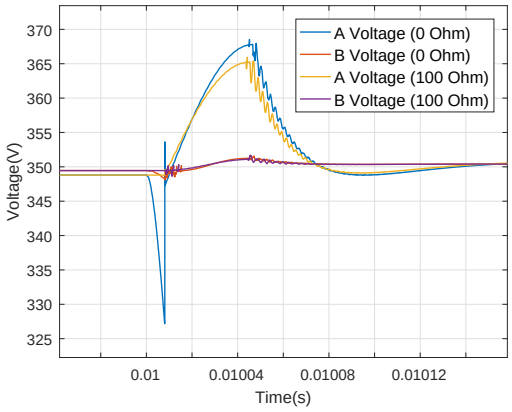

Figure 4.8: Voltages in case of + to Neutral fault

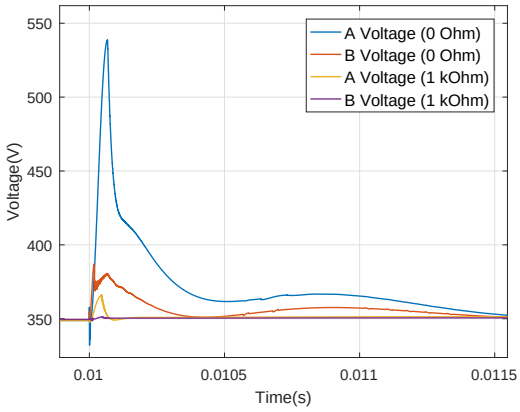

Figure 4.9: Voltages in case of + to earth(PE) fault

Another important case to look into is the one when the protection circuit does not operate as intended, as per the relevant research question from Section 1.5. If the circuit is not interrupted after a fault, it is easy to realize that the system will simply end up in a different steady state condition, where the large currents cannot be sustained by the system components. The opposite is also worth investigating; what are the effects when the circuit is interrupted when there is no fault, and how those effects differ from what was already shown. It is expected that the effect will be somewhat smaller, because the current that is interrupted in the no-fault case is just the steady state current, while the fault current that is interrupted in the other case is larger. The difference between the two currents is not big, as the MOSFET interrupts quickly after the fault occurs.

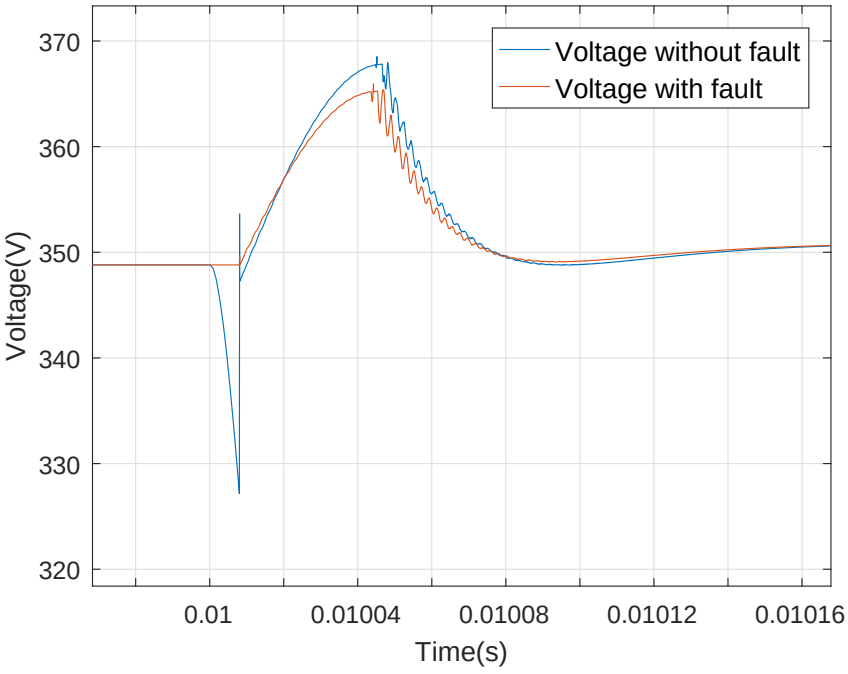

Figure 4.10: Clamp voltage comparison at point A with and without fault

Figure 4.10 confirms these expectations. The biggest difference between the two plots is the sudden drop in voltage right when the fault occurs. The slightly higher current that is interrupted in the fault case is charging the same capacitor, which results in a slightly higher overvoltage. It is clear that the difference is very small when it comes to a bolted pole fault. In the earth fault case, it is possible that the difference will be

larger because the circulating current through the ground will charge the capacitor much more. The conclusion is that the answer to the research question can vary depending on factors such as the type of fault or the time delay between fault and interruption.

A final point to make using this system is a basic comparison with the results of the DC street lighting measurements of Chapter 5. This is concerning the bolted earth fault case. Figure 4.11 shows the potential at each conductor close to the fault position.

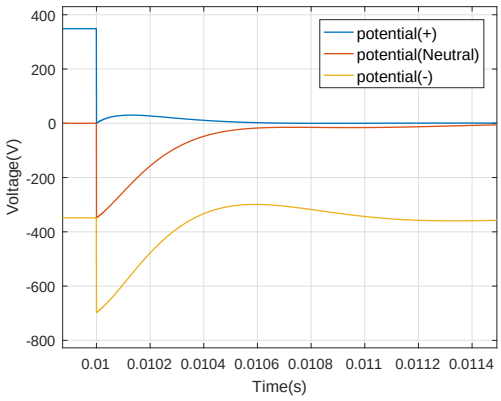

Figure 4.11: Potentials at fault point (simulation)

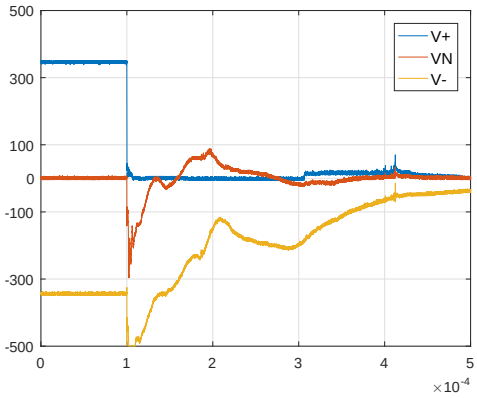

Figure 4.12: Potentials at fault point (system)

The two plots refer to completely different systems, but one common characteristic that is always observed in these types of faults is the simultaneous drop in all three potentials. Because one of them is forced to 0 due to the fault, the system capacitance momentarily drags the other two down as well.

With regards to one of the research questions in Section 1.5, it should be noted that this system was first tested in a unipolar configuration to better understand the behavior of the components that were used. The simulations for the unipolar system are not shown here, simply because the bipolar system allows for more interesting results to be shown simultaneously. The simplicity of the unipolar system means that there is no problem with a pole fault severely affecting the other side. It is obvious that many more parameters need to be monitored in the bipolar system, because the non-faulted pole is always affected in some way, due to the shared neutral conductor. During a bolted pole fault this effect does not seem to be big enough to disrupt normal operation, but it appears that the other pole will definitely be affected by a low impedance earth fault.

4.3.2. BRANCHING MODEL

The next model that will be discussed is the branching model seen in Figure 4.13.

The source is placed to the left, and is accompanied by its protection circuit. The node (bus) is where the three loads are connected through cables. Each load has of course its own protection circuit. The cable for both the top and middle loads is 200 m long, while the cable for the bottom load is 250 m long. The purpose of the simulations on this system is to show how a fault affects the voltage close to the rest of the loads, as well as the source. With this is mind, Figure 4.14 contains the voltages close to the source(A) the load where the fault happens (C), the load with the cable of 300 m (B) and the load with the somewhat longer cable of 250 m (D).

After the fault occurring at 10 ms, the voltage close to the fault point unsurprisingly drops the most with a decrease of 22 V in the 8 µs it takes for the fault current to be interrupted. In the same amount of time, the voltage at the other loads is affected to a lesser degree, with milder drops of 2 V. The effect on the source voltage is imperceptible, which is most probably because of the large output capacitors. After interruption, a voltage spike is observed, which is caused by the inductors' reaction to the abrupt current change. This is observed in all three of the loads, and the time difference between those three spikes can be used to calculate the propagation speed of the voltage pulse from the fault location to the other measuring positions. To be more specific, measuring the time difference between position A (red) and B (green), we get 3.12 µs s of delay. The distance between them is 200 + 200 = 400 m, so the speed would be:

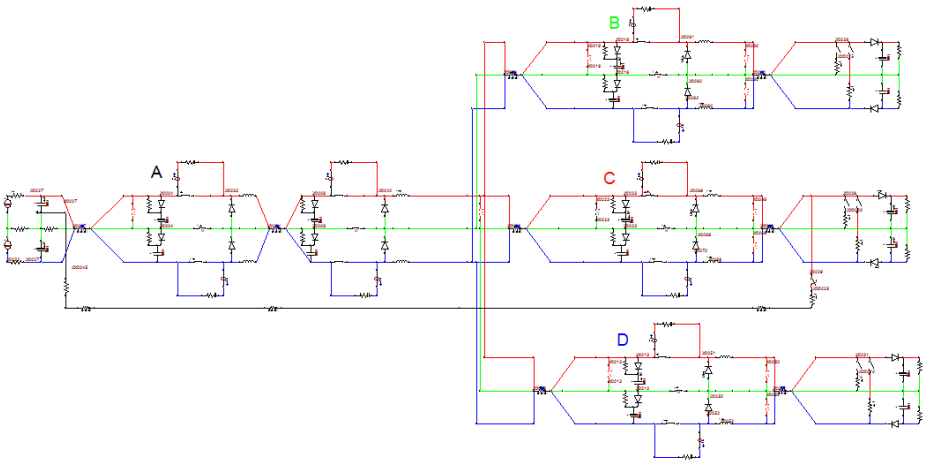

Figure 4.13: Branching model with three separate loads

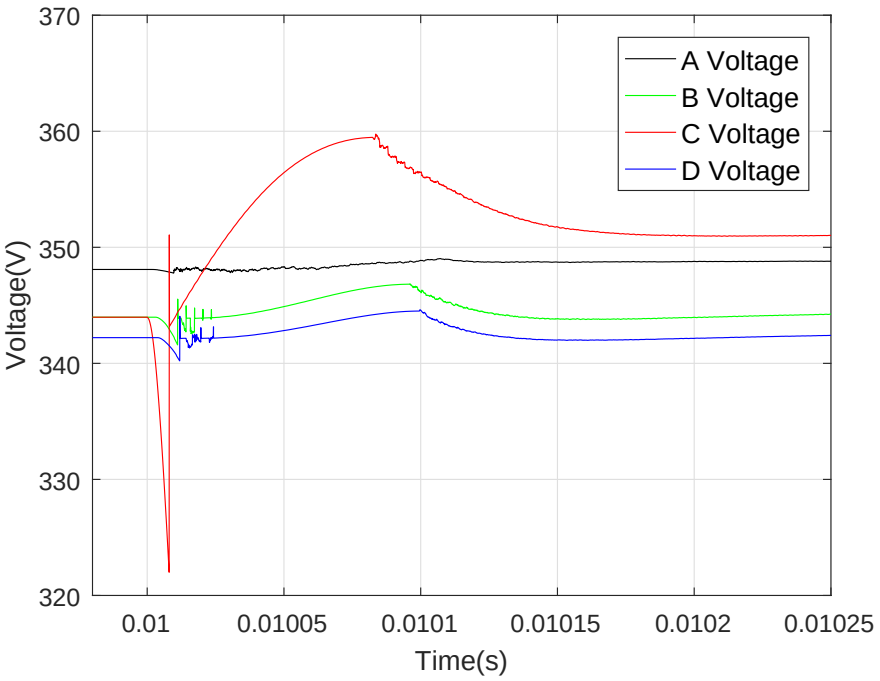

Figure 4.14: Voltage transients after bolted short near C

$$\frac{400}{3.12 * 10^{-6}} \approx 1.28 * 10^{8} \text{ m/s}$$

which is very close to the speed of $1.27 * 10^{8}$ m/s that was set in the cable parameters. Notice also the slight difference between positions B (green) and D (blue), which is due to the longer cable in the latter. The extra 100 m in the cable should add a further delay of t = $\frac{100}{1.28*10^{8}} \approx 0.8$ µs , which is very close to the delay measured in the ATP plot.

The capacitors will absorb the residual current and their voltage will increase. The biggest overvoltage is always observed at the capacitor of the protection circuit that trips, of course. A noteworthy observation is that the effect on the voltage on the healthy loads can vary with their distance from the fault. The overvoltage in position B is measured at 3.5 V, while the one at D is measured at 2.5 V. The difference is not visible in this

case, but it is easy to picture a larger difference in a bigger system. The conclusion is that a position that is closer to the problematic area will exhibit a more severe disturbance, which makes sense, but is nonetheless important to confirm.

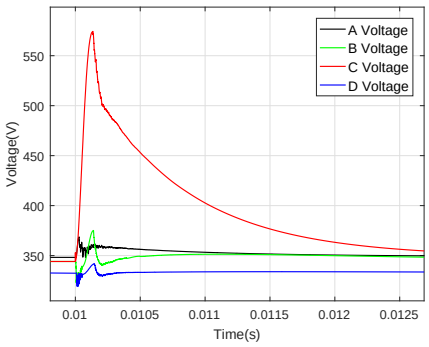

Figure 4.15: Voltage transients after bolted earth fault near C

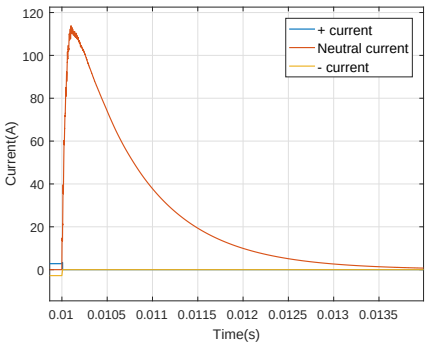

Figure 4.16: C currents during bolted earth fault near C

Figure 4.15 shows the voltages at points A, B, C and D during an earth fault at the same position as before. The voltage effect to the closest load is more visible here, as the green voltage increases significantly more than the blue one. Even the effect on the source voltage can be observed, as the pulse originating from the fault position is big enough to cause a small increase there too.

This time, both top and bottom switches were set to turn off as can be seen in Figure 4.16 but it is clear that the previous problem was not solved, as the neutral conductor current is still allowed to flow in the loop through the ground. This loop is shorting the load capacitor close to the fault, causing this large current to flow. Nevertheless, this current is significantly smaller than the one seen in Figure 4.6, which can be partially explained by the larger distance from the shorted earth (more than 400 meters compared to less than 100), resulting in a longer loop. The most prominent reason, unfortunately, is the fact that the other two load branches are affected. As the current flows through the fault towards the grounding point of the source, most of it flows back towards the fault position though the neutral conductor, as this is the path of least resistance. Some of it, however, is flowing through the two poles, charging the clamp capacitors in the case of the disconnected branch as we already saw in Figure 4.7, and also flowing through the other healthy loads and disrupting their operation.

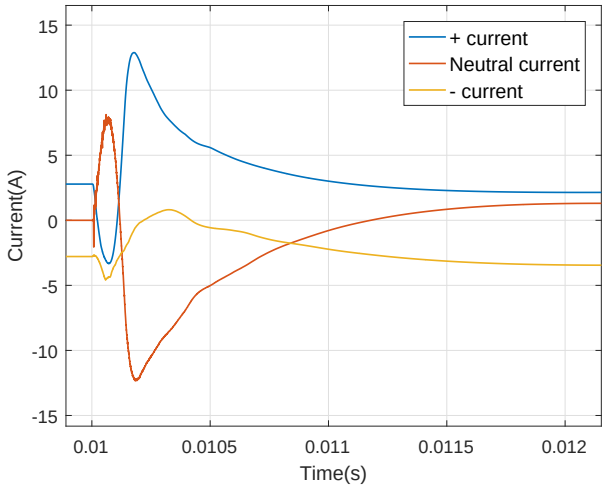

Figure 4.17: B currents during bolted earth fault at middle load

The currents flowing in all three conductors in the top load (B) are plotted in 4.17, and it is clear both the clamp and the load capacitors are involved. It is to be expected that the positive pole of the other loads is

affected the most. The capacitors discharge at first, as evidenced by the drop in voltage for some time after the fault. The current then reverses direction, and the capacitors are charged, as their voltages increase. In this way, all the loads in the system are taking part in these oscillations due to this loop.

A proposed solution to mitigate the effect on the other loads is to add diodes in front of the load capacitors, so that the discharging can be avoided. This is implemented in this system, and the voltages, currents close to the fault and currents at the top load are in Figures 4.18, 4.19 and 4.20 respectively.

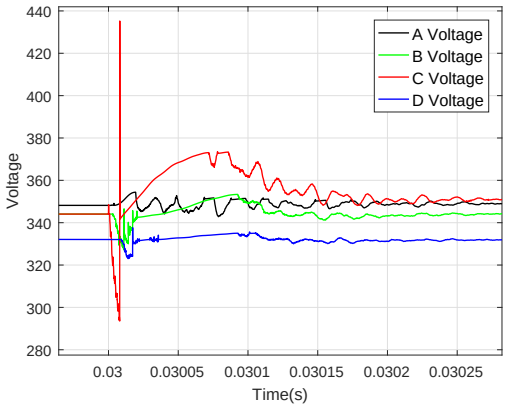

Figure 4.18: Voltage transients after bolted earth fault (with diodes)

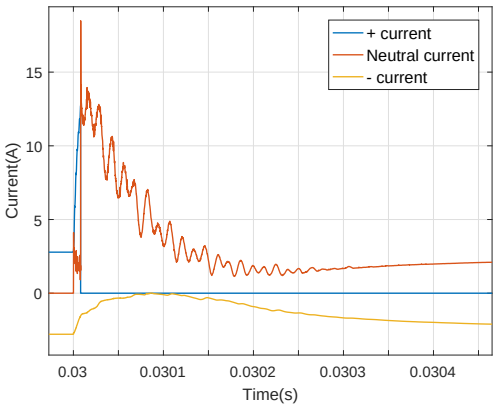

Figure 4.19: C currents during bolted earth fault (with diodes

It is obvious that the effects have been mitigated significantly, since the voltage close to the fault point does not increase nearly as much and the effect on the other measured positions is also smaller than before. The currents on the right figure are also limited. The largest current appearing through the neutral conductor flows because, after the switch turns off, the top diode is suddenly forward biased (due to the load diode not allowing the current to reverse). Through the forward biased diode, current flows from the neutral to the positive conductor until the former takes over the current from the latter, the diode stops conducting and the bottom load returns to steady state. The bottom switch was left open, as the current transient on the other pole appears to change slowly enough so as not to trigger the protection's $\frac{di}{dt}$ detection. As for the other loads, the impact is not completely avoided, since the loop still exists, it's just that the load capacitors are not allowed to discharge. In any case, the current only goes up to barely 5 A, which is much better compared to the previous case. The current rate of change should be low enough not to trigger the protection, while the negative pole is certainly able to operate.

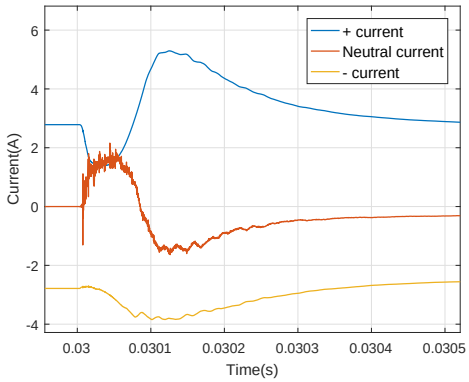

Figure 4.20: B currents during bolted earth fault at C (with diodes)

A final issue that was encountered while studying this particular system is the fact that, in some cases, the load side diode of the protection circuit can be permanently forward biased after the fault. This can occur whenever only one pole remains operational after a fault. After a bolted short, current will still be flowing through the neutral conductor to feed the load on the negative pole and a small voltage drop will appear along it. Since there is no current flowing in the positive conductor, a small positive voltage is applied across the diode. If the distance of the fault from the protection circuit and the diode is long enough, this small voltage will be enough for the diode to start conducting. The diodes have a typical voltage threshold of 0.7 V, and once this is crossed, current flows from the neutral to the positive, feeding the fault with the current seen in Figure 4.21.

The current supplied can make up a significant part of the current that flows through the bottom load. This current cannot cause damage as it is quite low, but the fact that current can still flow through the fault in

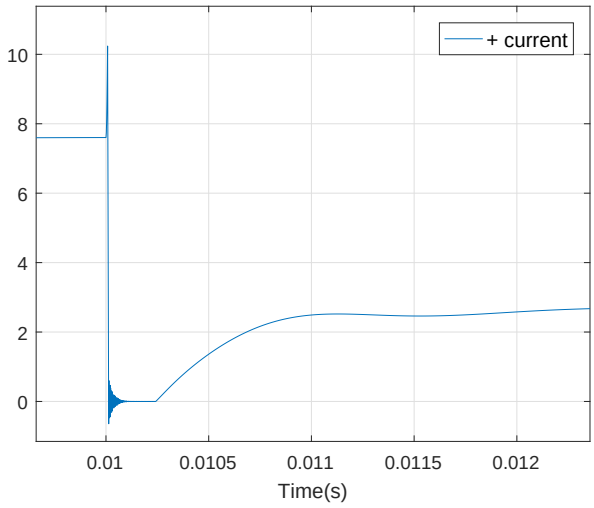

Figure 4.21: Forward biased diode feeds fault in steady state

steady state should be taken into account for protection design. It is clear that many parameters need to be considered to keep one pole operational.

4.3.3. ROAD SYSTEM

Moving on to more complicated models, the following one is a small street of houses supplied directly with DC via a central converter.

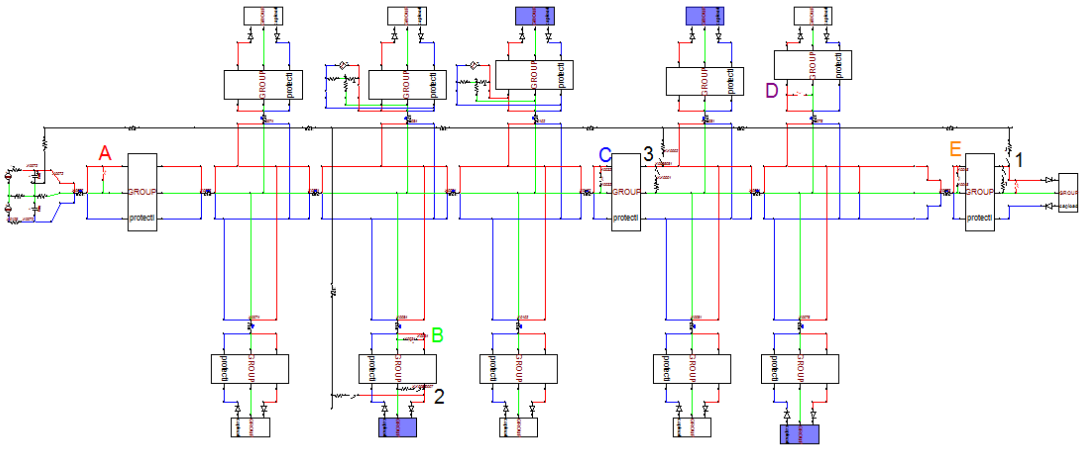

Figure 4.22: Road with houses model

In Figure 4.22, the DC converter is placed on the left. Loads and protection circuits are grouped together in the boxes seen, as it is easier to control everything in such a big system by grouping repeating components. The numbers indicate the positions where faults are simulated, and the colored letters the measurements. The whole main cable is 1.2 km long and every load connects to a node through a cable of 200 m. The blue-colored loads are operating at half load, and the second and third houses on the top side also have solar panels installed, represented by a constant current source. The panels are simplified, of course, since they do not supply constant power. For reference, a small panel installation of 1 kW would provide this system with a current of:

$$I = \frac{1000\text{W}}{700\text{V}} \approx 1.43\,\text{A}$$

It is also important to state that the current sources are grounded, just like the DC converter. This is expected to have an impact on system response, especially when it comes to earth faults.

Since this is the maximum theoretical current that can be provided, the constant current source is set at 1 A.

As this is a more complex system than the previous two, faults at more positions will be simulated, but only the voltages will be presented here. The idea is to give some insight to the impact of disturbances along the road on the rest of the system instead of focusing on specific locations.

The first faults are conducted at position 1, the load furthest from the source.

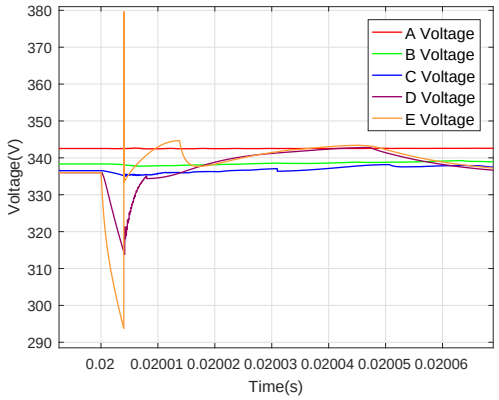

Figure 4.23: Voltage transients after bolted pole fault at E

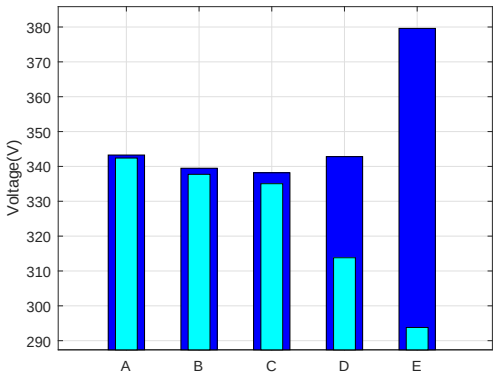

Figure 4.24: Voltage variation (min-max) after bolted pole fault at E

Figure 4.23 shows the measured voltages at the positions A, B, C, D and E. It is obvious that, beside the fault position E, the greatest impact is observed at the closest load D. Both voltages drop (approximately 20 and 40 V respectively), and charging of the clamp capacitors commences after the MOSFET switches off. The sudden spike in voltage at point E is due to this switch off, but it seems that the height of this spike changes depending on the chosen timestep. An even smaller timestep than the one that was used now (10 ns) produces an even smaller spike. The reason for that is that in the step right after the switch turns off, the change in voltage can be too fast for the software to keep up with, resulting in an error. The conclusion is that this spike is in reality smaller than what it is pictured to be here.

After the clamp capacitor at E is charged, it starts discharging and from then on follows the “local” voltage, as the capacitor at D and the other nearby loads are also charged and discharged. We see in this way not only how the effect is delayed from the origin to other positions, but also the damping effect. The impact on position C, which is roughly in the middle of the road, is much smaller, but the pattern is still recognizable. The other two positions A and B are practically unaffected by the fault at the end of the line.

On the right, Figure 4.24 offers another view on the same results; the maximum and minimum voltage of each position is presented in the bar graph, which illustrates the varying impact on each position and emphasizes the fact that the further we move away from the fault, the smaller the impact observed.

Figures 4.25 and 4.26 show the same for an earth fault at position 1. As can be seen from the left figure, the response is very different to the bolted pole fault. The main reason for the difference is the forming of the neutral ground loop that was also described in previous models. The effect is amplified here because we have three grounding points, with the distributed generation contributing significantly to the circulating current. The grounding points of the two current sources carry in fact most of the loop current.

It is true that the effect is diminished somewhat since the large load capacitors cannot discharge directly on the fault, but there are still the capacitive elements of the clamps in this loop path that along with the inductors, can cause voltage oscillations like the ones shown in the plot. The fact that all voltages are oscillating is proof that the earth fault affects the whole system. It is also clear that the proximity of the load with the current source close to the C position is causing its voltage to oscillate significantly more than the other positions. B and D have the mildest oscillations, since they are not part of the loop.

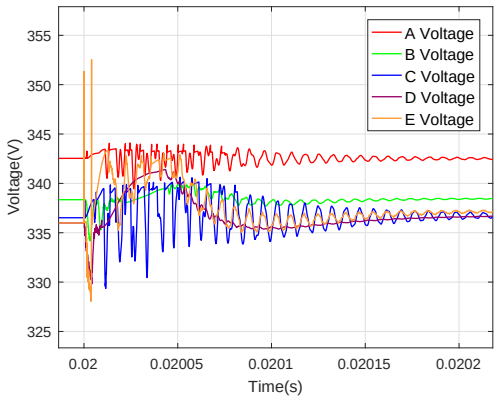

Figure 4.25: Voltage transients after bolted earth fault at E

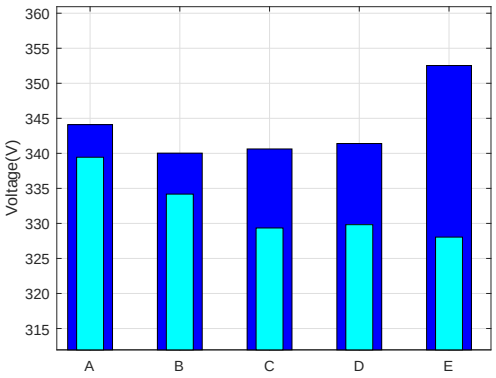

Figure 4.26: Voltage variation (min-max) after bolted earth fault at E

The above analysis agrees with the bar plot; there is a variation on all five measured voltages, with the size being dependent on a mix of a) proximity to the fault and b) whether or not the particular position is part of the loop formed by the earth fault.

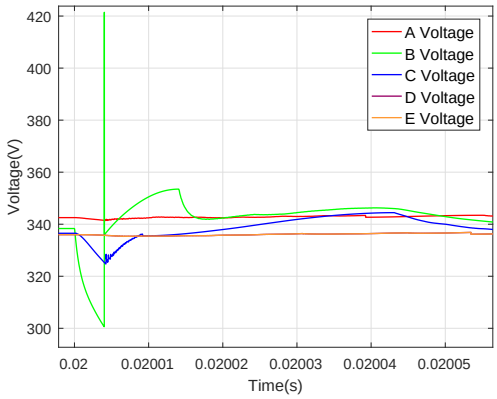

Figure 4.27: Voltage transients after bolted pole fault at B

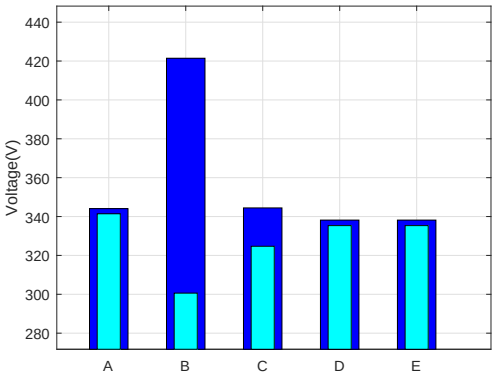

Figure 4.28: Voltage variation (min-max) after bolted pole fault at B

Moving on to the faults at position 2, the same bolted pole and earth faults are performed, and the previous illustration method is used again to discuss the simulation results. The fault position reacts in the same way, with a large drop at first and a spike which may not be as high as it seems in reality as we already discussed. Measuring position C seems to be the one affected the most from the other measurement positions. Overall, we get the same image as the previous pole fault, as the impact of the disturbance is mitigated the further one moves away from the fault.

An earth fault at position 2 presents a significantly different outcome than the same fault at the end of the road (position 1). The oscillations have the same pattern as before and take much longer to damp than those in the pole fault, but in this case, the ground loop is limited to the left half of the street. This means that the effect of the circulating current is mostly contained to that subsystem. Oscillations are most prominent in positions A, B and C, with the two other positions displaying a very mild response exactly because they are far from the loop. This interpretation is further backed up by the bar chart which shows the small impact on D and E.

Overall, the results from faults in 1 and 2 were fairly comparable. This is, however, not the case with faults on position 3.

In this position, only the voltages from A, B and C are shown since the rest of the system will be discon-

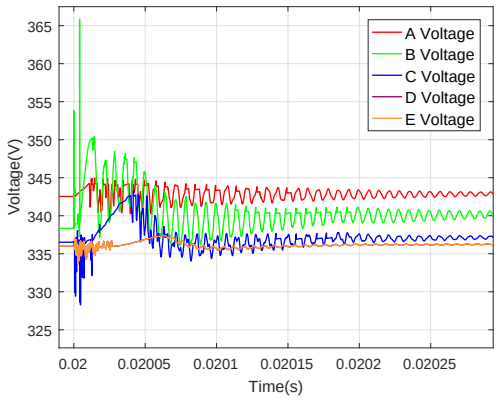

Figure 4.29: Voltage transients after bolted earth fault at B

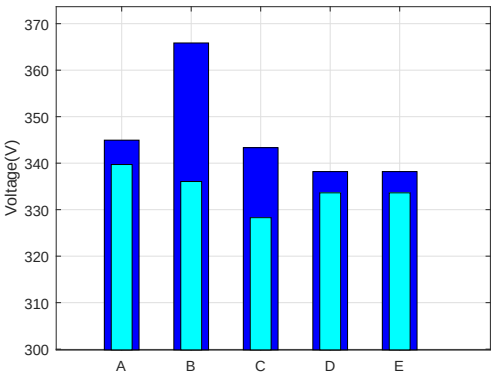

Figure 4.30: Voltage variation (min-max) after bolted earth fault at B

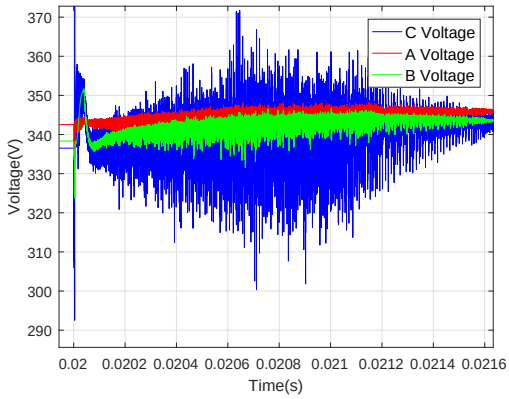

Figure 4.31: Voltage transients after bolted pole fault at C

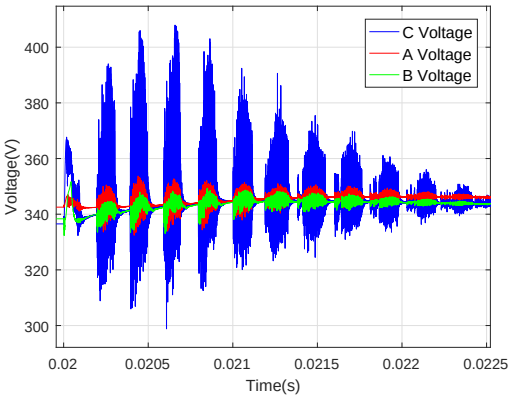

Figure 4.32: Voltage transients after bolted earth fault at C

nected. In the previous fault positions, the bottom pole was kept operational after the pole fault, but the impact here is somewhat more severe, and it would most probably trigger the protection on that side as well. Figure 4.31 shows the results from the bolted earth fault. By far the most extreme reaction is noted in the C voltage. After the initial drop just below 300 V and the inaccurate overvoltage spike which is not included whole in the image, the charging of the clamp capacitor takes place. This time the capacitor will be charged to a higher voltage than that seen before, since the current of the main line is interrupted. After that, severe oscillations occur. Even with the load diodes preventing the load capacitors to discharge, the clamp capacitors from all the loads can still discharge through the fault and the neutral conductor. This has some impact on the healthy side, as some of that current flows through the neutral conductor and seems to impact the voltage in the way seen. It also appears that removing the diodes from the loads would result in much smoother voltages overall, because the current would be allowed to flow and of course very large currents would be observed through the cables and the fault point itself. That is not acceptable, as it can lead to premature aging or even destruction of the components. The case for using the diodes is further supported by the fact that the large oscillations are severely diminished near the loads and the source, where the amplitude seems to be around 10-15 V at most. It is also important to remember that the filtering effect of the cable is not seen here, and we can expect 400 m of cable to smoothen those rough oscillations.

The same holds true for an earth fault at position C. The major difference here is the fact that current can flow through the earth and affect the healthy section more visibly now. This leads to somewhat larger currents on the healthy side, but the takeaway should again be the very diminished effect on the remaining measured loads, with oscillations up to 10-15 V.

4.3.4. RING SYSTEM

The final model that will be tested is the ring shaped system seen in 4.33.

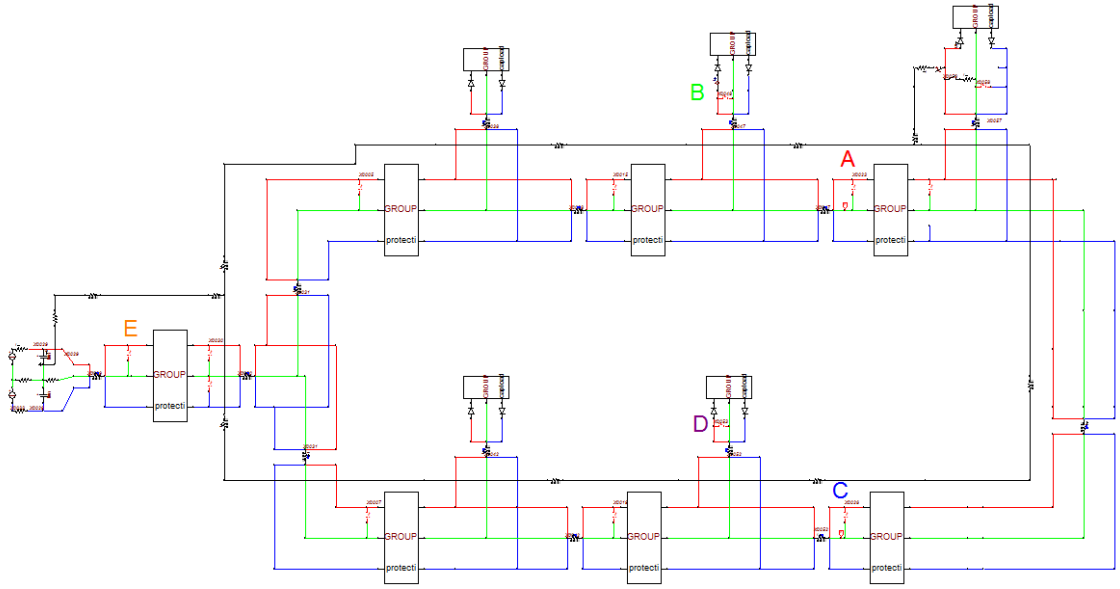

Figure 4.33: Ring model

In this model, the same components from the Road system are used. The DC converter is on the left, and the ring structure is made up of several connections to loads. As can be seen, the protection circuits are now on the line itself instead of close to the loads, so the current is interrupted there. However, the protection is placed in such a way that redundancy is guaranteed; one load alone can be isolated, while the rest can continue operation. The top part of the ring is 600 m long, while the bottom is 600 m long.

The purpose of this system is twofold: First, to show the effect of two opening switches located in different parts of the system on the healthy remaining system. Second, to demonstrate the difference in arrival times of the two pulses close to the source, this time in a more complex scenario. Both pole and earth fault will be simulated at the load close to location A (top right). The measurement positions are indicated by the colored capital letters A-E, just like before.

The voltage results for the (bolted) pole fault are presented in 4.34. Only the top MOSFET at A is switched off. The first thing to notice is the voltage spikes in positions A and B (where the current is interrupted) caused by the large $\frac{di}{dt}$ in the system inductance. After that, the voltage at A is increasing due to the clamp capacitor being charged, while the clamp capacitor at C is discharging. This may seem strange until we realize that the load at D is fed by the top part of the ring. The reason for the different voltage response at C is the fact that the protection circuit is not bidirectional, which means that the clamp cannot function in the intended way if power is reversed. It is also the reason behind the steady voltage drop of C and D, as their voltages will settle at a lower steady state position after the capacitors' slow discharge.

In a similar manner, the voltage at B follows the one at A, with a significantly smaller impact. The curious intermittent voltage oscillations of A at 29 ms appear to be detached from the previous oscillations, but can be explained if we take a look at the currents flowing through the protection circuit in A. Figure 4.37 shows the current through the top MOSFET, the current through the neutral and the current flowing through the top diode (from neutral to positive conductor).

The MOSFET current is of course interrupted immediately. Due to the inclusion of the load diodes, the top diode of the protection circuit is forced to conduct. Meanwhile, the neutral conductor takes over from the positive to provide current to the bottom load. When the current through the diode is depleted, it does not turn off completely, but is instead forced to turn on and off by the voltage oscillations. The diodes used in the model had a deionization time of 100 ns, which is considered to be relatively fast. Slower diodes with a reverse recovery time of 2 µs would most probably not be able to conduct as much in a similar situation.

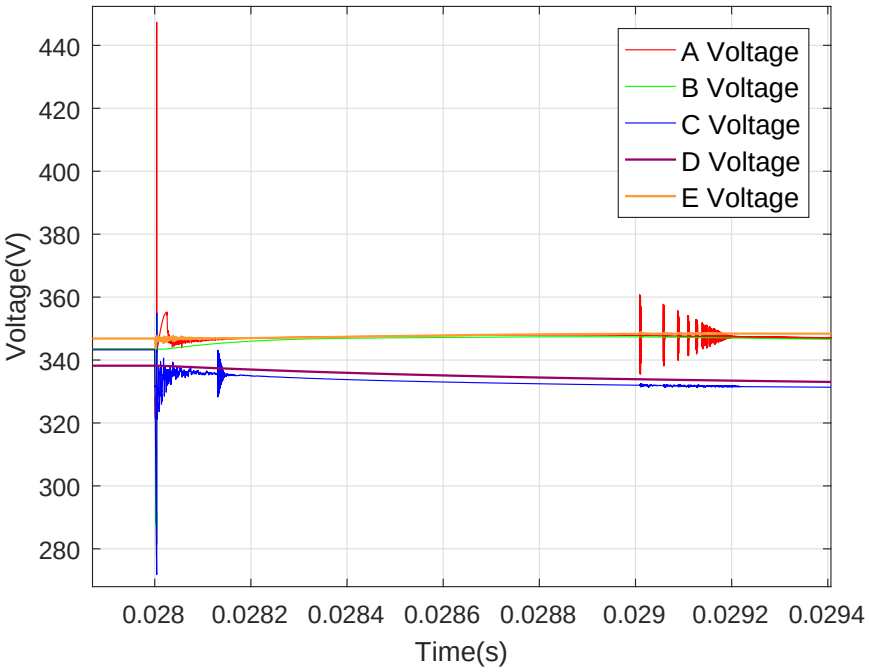

Figure 4.34: Voltages in the system after bolted pole fault at A

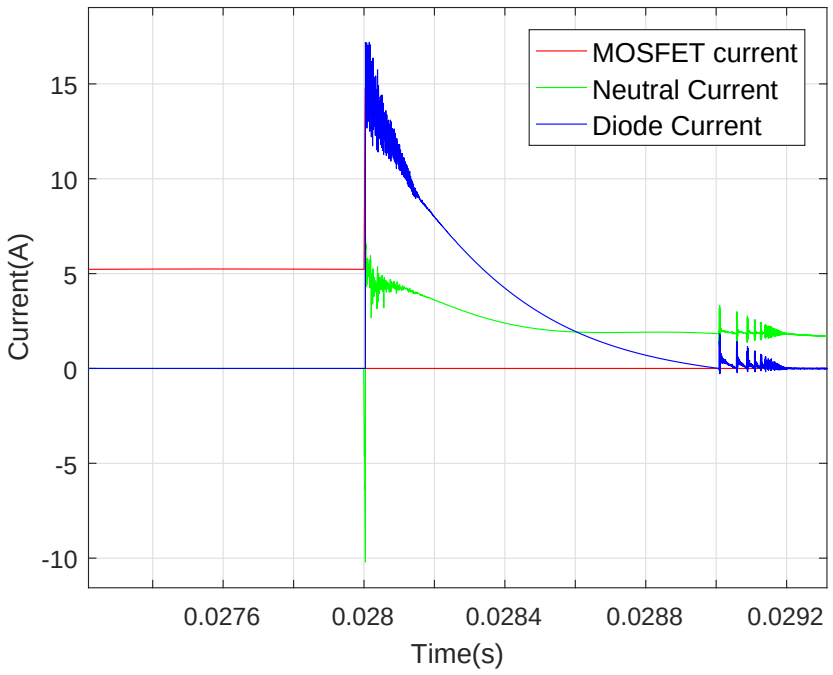

Figure 4.35: Currents in the protection circuit near A after bolted pole fault at A

The focus is as always on the healthy part of the system and it is clear from the plots that the disturbance is minimal.

A similar picture is given by the results of the earth fault at the same position. In this case, both MOSFETS at position A are disconnected.

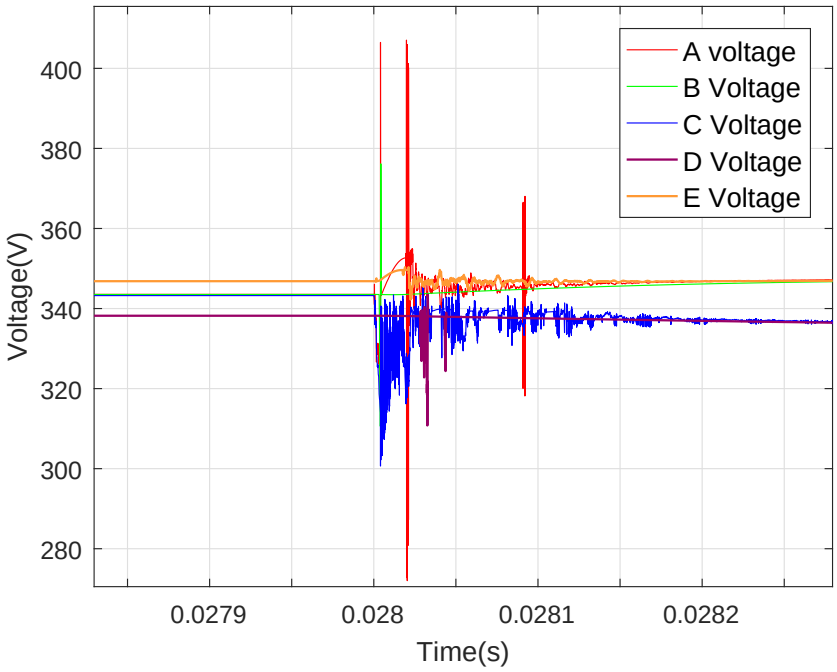

Figure 4.36: Voltages in the system after bolted earth fault at A

The voltages of the five measured positions in Figure 4.36, show that the positions A and C display the again the largest disturbance. Once again, the same ground loop is formed with the neutral conductor. After the MOSFETS switch off, the top diode near the inductor is forward biased and conducts current towards the ground fault(as seen in Figure 4.35). There are many elements that affect the oscillations of the current through this loop, unlike the much cleaner discharge in Figure 4.37. Because of that, the diode current actually drops to zero on two instances, and it is on those instances that we see the two voltage oscillations in A.

The voltage of C and D is again explained by the power flow during steady state; the capacitors are discharging instead of storing energy. The effect on position B and E is comparatively smaller and they are considered safe, but the drop in voltage at the load D at around 310 V could mean that the specific load is affected. The conclusion from that is that a bipolar version of the protection circuit needs to be developed, so that it can handle breaking the current in both directions without adversely affecting nearby loads.

Finally, Figure 4.38 shows the time difference in voltage reactions at two positions closer to the source, right after the pole fault at A.

The time difference, as measured in ATP but also seen here, is approximately 2.5 μs, which, with a cable length difference between the two parts of the ring of 300 m equates to a propagation speed of:

$$u = \frac{\Delta x}{\Delta t} = \frac{300\ m}{2.5 * 10^{-6}\ s} = 1.2 * 10^{8}\ m/s$$

Which is again equal to the speed that was set in the parameters for the cable.

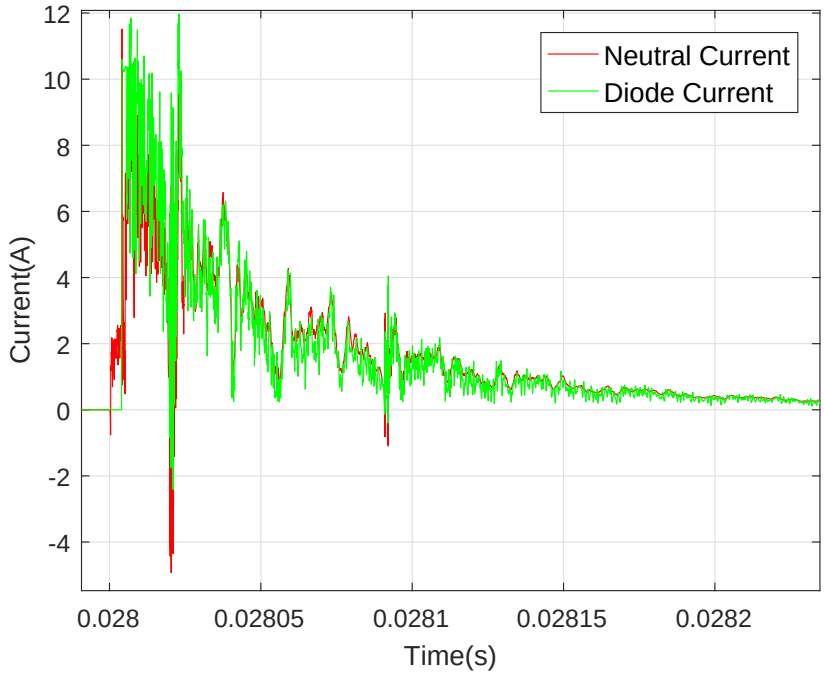

Figure 4.37: Currents in the protection circuit near A after bolted earth fault at A

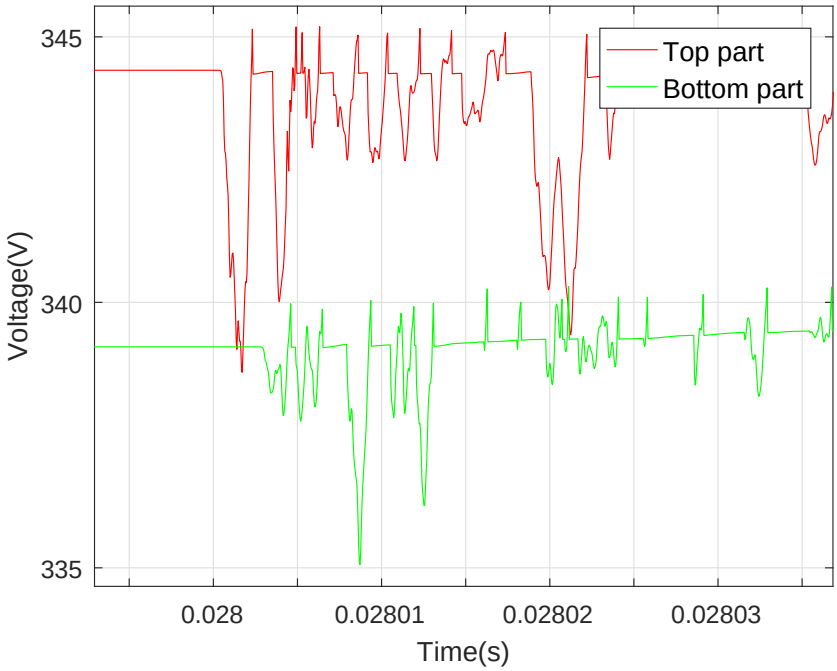

Figure 4.38: Voltages closer to the source after bolted pole fault at A

4.4. CONCLUSION

This chapter is the culmination of the preparations that was discussed in Chapter 3. At first, the propagation experiment results were presented, so that a connection could be made later on with the simulation results. The first model was a simple line system, to explain the behavior of the basic components used (also in con-

tinuation of their analysis in Chapter 3. A somewhat more complex system followed, where the effect of faults at one position on the other loads and at the source were investigated.

Along with the presentation of the results from those two systems, two challenges that arose were also discussed. The first was the formation of the ground loop with the neutral conductor during earth faults and the discharging load capacitor through the fault. The result was very high currents flowing through the whole system in case of a ground fault, while in the pole fault the huge current was limited to the load capacitor. The solution proposed to include diodes in front of the loads proved to significantly diminish the currents. The unfortunate side effect was that additional voltage oscillations were introduced due to those diodes being reverse biased, but the high currents that could damage a large part of the system are avoided. Another solution would be to include a third MOSFET so that the neutral is also disconnected, but that would certainly bring more issues.

The second challenge was the unintentional forward bias of the diode in the protection circuit at steady state in some cases. The result was a permanent current flowing in the disconnected conductor through the fault. The current was not large, and the voltage would probably not pose a danger to humans, but it is still an undesirable side effect. A possible solution would be a double neutral scheme, so the load at the other pole would be fed independently.

Following that, a model of a road with multiple houses was presented, with various faults occurring at multiple locations. The analysis focused more on the effects on the healthy part of the system instead of the details of the oscillating pattern close to the fault. It became clear that faults at the line produce significantly different results compared to those closer to the loads. The same strategy was followed for the last system, a ring structure with multiple loads attached to it. Here the intention was to observe the effect of two protection circuits interrupting the current in order to ensure selectivity. The bidirectional nature of the system, however, caused some of the results to be worse than expected, because the protection circuits are unidirectional. It is therefore imperative to come up with a protective circuit that can operate effectively in such complex configurations.

Finally, the propagation delay in the second and last system were measured to calculate and confirm the speed that was a parameter in the components discussed previously.

5

DC Street Lighting System Measurements

5.1. Introduction

To analyze DC system faults and obtain conclusions for the interaction between the protection and the rest of the system data obtained from a real system is required. Simulations are of course important for research, but any results obtained from models should ideally be compared against measurements from a real system to verify their validity. The reason for that is that simulations are, by their nature, a compromise between model accuracy and limited time and computational resources. Modern engineering software has evolved to include a multitude of options for customizing simulation settings, so one can get a very fast model for a rough idea of a system's characteristics up to a very detailed model that approaches the behavior of the system. However, real measurements are always desired alongside the results from those models. This is especially true for DC systems, as they are uncharted territory in many ways, as discussed in detail in Ch. 2.

For the above reasons, fault measurements from a DC system are a big part of this thesis. There are some small-scale distribution level DC systems in the Netherlands, most of them for efficient street lighting. These measurements were possible through the cooperation between TU Delft, the converter manufacturer Direct Current B.V. and the system owner Luminext B.V. One of those systems were chosen for the measurements.

This chapter is split into two parts; the first one describes the preparation needed for those measurements, while the second one discusses the takeaway from the procedure itself, a few selected measurements and some analysis based on them.

5.2. Measurement Preparations

Before discussing the various preparations for the measurements, it is important to introduce the system and explain its characteristics.

5.2.1. System Introduction

The measured system is one line of lamps over a distance of approximately 800 m, and is a part of the larger street lighting system of De Liede industrial area, close to Haarlem, where more converters and lines are installed. Figure 5.1 shows the whole system with the measured line in orange, with letters S, A, B and C indicating the 4 measuring positions, Source, Lamp A,B and C, respectively. Figure 5.2 indicates the line in question on the map. This specific line was chosen because it contains the minimum amount of branching and thus could be easily approximated by a straight line. This means that the two lamps that form the small branch in the middle of the line can be ignored without significantly altering the results of the research conducted.

As seen in figure 5.3, the source of the DC system comprises two identical AC/DC converters, each gen-

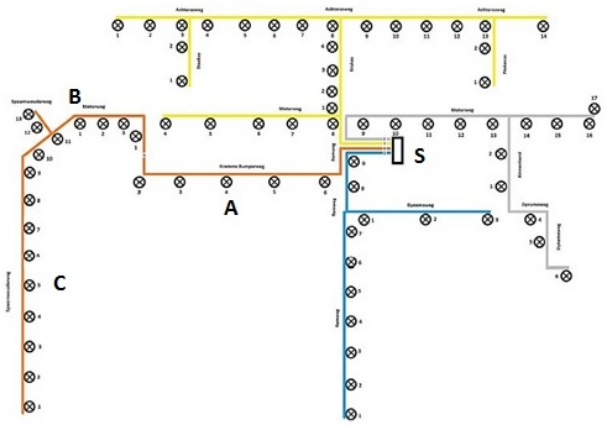

Figure 5.1: Schematic of street lighting installation

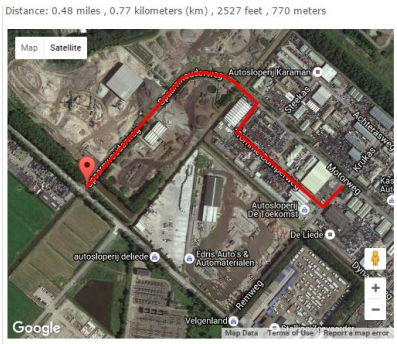

Figure 5.2: Map of De Liede area

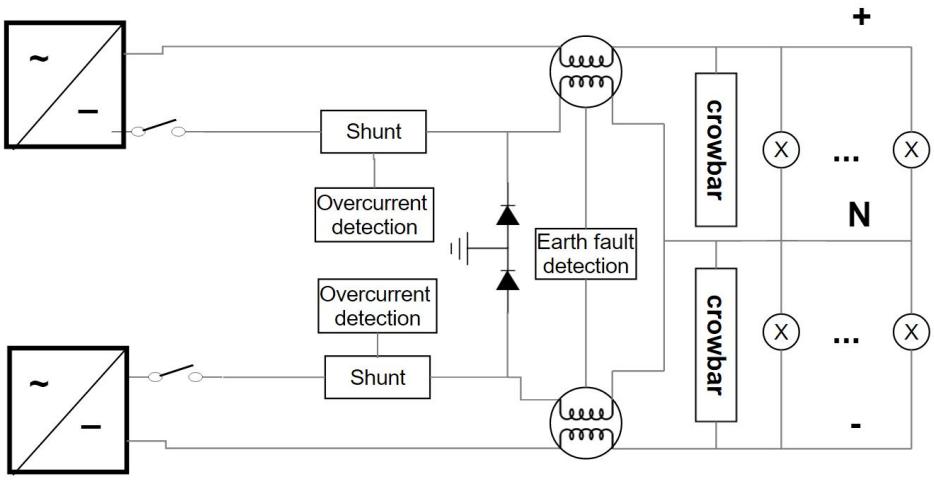

Figure 5.3: Schematic of DC lighting installation

erating 350 V DC from supply distribution voltage (380 V AC). The two converters form a bipolar system of 700 V(+-350 V). What is not shown in the diagram are the bleeders. One of those is in each converter, and is discharging the output capacitor before startup. This is done in order to prevent any risk to system damage when the system restarts after a fault with charged capacitors.

The two middle conductors at the output of the two converters are connected through the two diodes in series with the earthing rod between them. The purpose of the diodes is to prevent any earth leak from flowing to the other half of the system and affect its operation. Essentially, the diodes are supposed to facilitate independent operation of the two poles of the system. Their effectiveness will be discussed later, when discussing the results. The two middle conductors then connect to form the neutral conductor, with a standard bipolar configuration where the neutral will carry zero current in balanced operation. This is obviously a TN earthing configuration, with the load connected to a neutral which is earthed close to the source.

The load of the system are 20 LED lamps of 50W at 350 V connected intermittently on the top and bottom converter. The connection is done with a standard 3-phase AC cable. Each lamp has a PLC unit in parallel, which is used for controlling each lamp individually via communication. These PLC drivers are installed at the base of each lamp structure for ease of access in case of maintenance. Their placement was vital to the measurement process as will be explained later.

As for the protection of the system against faults, both overcurrent and earth leak detection are implemented. Two MOSFETs are used in parallel for each converter. The reason for that is that the current after the fault increases, and despite the fast reaction time of the MOSFET (200 ns), it may still be too large (depending

on the fault) for just one solid state device to interrupt. For the detection of overcurrents a simple shunt is used to measure the current, and if that is larger than 3.5 A a trip signal is sent to the two MOSFETs. For the earth leak detection the two conductors are wrapped around a coil, and if their current difference is above 30 mA the same signal is sent to the protection devices. The limit of 30 mA is chosen as a compromise between the need to have a low limit so the current is not dangerous for people and the need to have a higher limit to avoid oversensitivity.

Finally, the crowbars in parallel with the load are essentially thyristors with a temperature dependent resistance that conduct as soon as the protection interrupts the current flow from the source in case of a detected fault. Their purpose is to quickly discharge the leftover energy stored in the cable and PLC capacitors in order to lower the chances of people getting hurt.

5.2.2. MEASURED VARIABLES

At first, we need to identify what should be measured. Ideally, we would like to measure the voltages and currents of the system at several points along the line in response to different earth faults and short circuits. In the end, it was decided to have 4 measurement positions, one at the source and 3 along the line. The fault location will be moving along the measurement points. Table 5.1 illustrates the measurements in the different positions and for the different fault locations:

Table 5.1: Planned measurements

	Source Faults			
	Source	**Lamp A**	**Lamp B**	**Lamp C**
Channel 1	+ voltage to G	+ voltage to G	+ voltage to G	+ voltage to G
Channel 2	N voltage to G	N voltage to G	N voltage to G	N voltage to G
Channel 3	Fault current	+ pole current	+ pole current	+ pole current
Channel 4	+ pole current	- voltage to G	- voltage to G	- voltage to G
	Lamp A Faults			
	Source	**Lamp A**	**Lamp B**	**Lamp C**
Channel 1	+ voltage to G	+ voltage to G	+ voltage to G	+ voltage to G
Channel 2	N voltage to G	N voltage to G	N voltage to G	N voltage to G
Channel 3	+ pole current	Fault current	+ pole current	+ pole current
Channel 4	- voltage to G	+ pole current	- voltage to G	- voltage to G
	Lamp B Faults			
	Source	**Lamp A**	**Lamp B**	**Lamp C**
Channel 1	+ voltage to G	+ voltage to G	+ voltage to G	+ voltage to G
Channel 2	N voltage to G	N voltage to G	N voltage to G	N voltage to G
Channel 3	+ pole current	+ pole current	Fault current	+ pole current
Channel 4	- voltage to G	- voltage to G	+ pole current	- voltage to G
	Lamp C Faults			
	Source	**Lamp A**	**Lamp B**	**Lamp C**
Channel 1	+ voltage to G	+ voltage to G	+ voltage to G	+ voltage to G
Channel 2	N voltage to G	N voltage to G	N voltage to G	N voltage to G
Channel 3	+ pole current	+ pole current	+ pole current	Fault current
Channel 4	- voltage to G	- voltage to G	- voltage to G	+ pole current

The positive and neutral voltage (potential) to ground should be measured at every position. The fault position measures the fault and positive pole current, while in the other positions the positive pole current and negative to ground voltage are measured. As will be explained in section 5.3, not all of the above measurements were possible for various reasons.

5.2.3. FAULTS

After deciding what is going to be measured at which position, the next step was to determine the kinds of fault that would be performed on the system while its transient response is measured. Naturally, both earth

faults and short circuits should be investigated, but the effect of the fault impedance would also have to be taken into account. After taking into account the time limitations, it was decided that the following faults would be tested:

Table 5.2: Faults summary

		Fault Type	
		Short Circuit	Earth Fault
Fault R(Ω)	0	✓	✓
	100	✓	✓
	1k		✓

The reason for which the short circuit is not tested for the 1 kΩ fault resistance is that the resulting fault current (~0.35 A) would not be high enough for the overcurrent detection to trigger the protection and interrupt the current. This would result in a constant power flow of $350 * 0.35 = 122.5$ W through the fault generator circuit (shown in the Appendix A). As it would be impossible to use resistors that can take this amount of power in a small circuit, it was decided that the short circuit would only be tested for 0 and 100 Ω .

Another important point is that each measurement needs to be verified with a repeat. However, it would be impossible to decide which one between two different measurements of the same thing is the 'correct' one, which means that 3 runs for each measurement are needed. With tables 5.1, 5.2 in mind, this translates to 5(faults)∗3(repetitions)∗4(fault locations)= 60 measurements in total.

More detailed information regarding the preparation for the measurements as well as the hardware for them, can be found in section A of the appendix.

5.3. MEASUREMENT RESULTS

5.3.1. SETBACKS

During the preparations for these measurements, great emphasis was put on two main goals. First, to complete the desired task while making sure that the safety of everyone who would be involved was guaranteed. Second, to make a thorough plan detailing the procedure step by step, so that any unforeseen obstacles could be solved beforehand. Despite that, some events prevented us from taking the full range of measurements that was planned.

Specifically, time was more limited than anticipated, mostly due to the longer travel time during rush hour and the extra time it took to set up all the measuring equipment and explain to the responsible technician from Luminext what needed to be done. What's more, there was a small accident as soon as the measurements started. After the first test, the technician (who was performing the faults) did not clear the fault on the fault generator circuit before turning on the converter. As a result, the source started charging the system with a fault of 100 Ω present. Because the output capacitors were not fully charged, the current was low enough to not trip the protection, but high enough to melt the fault resistor (rated at 7 W) after a few seconds. The result was that the measurements would have to be done with just the 1 kΩ and the 0 Ω faults.

There were also some problems with capturing the desired results. Some flash drives were not saving correctly, and the scope connected at the source, while seemingly working, did not capture what was needed during most of the measurements. It was also not possible to measure currents at the three non-fault measurement points due to physical constraints. Finally, there are the errors of the people who were handling the measuring equipment to consider. Nevertheless, a great amount of data was collected, which can be very useful in shedding some light into the transient behavior of DC systems.

5.3.2. SELECTION OF RESULTS

From the great amount of data that was collected, some of them are chosen and presented here.

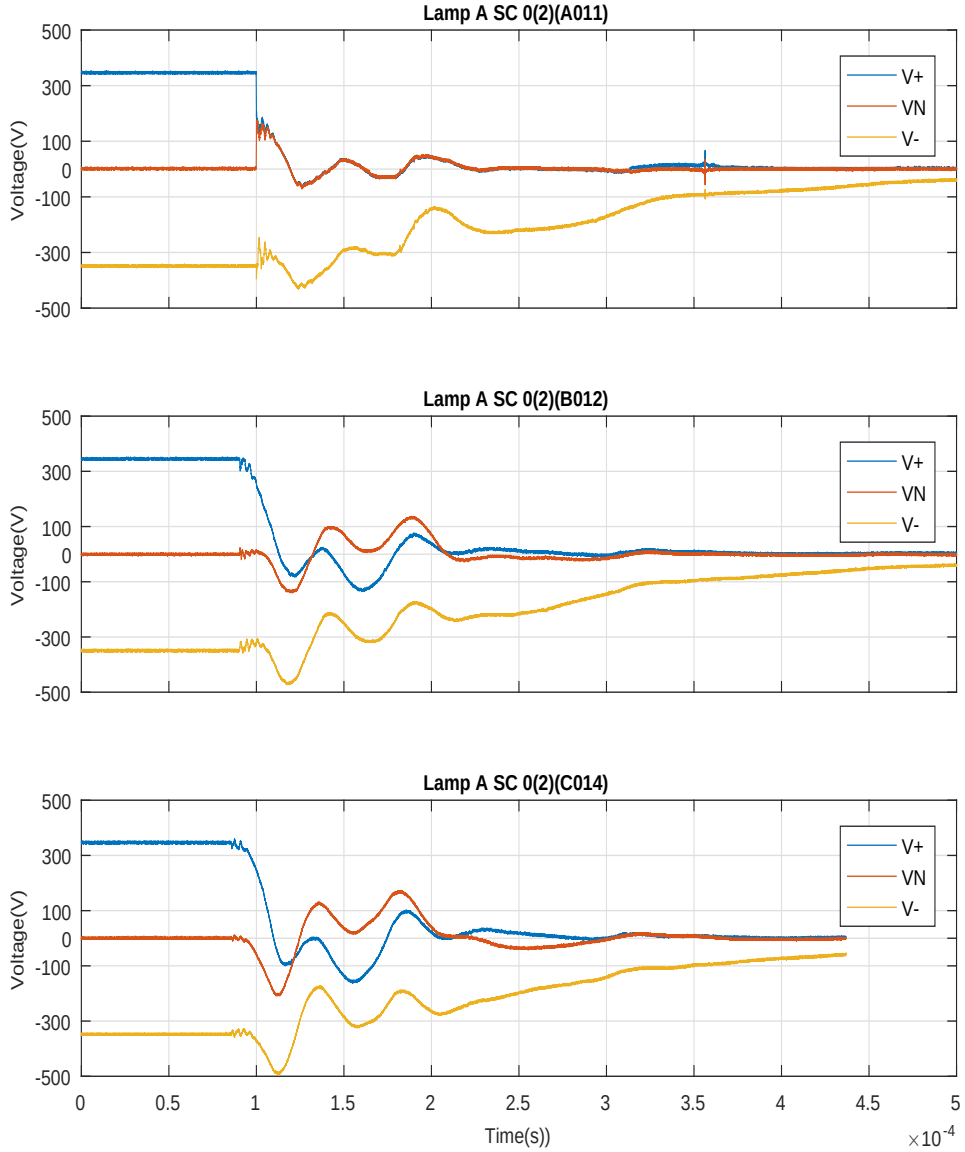

Figure 5.4: Voltages at lamps A, B and C during bolted short at lamp A

The plots in 5.4 show the voltages on the positive, neutral and negative conductors during a bolted fault between the positive and the neutral conductors at Lamp A (the third lamp along the line).

The type and location of the fault can be easily identified. In the first plot, which shows the voltages at Lamp A, the positive and neutral potentials are forced to be equal, therefore a bolted short between those two conductors occurs.

Another interesting point on the first subplot is the small bump in the positive voltage, even after it seems to have settled to zero. This is due to the imperfect operation of the mechanical switch of the fault generator. When that switch makes the fault connection, bouncing occurs across its contacts, as an arcing phenomenon takes place. This same bump was also observed during lab tests of the switches, and it can take u p to 1 ms after the initial connection for the arcing to cease. This bouncing is not thought to affect the measured voltage in a way that distorts the results significantly, because the highest voltage that was observed due to bouncing was less than 10% of the system voltage.

Other characteristics to comment on are the similar shapes of the measured voltages in the other two positions (Lamps B and C) compared to those in A, and the fact that the bottom pole is severely affected and trips, despite the design at the source to prevent that. A rather surprising observation that was not expected is the temporary reversal of the voltage between the positive and neutral conductors, exceeding even 100 V at Lamp C, further from the fault. This reversal, temporary as it may be, could have unforeseen repercussions on components that were not designed to withstand a voltage reversal across them, especially after several faults and more exposure to this reverted voltage.

Finally, the negative increase of the bottom pole voltage drops could also be potentially dangerous, reaching almost 500 V temporarily.

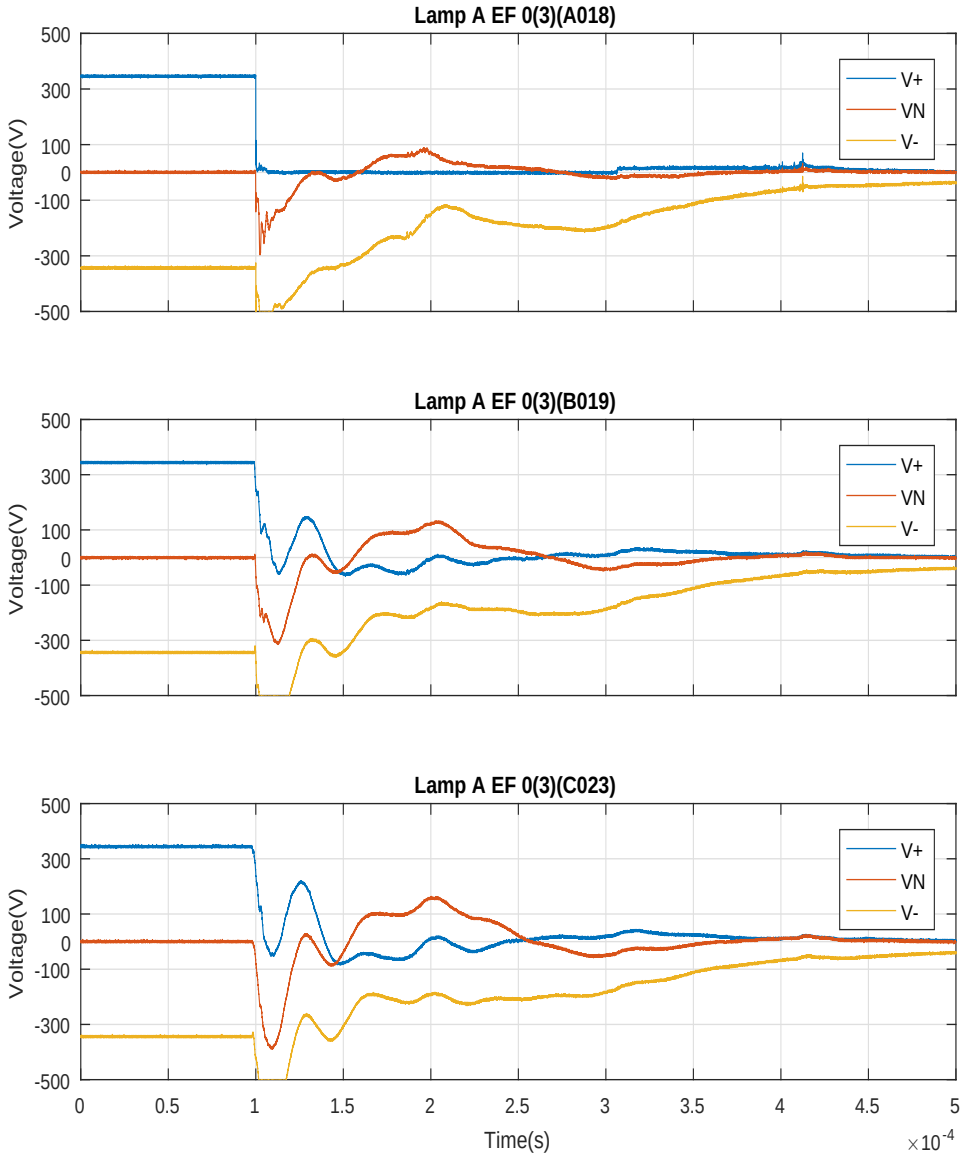

Figure 5.5: Voltages at lamps A,B and C during bolted earth fault at lamp A

Figure 5.5 shows a bolted earth fault at Lamp A. In contrast to the previous example, the voltages at the faulted lamp behave quite differently. Because this is an earth fault, the positive pole is abruptly brought to the zero potential of the ground. Because of the charged capacitance of the system, the potential difference

(voltage) between the conductors cannot change instantaneously, which explains the downward surge of all the voltages in the figure. This is in contrast with the conductor-to-conductor short.

As before, the voltage reversal between positive and neutral conductors appears here, too. What is more worrying, however, is the surge of the negative conductor to even higher (negative) voltages, due to the capacitance effect explained above. Unfortunately, the scope could not capture the full waveform, but based on the voltage of the neutral, we can safely say that a voltage of at least -700 V is attained. The duration of this spike is approximately 100 µs and under certain circumstances could be very harmful to the insulation the conductor, especially after several low impedance earth faults have occurred. The specific cable used here is designed for an operating (phase) voltage up to 600 V, so exposure to multiple earth faults through the years could negatively impact the insulation and therefore the safety of the system. It is furthermore very important to be aware of the system's transient behavior in such extreme circumstances before choosing equipment.

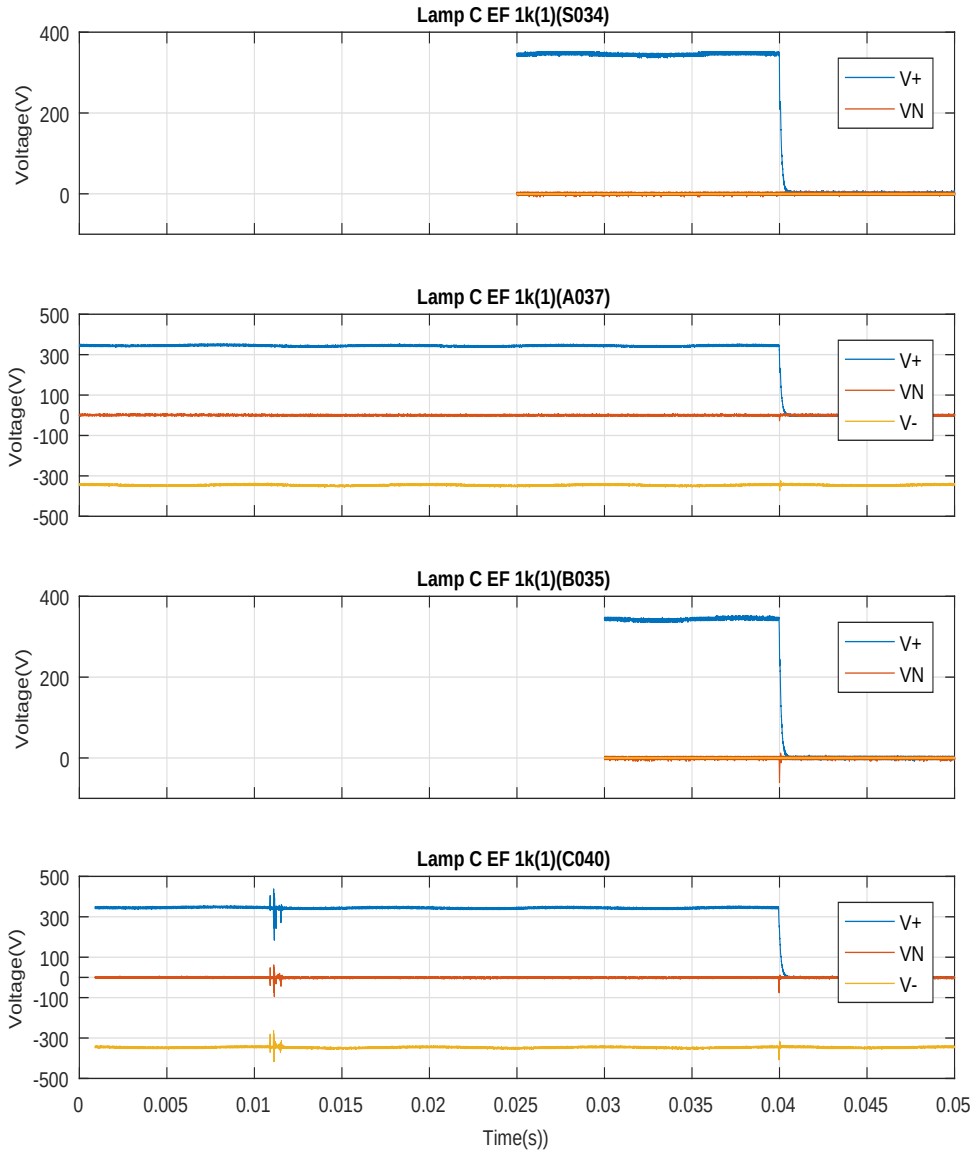

Figure 5.6: Voltages at lamps A,B and C during 1 kΩ earth fault at lamp C

An earth fault of 1 kΩ at lamp C is shown in Figure 5.6. Note that the data has been shifted so that all the

subplots are vertically aligned. The missing part for lamps A and B is because the respective scopes were set to capture a different portion of the voltage around the trigger point.

The fault occurs close to the 0.01 mark as evidenced by the minor disturbance in the last subplot, but the system continues its operation for almost 30 ms more before interrupting. This is most probably due to the very low fault current. There is a delay in the control system after a fault is detected. Since the current is much lower, this delay is larger, and because the fault is not cleared the system eventually trips.

What is also noteworthy is the fact that the negative pole does not trip, as it is apparently not affected enough by the small fault current. It is very possible that there is again some current circulating to the bottom pole, but the high impedance fault makes it small enough so that neither the overcurrent nor the earth leak protection of that side is tripped.

If the results are plotted in a different way, we can discuss even more details. If every subplot contains the voltages from each conductor, it is possible to see the difference in reaction time with regards to the distance of each measurement position to the origin of the fault.

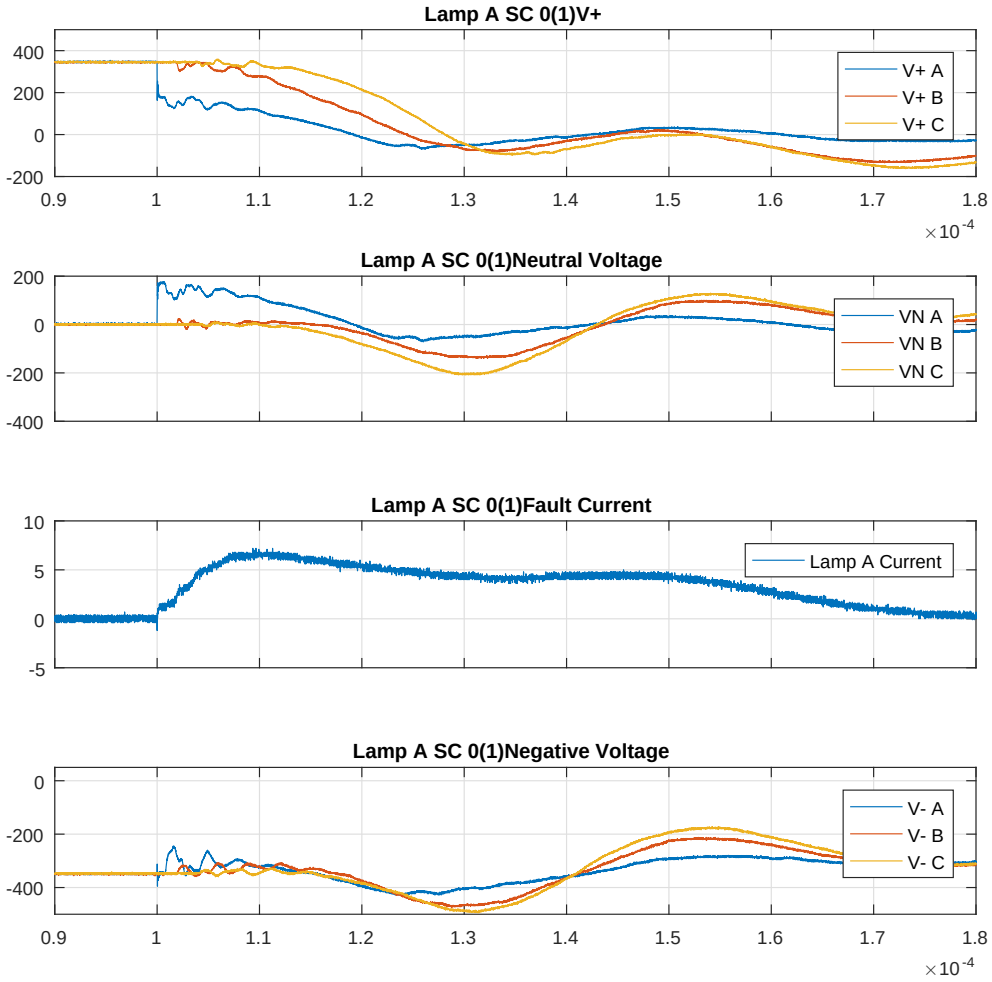

Figure 5.7: Voltages per conductor for bolted short at Lamp A

For example, in Figure 5.7 it is very clear that the voltages react to the fault at a different time. That happens because the distance between the points is long enough to make the time it takes for the voltage wave to travel between them noticeable. From lamp A to lamp B, that would be around 2 µs and from lamp B to lamp C it

is bit more than that. By taking an average length of 40 meters between each lamp the propagation speed can be estimated, which in this case would be approximately $1.2 * 10^8$ m/s or 0.12 m/ns. This is lower than the $1.2 * 10^8$ m/s speed from the lab experiment, but we should keep in mind that the speed depends on the permittivity of the surrounding medium. Because the lab cable was rated lower and therefore had insulation with lower permittivity (PVC instead of XLPE for big power cables) , it makes sense that a wave would travel much faster along it.

What is also important to investigate is the behavior of the voltages after the fault occurs, until they stabilize.

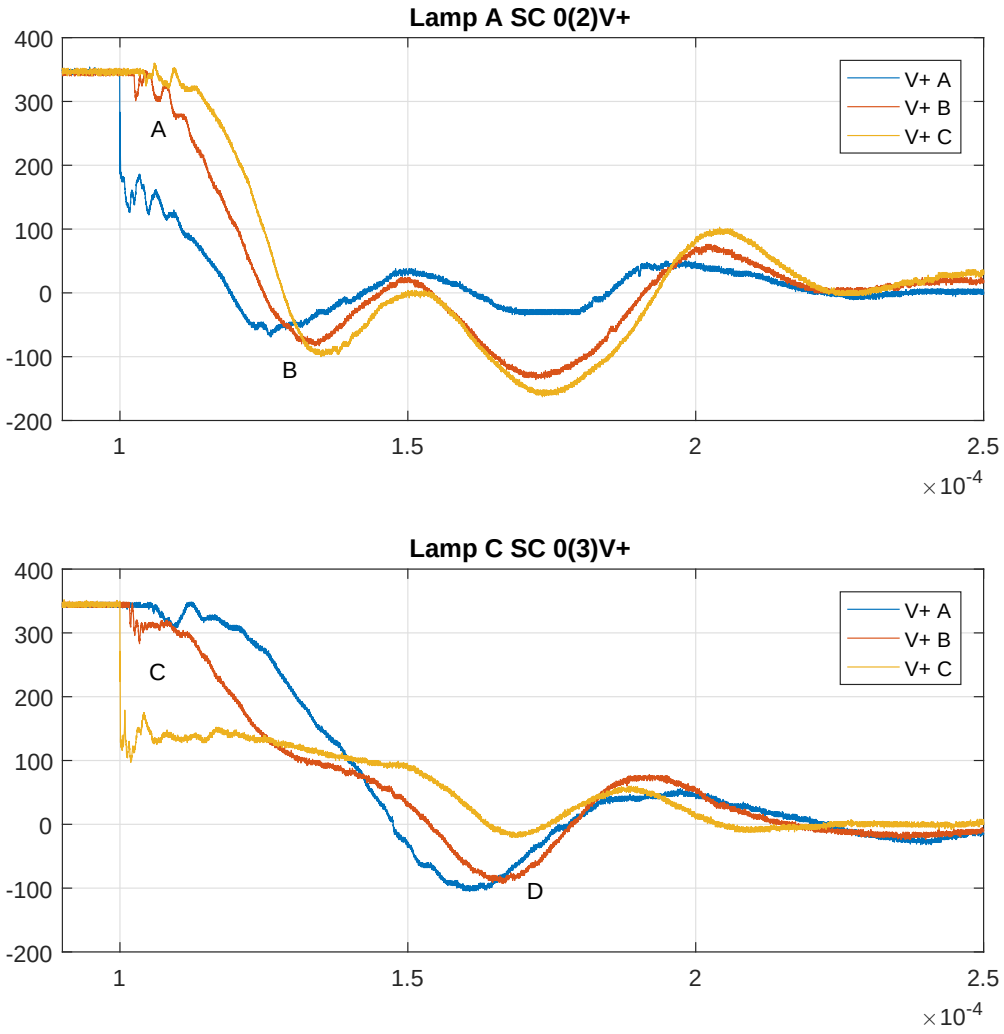

Figure 5.8: + Voltage comparison between two faults

In the first subplot of Figure 5.8 (point A) the voltages react to the fault as explained before: The voltage at Lamp A is dropping immediately, while the rest have a delay depending on their distance from the fault point. After that, at some point the crowbar is activated. Unfortunately, due to the scope at the source not capturing correctly, we do not have a clear picture of the crowbar's behavior and its exact contribution to the response of the system. What is known is that, once the crowbar closes, a path is formed for current to flow. The resulting RLC circuit is causing the voltages to oscillate at a specific frequency, which is determined by the cable inductance and capacitance and the PLC capacitors. At point B, we can see that voltage A leads, and the others follow, which is to be expected.

This is not the case in the second subplot, where the voltage at the faulted lamp C does lead at first (point C), but once the decaying oscillations begin, the order is switched (D), and A is leading again. The reason for that is that the crowbar is closest to lamp A, so naturally voltage A will react first to the closing of the crowbar, even though the fault is elsewhere. We can therefore conclude that the position closest to the crowbar will always oscillate first, with the others following, depending on their distance.

5.4. SYSTEM SIMULATION

After the measurements were completed, an attempt was made to build a model that is a replica of the system that was measured.

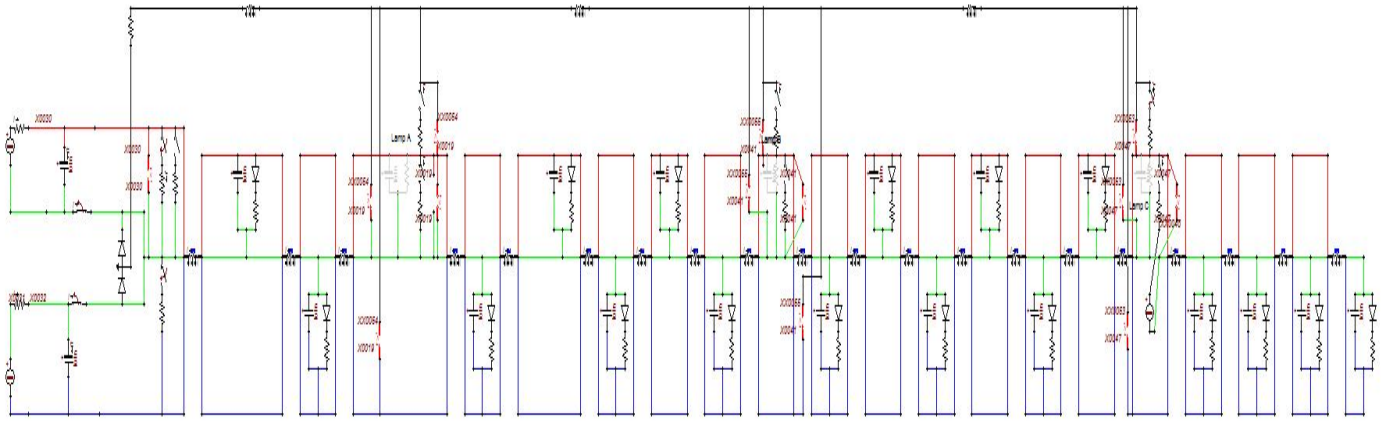

Figure 5.9: Model of the street lighting system

The model in Figure 5.9 includes the lamps as resistors with parallel capacitance for the PLC. They are interleaved, but the last part of the line contains only lamps connected to the negative pole, as in the real system. The fault positions are at the 3rd lamp (A), the 9th (B) and the 16th (C). The extra conductor on top of the system is protective earth. The source is constructed in the same way as in 5.3 and the crowbars as well. The cable utilized is the same as in the simulations for Chapter 4.

What was not implemented was the overcurrent and earth leak detection parts, because of the difficulty of ATP regarding initialization. Since simulation always starts at time 0 and pre-initialization is not possible, the initial inrush current that charges the system also triggers the protection, since it is larger than the steady state current, even when using initialized capacitors. For this reason, the protection switch and crowbar are tripped manually with a timed switch, a few microseconds after the fault.

Below, the measurements and simulation results are compared in two fault cases. An earth fault at lamp C is the first comparison in Figure 5.10.

The two plots are quite similar. It is clear that both illustrate a low impedance earth fault based on the drop of the voltages. Comparing the neutral and negative voltages, we see that in both cases the neutral reaches -350 V before the oscillations. The overall shape and discharge time of the voltages are also similar.

On first sight, two differences can be immediately spotted. The first one is the chopped negative surge in the measurements which is actually simulated in the model, and seems to reach -700 V as discussed before in the presentation of the measurements' results. The second one is the bouncing seen in the otherwise zero voltage of the plus conductor after the fault. This of course cannot be seen in the model equivalent.

Two other differences between model and reality are the frequency and damping of the oscillations.

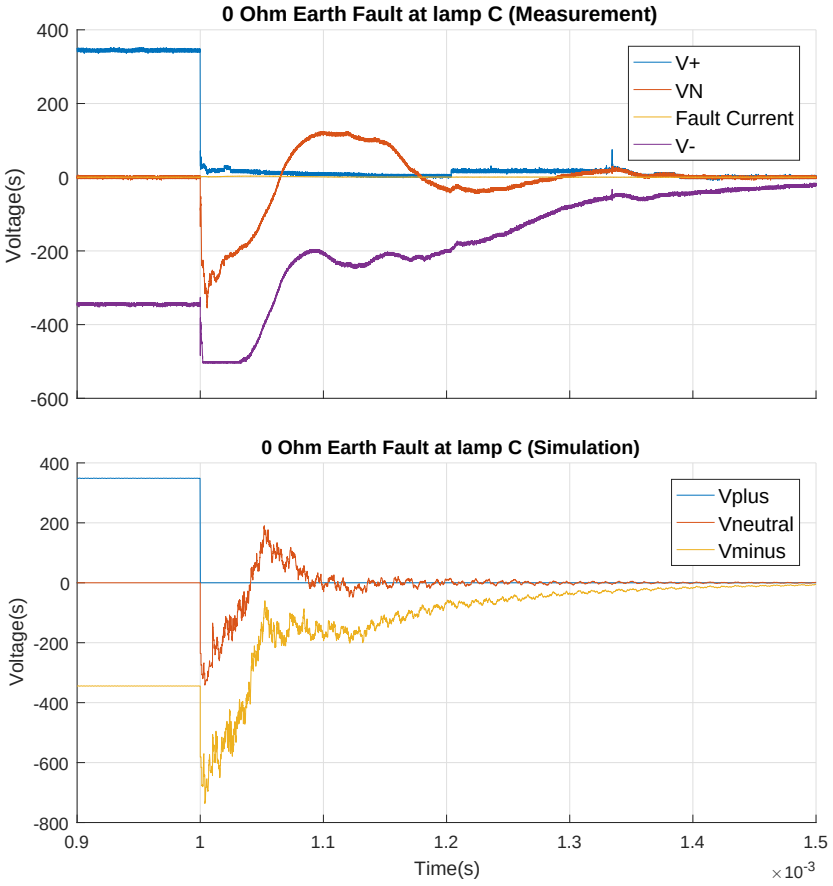

Figure 5.10: Comparison between simulation and measurements for bolted earth fault at lamp C

The oscillations in the simulation seem to be damped faster than those in the measurement. This is mostly affected by the way the crowbar is modeled. In this specific model, the crowbar was modeled by a switch and a resistor, with a low value at first (below 1 Ohm). This low resistance gave unrealistic results compared to the measurements, however, as the oscillations were more severe in both poles. With subsequent simulations, it was found that a higher crowbar resistance (around 10 Ohms) would produce the results seen in the above figure, which are certainly closer.

As for the frequency, it is clear that the measurement signals oscillate somewhat slower. This can be attributed to the differences in the rest of the RLC discharge circuit, namely the cable capacitance and inductance. As seen in Chapter 3, some assumptions were made in order to calculate the information needed for the cable model, due to lack of enough data from the manufacturer. It is therefore very possible that the resulting values differ from the actual ones, which would result in a different frequency during the RLC discharge.

Another difference that can be easily explained is the depiction of the very high-frequency transients in the model but not in the measurements. These high frequency components are a result of the reflections between the lamps. This can be proven by measuring the time difference between two peaks and calculating for the distance.

In Figure 5.11 the time difference is shown to be $0.6\mu s$. A pulse will cover the 40 meters to the next lamp, partially reflect and travel another 40 meters until it returns. Then the speed will be:

$$u = \frac{d}{t} = \frac{2 * 40}{6 * 10^{-7}} = 1.33 * 10^{8} \text{m/s}$$

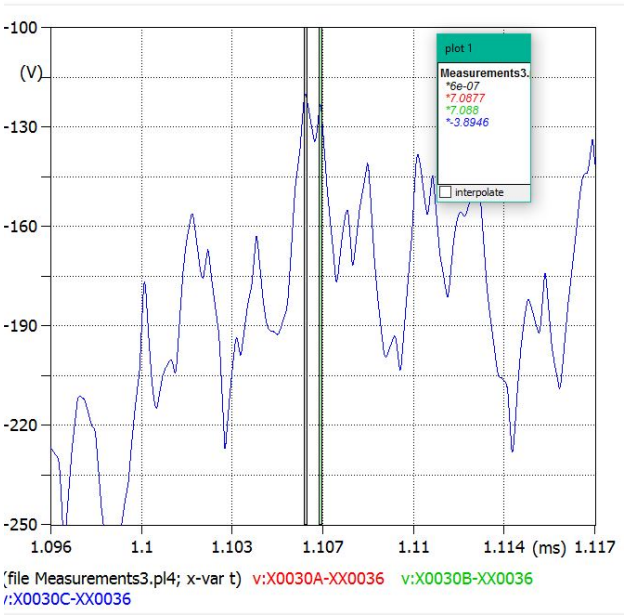

Figure 5.11: High frequency transients as a result of reflections

, which is very close to the $1.27 * 10^8$ speed that was set for the cable component in Chapter 3.

In any case, those pulses travel along the line and get reflected at every lamp, contributing to what we see in the second subplot of Figure 5.10. The reason we do not see a similar effect is possibly because the real cable tends to filter out the very fast transients due to its frequency dependent response. The cable model that was used does not contain frequency dependent elements.

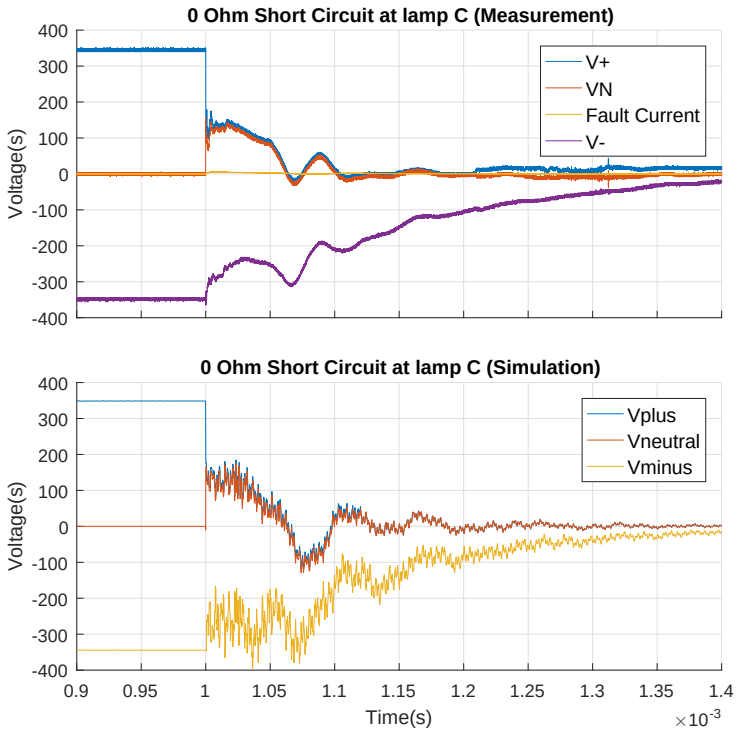

Figure 5.12: Comparison between simulation and measurements for bolted short at lamp C

The second comparison can be seen in Fig. 5.10. We observe the same differences as before, with the unfiltered high frequencies being the most prominent one. The mean of the lines in the simulation, however, more or less closely follows the measurements, with the exception of the dip of the positive (neutral) voltage to -100V.

5.5. CONCLUSION

The overall result of the measurements project is very positive. It was possible to complete most of the measurements that were planned on site and a great amount of data was gathered. The measured quantities were collected, sorted and plotted in different ways. Depending on the manner they were plotted, different ways of interpreting the results were possible. The presentation of the results in different ways was essential for understanding the transient response of the system. The comparison between the model and the measurements showed that the model was approaching the measurements, but also gave some indications regarding the differences and what could be done to further improve the model. The picture would be certainly much clearer if all the data was available so the behavior of the source and the crowbar could also be analyzed. It has nevertheless been a lesson for possible future measurements, where previous experience will prove invaluable in obtaining even more information.

Since we now know what can and cannot be measured on that system, planning for a new set of measurements should prove easier. Any future repeats should focus on retrieving more measurements regarding the behavior of the converter and its assorted components (crowbar, diodes). It would also be interesting to investigate the behavior of the system after faults with the 100 Ohm resistor. Furthermore, previous knowledge of what might go wrong in this endeavor will definitely assist in measuring in the most time efficient manner. This will in turn ensure retrieval of maximum data in the limited amount of time that is available.

6

CONCLUSION

This chapter summarizes all the conclusions from the work done in chapters 4 and 5. Some recommendations for future work is also included in the second part of the chapter.

6.1. ANSWERS TO RESEARCH QUESTIONS

Each answer already given within Chapters 4 and 5 will also be included here, corresponding to the relevant research questions. The answers to the questions will mostly be referring to the results obtained from testing networks with the protection circuit explained in paragraph 3.2.1. The questions and their respective answers are grouped according to their relevance, just like in Section 1.5.

1. *What are the fault after effects and how can they be handled?*

   (a) What happens to the system variables right after a short circuit occurs?

   (b) What is the cause of the over-voltages and under-voltages that appear after the fault and after tripping?

   (c) How can we limit the transients caused by the interruption of the fault current to minimize the negative impact on the system?

   (d) What happens if the protection is not operating as intended and trips when there is no fault or does not trip when there is one?

   Strictly speaking, only the reaction of these variables after the fault *and* the current interruption was investigated. This is because it is assumed that faults will always be detected and interrupted by the protection system. In the vast majority of cases an uncleared fault will result in the destruction of some component of the DC distribution system, so the focus is on what happens when everything happens as intended.

   The system variables of interest after current interruption in various fault conditions are shown in 4.3 for a simple system. The abrupt interruption of the fault current leads to the overvoltage, which is the reason the protection circuit includes the clamp. Further simulations in other, more complicated systems showed a similar overvoltage at a position close to the tripping switch. It is clear that such an effect cannot be completely avoided, but designing the protection circuit in a way that absorbs the transient lessens the impact of that overvoltage even at the point of interruption, while the effect is even less noticeable in positions further from the fault point.

   Due to the capacitive nature of the DC loads, a potential fault close to the loads would make its capacitors rapidly discharge through the fault. in the pole fault case, this current would just go through the relatively small, isolated path between the capacitor and the nearby fault, but in the case of the earth fault, the loop included the healthy part of the system, making this unforeseen effect even more alarming. This discharge current would be extremely high, directly linked to the

proximity of the fault to the capacitor and would undoubtedly cause damage to the loads if left to flow. For this reason, diodes were inserted in front of the load capacitors, so they would not be able to discharge into the fault. The result, as seen in 4.3.2, is that the capacitors cannot discharge and the current through the fault is significantly smaller, but some small side effects appear, such as the additional voltage oscillations close to the fault. In any case, the dangerous currents from the load capacitors are avoided. For faults that occur close to nodes or buses, however, it is possible for this phenomenon to occur despite the included load diodes. The clamp capacitors further down the line can also discharge backwards into the fault through the clamp resistors, which means that they should be rated low enough to avoid large discharge currents.

Regarding question 4, there are two separate questions here. As stated before, it is clear that a fault current that is not interrupted will damage one or more parts of the DC distribution grid. Therefore, only the first part of the question was investigated, which is the unwanted interruption at a specific part of the system when no fault has occurred. This could be caused by a number of reasons, such as a change in steady state that creates a reaction which could be considered as a fault by the control system, a fault in the control system itself, or even a malfunctioning MOSFET switch. Whatever the reason, this particular situation was investigated in the simple system introduced in Section 4.3. The voltages close to the tripping MOSFET switches were measured, with and without a fault occurrence, and the results were shown in 4.10. The sudden drop in voltage was only seen in the case where a fault takes place, and in the other case the voltage remains in steady state before the switch turns off. The transient overvoltage observed in the non-faulted case was slightly lower than the other one, which is attributed to the fact that the former voltage occurs when the steady state current is interrupted, while the second results from the interruption of a fault current which started increasing in the few μs between fault and interruption. This current difference charged the clamp capacitor a bit more and caused the difference in the transient response seen in that figure. In that particular instance, the voltage difference was merely a few volts, but the difference could vary, for example in case of a slower MOSFET response, or an earth fault, where the circulating current through the ground would charge the clamp capacitor significantly more than the non- faulted case.

2. *Do the after effects change in more complex, large, bipolar systems, and how fast do transients travel across those large systems?*

   (a) How does the above change with the implementation of a bipolar LVDC microgrid? Which additional parameters should be considered in this case?

   (b) How fast does the fault (or any signal for that matter) propagate through the system?

   The implementation of a bipolar system in place of the simpler unipolar one introduces some difficulties regarding the operation of the system. At first, the changes in voltage and current rate of change during every fault should be closely monitored at the other pole, to make sure that it can keep operating.

   One of the issues that were discovered while working on the simulations came from the fact that, after a pole fault, the neutral conductor would start carrying current to feed the load of the intact pole. As documented in Section 4.3 and specifically figure 4.21, this current caused a small voltage drop along the neutral which would not exist in steady state and caused the load side diode of the protection circuit to be forward biased and carry current from the neutral to the faulted conductor. The current would then return to the neutral conductor through the fault and feed the intact pole's load. For the voltage drop of the neutral to be big enough to make the diode conduct, the fault must be far enough from the protection circuit. The exact distance would be a factor of the steady state current, the specific forward voltage bias of the diode and the cable parameters. Although this phenomenon may not present an actual danger as the voltage at the disconnected pole would be very low, it is still important to keep in mind that, in some cases, it is entirely possible for current to flow through the disconnected pole.

   Another issue was encountered in the first simple system in Subsection 4.3.1. Some very large currents were circulating in the whole system after an earth fault (seen in figure 4.6), before the load diodes were implemented. Part of this large current would flow through the healthy pole source capacitor, which could very easily disrupt that pole's operation or even cause damage. The

inability to stop these currents even when both poles were switched off led to the diode solution explained before.

In general, the bipolar system in its current configuration is very vulnerable to bolted faults. Depending on their location and type (pole or earth), it is likely that the measured quantities of $\frac{di}{dt}$ and voltage will be out of bounds and the healthy pole will not resume operation. In the case of the earth fault it is common practice to disconnect both poles in order to ensure there are no safety concerns, but the impact can still be severe during a pole fault. To facilitate the operation of the healthy pole in such scenarios, it would be beneficial to design a split neutral system, where the neutral would split at certain positions to ensure that the effect of a fault on one pole to another is minimal.

As for the travel speed of pulses in the cable, it was expected to be a fraction of the speed of light. The lab experiment that was carried out to get a feel for the travel speed indicated (4.2) that it can be expected to be around 66% of the speed of light, namely $2 * 10^8$ m/s. The result agrees with the relevant documentation[31], where a pulse showed a 0.5 ms delay along 100 km of cable.

However, during the calculations for the specific cable used for the street lighting DC system, a speed of $1.3 * 10^8$ m/s was calculated. For this reason, all the cable parameters used the latter speed even though it deviated from the one in the experiment, because a different cable will not produce the same propagation speed, as explained in Subsection 3.2.2.

3. *Does the comparison with real measurements validate the constructed models?*

   (a) How do the simulation results compare to measurements from an actual DC system, such as the street lighting system constructed by the company Direct Current BV?

   In order to make a direct comparison between the measurements from the DC street lighting system and the simulation, a model was built to resemble the system. While trying to build the model as accurately as possible, the results did not seem to resemble the simulations. It seemed that the simulation transient was damped much faster than the one in the measurements, which indicated that the crowbar had a higher resistance than what was first considered, and a value of 10 Ohms produced the results seen in 5.4. The simulation results seem to be much closer to what was measured with this adjustment, and the differences that are seen are down to higher frequencies being filtered by the real cable and the assumptions and simplifications that were made when calculating the cable components in 3.2.2. Differences could also result from the fact that the switches in the model were not controlled but were switched on and off manually.

   As for the measurements themselves, they have provided insight on how an actual DC system handles severe faults. The oscillations after the fault are mostly due to the crowbar discharging the PLC capacitors, and its importance and effect on the shape of those oscillations was shown in the model of the system. The effect of a fault on other parts of the line was shown, and the potential danger to system or measuring equipment due to the transient voltages was also discussed. Other issues such as the inability of the system to resume operation with one pole after a fault, much like the models from Section 4.3 was pointed out. Some more information regarding the crowbar operation would have been desirable, but due to one of the scopes not capturing properly, it was not possible to measure the currents and voltages at the output of the converter.

6.2. FUTURE WORK

Regarding the simulations, the models built for this thesis need to be expanded upon with more sophisticated cable, converter and load components. Cables which include frequency dependent response will prove especially useful, as the depiction of transients will be more accurate due to the filtering of higher frequency components. On the other hand, it is important not to forget that such additions may be computationally expensive at first, to the point which simulations may become slow and cumbersome. It is therefore important to keep the balance between accuracy and computation complexity, especially as the simulated systems will undoubtedly be larger. Something else that would contribute to the completeness of the models would be to add control to the models, so that there is no need to manually switch the MOSFETS. That will, however, require a solution for the initialization problem in ATP (briefly discussed in 5.4), where very large initial

transients would disrupt the normal operation of the control. Finally, a true bidirectional system still remains to be built, along with the bidirectional protection circuits needed to be able to successfully interrupt and mitigate the transients in both directions.

As for the measurements, there is still room to obtain even more information from the same street lighting DC system. As was already discussed multiple times, no data could be retrieved from the converter itself, and thus more information is needed to fully understand the behavior of the system and therefore explain the results from the measurements. Since we now know exactly what we can measure from the system and the time that is needed, preparations for repeat measurements should be easier. Any potential problems can be more easily avoided as well. In the next set of measurements, the focus should be on making sure that all the scopes can capture properly and gathering data from the converter output as well as the 3 measurement points along the line.

DC distribution systems are still in their infancy, which means that there is still considerable research to be done in order to design a system that performs satisfactorily. Transient analysis is of exceptional importance, as it always feeds into protection design. It is crucial to deeply understand the behavior of the system we are trying to protect in all circumstances, and that is why transient analysis is especially needed in such a new industry.

A

DC System Measurements Specifics

In this section, the details of the DC measurements project will be presented.

Hardware

The first problem that needed to be addressed in order to obtain any measurements from the system was to find a way to measure voltages and currents given its physical limitations. Especially voltages would be impossible in a system where no bare conductor is available for obvious safety reasons. In other words, it was important to somehow add a part to the existing system to allow for voltages to be measured. This is where the previously mentioned PLC drivers come into play. Those drivers have three pins on their bottom in order to monitor and control the operation of their respective lamp. The pins correspond to the two conductors across which the lamp is connected (Plus and Neutral or Neutral and Minus) and the ground conductor (PE). They can be seen in Figure A.1.

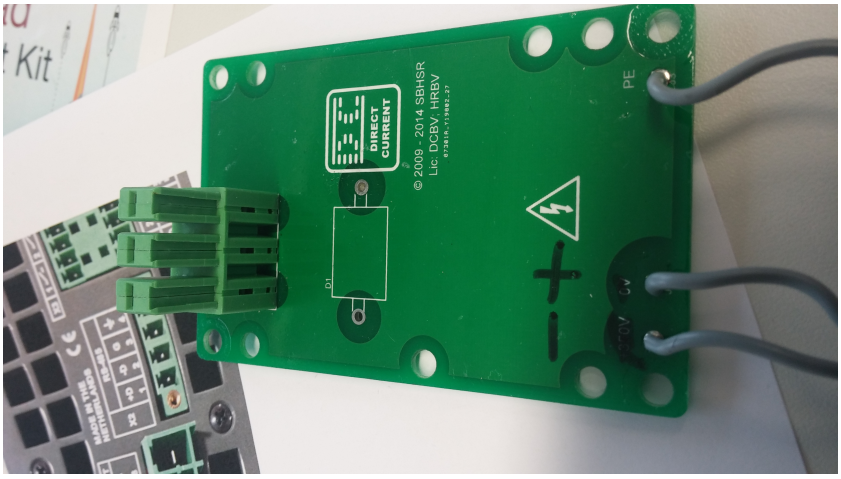

Figure A.1: PLC driver base with 3 connection pins visible. Property of Direct Current B.V.

Therefore, it would be possible to measure these voltages (or potentials) if the pins were accessible. For this reason, it was decided that the drivers at each measurement point would have to be removed. Of course, doing that would result in removing the capacitors from the measurements, which could change the response of the system. However, there was no alternative to access the conductors, and the removal of just 3 of the 20 capacitors should in theory not cause a big difference in system transient response. By using plugs corresponding to those at the base of the driver, it would be possible to connect a measuring circuit.

The above solution could not be applied to the source. Instead, it would be necessary to interrupt the connection of the converter to the rest of the system at its output to measure the source output voltages.

To achieve this, the configuration shown in Figure A.2 was interjected between the plug at the output of the converter and the cables coming out of it. This way, it became possible to access the conductors for measurements at the source as well.

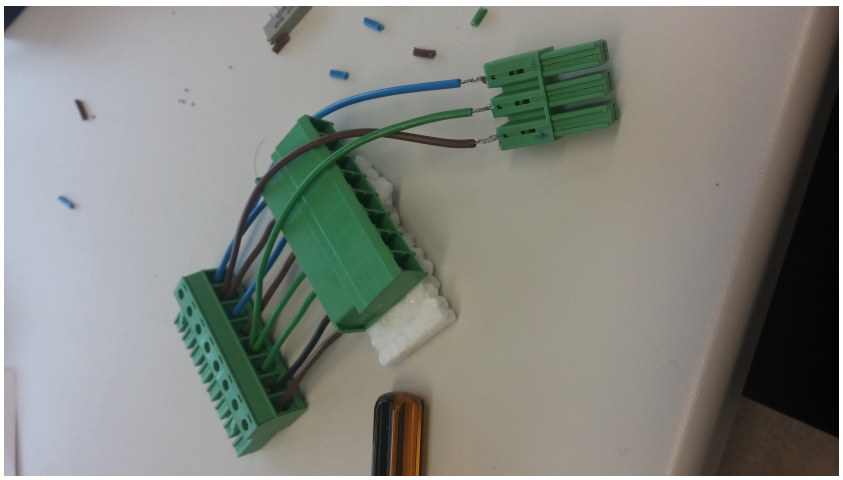

Figure A.2: Source connection

Another problem with measuring voltages of this level was ensuring the safety of the people handling the equipment during the measurements. The cables coming from the plugs should not just be connected to the scope, as touching a bare conductor at 350 V could be lethal. For this reason, a box was used to connect the plugs from each measuring point to the scope probes. One of them can be seen in Figure A.3.

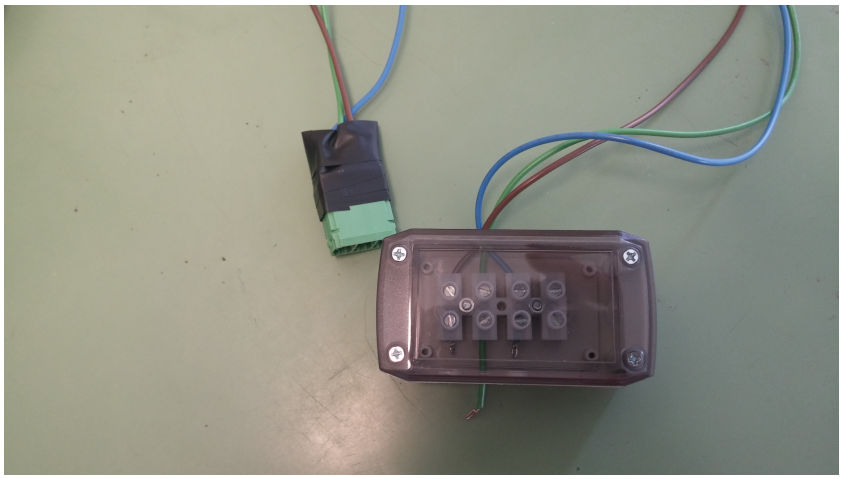

Figure A.3: Measurement Box

Inside the box, the three colored cables are stabilized with the use of the small white component. Three holes were drilled on one side of the box, where the voltage probes could fit through and connect with the cables, the ends of which were soldered into loops to make said connection with the probes easier and more reliable. The green cable (ground) is the one that is pulled out of the hole, so that the ground connections of multiple probes can latch onto it. In this way, no conductor is exposed and anyone handling the box during the measurements can be safe.

Finally, a similar box needed to be made for the fault position. The box seen in Figure A.4 serves two purposes: to make the needed faults while choosing the necessary fault resistance and connecting the plug of the faulted position to the scope safely.

In this larger box, three holes on the top were made to put in the three switches that control the circuit, three holes on one side for the probes and three more holes on another side for current measurements. The circuit board was screwed on the bottom of the box. The circuit of the box is illustrated clearly in Figure A.5.

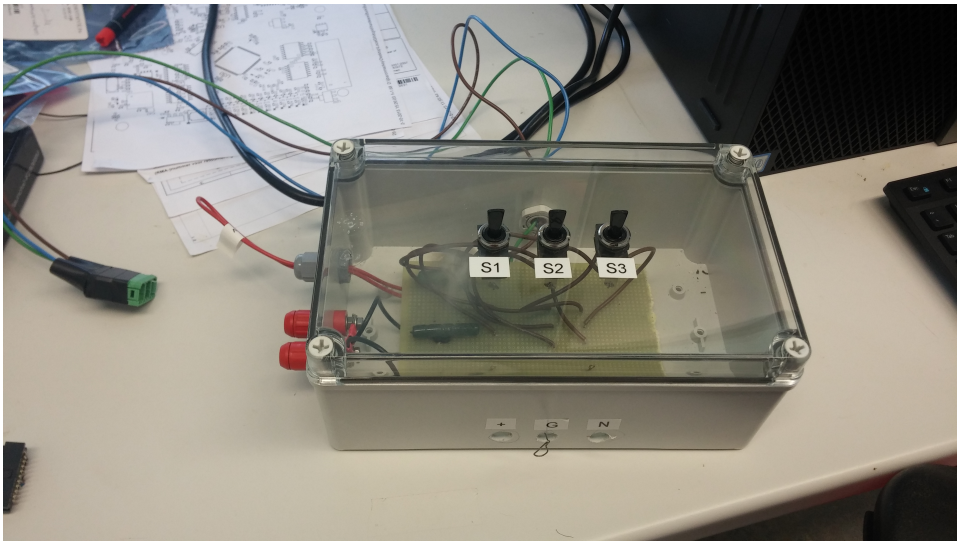

Figure A.4: Fault generation box

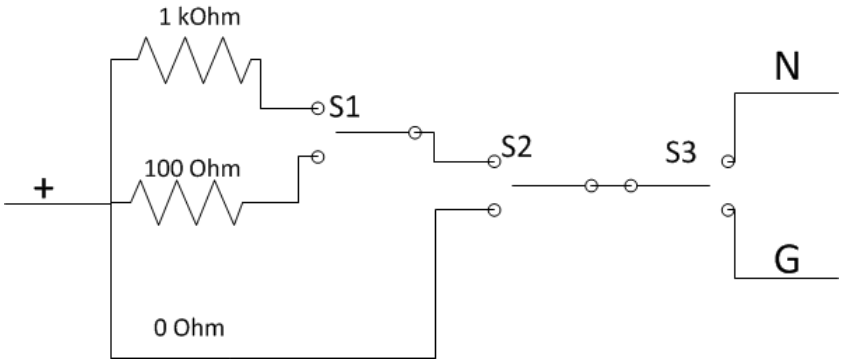

Figure A.5: Fault generation schematic

Each of the switches has three states. Two of them make a connection with a contact and the third is the non-connected state. The first switch(S1) chooses between the two resistors 10 kOhm or 100 Ohm. The second one (S2) chooses between one of the previous two or a bolted fault (0 Ohm) and the final one (S3) chooses between connecting the + to the Negative (N) or the Ground (G) conductor.

B

ATP Instructions

This short guide to ATPDraw (the graphical preprocessor to ATP) is meant to help new users come to grips with the peculiarities of the software. It is meant to be used alongside the official manual for ATPDraw and point out some difficulties that were encountered during the simulations for this thesis. It is assumed that the program has been installed correctly. Also make sure to install the plotting software PlotXY, which is separate to ATPDraw. Both of them are included in the zip folder. First, the groups of components used in the models of 4 will be analyzed. Following that, basic instructions to obtain plots from the existing models will be given.

In Sections 4.3.3 and 4.3.4, blocks were used in place of the usual protection circuit and the loads seen in the previous models. The reasons for this have already been explained, but it is important to include the manner in which these blocks function. Figures B.1 and B.2 show those two blocks and their contents side by side.

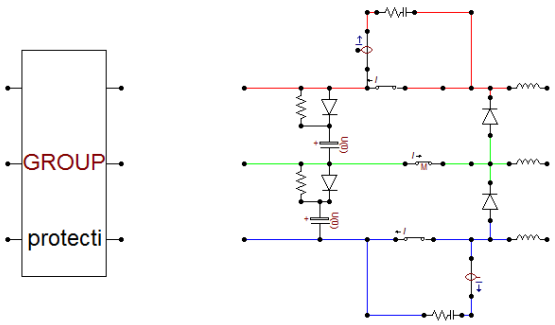

Figure B.1: Protection block and contents

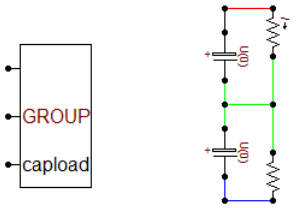

Figure B.2: Load block and contents

The manual thoroughly explains the grouping process and the selection of parameters to set. A handy tip is to use Ctrl+G in order to look into a group of elements, and press Ctrl+H to move out of the group. To change the values of the chosen parameters, double click or right click the group.

To get a plot from an existing model, first make sure that the desired quantity is being measured, either by a probe, or by the inner measuring capability of some elements. For example, the parameter setting window for the common resistor contains the output section, where the various quantities can be measured(Figure B.3).

Once all the required quantities are being measured, make sure that any parameterized components are configured correctly. When entering parameter values for any component, the user can type a text string instead, and ATP will ask if the user wants to add it to the list of ATP variables. By pressing F3 (or the buttons ATP→Settings) and selecting the tab Variables, all declared variables can be accessed. Their name can be changed, as well as the value assigned to them. There is a trick to assigning values to the variables. The manual in page 74 states that a period should always be use after a number in the value field, but that is not completely correct. A number below 1 can be written as 0.0333 without a period in the end or in the

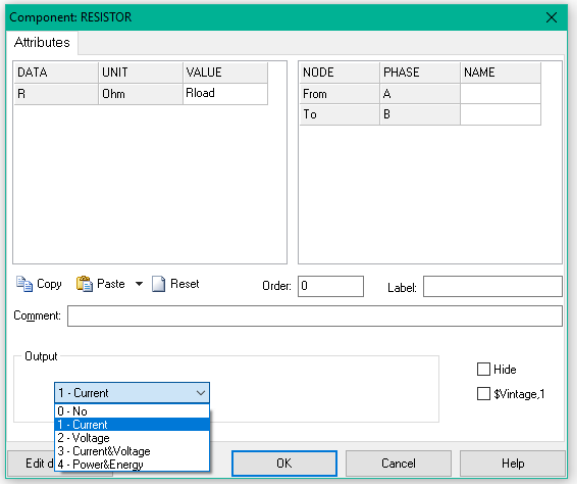

Figure B.3: Resistor measurement

exponential format 3.33E2 again without a period in the end. It seems that the period after the number is not needed if there is a decimal in the number's expression. Note that the number cannot be written in exponential format without a decimal, because even if a period is added after it, ATP will not be able to run. Finally, keep in mind that you can set variable values for multiple runs with the expression @[...] with the different numbers separated by space, without the need for a period in the end (for example @[0.1 100] works). Set the number of simulations you want to run at the bottom of the window.

In the Simulation tab of Settings, set the time step and finish time of the simulation. Unfortunately ATP can only start the simulation from 0 s. In the Output tab, the user controls how many of the time steps will be printed during the simulation with the print frequency, while plot frequency controls the amount of time steps that are simulated. To minimize simulation time, the user can input the maximum print frequency of 50000 while choosing for an appropriate plot frequency. 1 is the most accurate, but, depending on the size of the system, the user may chose 2 or more to reduce simulation time even further.

After setting everything up, the user can run ATP either with the Compile and Run button at the top or F2. In the black window that appears, the user can see the simulation being carried out. In most cases the message that appears if the simulation is not executed due to some error is very clear and helpful in identifying what is wrong with the model and what should be changed. The error can be read directly from the black window, but it is easier to press F5 and bring up the LIS file, which is basically the log of the simulation. Any node positions that are mentioned in the LIS file as part of an error can be found with the F6 shortcut. Even if the simulation is finished seemingly without problems, it would be good to check the LIS file, because some times the message 'floating subnetwork found' can be read. This doesn't stop the simulation, it just grounds the node at which the floating subnetwork was detected. It is therefore important that the system is properly grounded in order to stop ATP from grounding it wherever it sees fit.

Assuming that the simulation runs correctly, it is time to open the plotter with the F8 shortcut. Spotting the name of the node to see the respective measurement may not be easy, depending on the number of measurements that were set. For this reason, it is recommended to name the most important nodes beforehand, by double clicking on them to open the node data window and change their name to something different than the default name, which will make it stand out in the plotter's list. Each simulation run is saved in a different PL4 (output) file. If more than one was executed, the user should load the file manually by pressing the button load. If only one was executed, that single PL4 file is loaded. The chosen variables to be plotted are moved to the right. The user can right click any of them in case more than one units will be displayed in the plot to have a second y axis. To plot a variable in another figure, select a different tab.

After plotting, the user can add a title, set the scale, use cursors and show the difference between two cursors using the buttons on the bottom left of the plot window. The plot itself can be saved in an svg file with one of the bottom right buttons. To save the variables themselves for further processing in Matlab, however, the 'save vars' button on the plotter window. This will only save the variables of the current plot. The user can

choose to save the file in .mat format, which will allow for the further processing of the data in the Matlab environment.

BIBLIOGRAPHY

[1] International Renewable Energy Agency, *Renewable Power Generation Costs in 2014,* (2015).

[2] K. a. Nigim and W.-J. Lee, *Micro Grid Integration Opportunities and Challenges,* 2007 IEEE Power Engineering Society General Meeting , 1 (2007).

[3] R. M. Cuzner and G. Venkataramanan, *The status of DC micro-grid protection,* Conference Record - IAS Annual Meeting (IEEE Industry Applications Society) , 1 (2008).

[4] D. Nilsson and A. Sannino, *Efficiency analysis of low-and medium-voltage DC distribution systems,* Power Engineering Society General . . . , 1 (2004).

[5] A. Pratt, P. Kumar, and T. V. Aldridge, *Evaluation of 400V DC distribution in telco and data centers to improve energy efficiency,* INTELEC, International Telecommunications Energy Conference (Proceedings) , 32 (2007).

[6] T. Kaipia, P. Salonen, J. Lassila, and J. Partanen, *Possibilities of the low voltage DC distribution systems,* Nordac, Nordic Distribution and Asset Management Conference , 1 (2006).

[7] A. Sannino, G. Postiglione, and M. H. J. Bollen, *Feasibility of a DC network for commercial facilities,* IEEE Transactions on Industry Applications **39**, 1499 (2003).

[8] H. J. Laaksonen, *Protection principles for future microgrids,* IEEE Transactions on Power Electronics **25**, 2910 (2010).

[9] L. Mackay, T. G. Hailu, G. R. Chandra Mouli, L. Ramırez-Elizondo, J. Ferreira, and P. Bauer, *From DC Nano- and Microgrids Towards the Universal DC Distribution System – A Plea to Think Further Into the Future,* 2015 IEEE Power & Energy Society General Meeting , 1 (2015).

[10] T. Dragicevic, X. Lu, J. Vasquez, and J. Guerrero, *DC Microgrids Part I: A Review of Control Strategies and Stabilization Techniques,* IEEE Transactions on Power Electronics **8993**, 1 (2015).

[11] M. E. Baran and N. R. Mahajan, *Overcurrent protection on voltage-source-converter-based multiterminal DC distribution systems,* IEEE Transactions on Power Delivery **22**, 406 (2007).

[12] J. D. Park, J. Candelaria, L. Ma, and K. Dunn, *DC ring-bus microgrid fault protection and identification of fault location,* IEEE Transactions on Power Delivery **28**, 2574 (2013).

[13] P. Salonen, T. Kaipia, P. Nuutinen, P. Peltoniemi, and J. Partanen, *An LVDC Distribution System Concept,* NORPIE, Nordic Workshop on Power and Industrial Electroncis , 7 (2008).

[14] J. Messerly, *HVDC Europe annotated,* available at `https://commons.wikimedia.org/wiki/File:HVDC_Europe_annotated.svg#/media/File:HVDC_Europe_annotated.svg`.

[15] T. L. Feng Wang Lina Bertling, *An Overview Introduction of VSC-HVDC: State-of-art and Potential Applications in Electric Power Systems,* CIgre (2011).

[16] Ias, *IEEE Std 1709-2010 IEEE Recommended Practice for 1 kV to 35 kV Medium-Voltage DC Power Systems on Ships*, November (2010).

[17] T. Ioannis, *Domestic Bipolar LVDC Microgrid Protection*, Ph.D. thesis, TU Delft (2015).

[18] B. Dunstan, L. Atkinson, R. Schooley, and D. Froelich, *Universal Serial Bus Power Delivery Specification,* **1**, 66 (2012).

[19] V. Jankov and M. Stobart, *HVDC system performance with a neutral conductor,* 2010 International Conference on High Voltage Engineering and Application, ICHVE 2010 , 188 (2010).

[20] E. I. El-Masry, *The Electronics Handbook* (2005) pp. 677 – 687.

[21] T. Dragicevic, X. Lu, J. Vasquez, and J. Guerrero, *DC Microgrids Part II: A Review of Power Architectures, Applications and Standardization Issues,* IEEE Transactions on Power Electronics **8993**, 1 (2015).

[22] P. Nuutinen, P. Peltoniemi, and P. Silventoinen, *Short-Circuit Protection in a Converter-Fed Low-Voltage Distribution Network,* IEEE Transactions on Power Electronics **28**, 1587 (2013).

[23] a. Ouroua, J. Beno, and R. Hebner, *Analysis of fault events in MVDC architecture,* IEEE Electric Ship Technologies Symposium, ESTS 2009 , 380 (2009).

[24] K. Satpathi, *Protection Strategies for LVDC Distribution System,* PowerTech (2015).

[25] IEC, *Short-circuit currents in d.c. auxiliary installations in power plants and substations Part 1 : Calculation of short-circuit currents,* (1997).

[26] A. Berizzi, A. Silvestri, D. Zaninelli, and S. Massucco, *Short-circuit current calculations for DC systems,* Ind. Appl., IEEE Trans. on **32**, 990 (1996).

[27] I. Conference and E. D. Stockholm, *The effectiveness of using IEC61660 for characterizing short-circuit currents of future low-voltage DC distribution networks,* , 10 (2013).

[28] G. Byeon, H. Lee, T. Yoon, G. Jang, W. Chae, and J. Kim, *A research on the characteristics of fault current of DC distribution system and AC distribution system,* 8th International Conference on Power Electronics - ECCE Asia: "Green World with Power Electronics", ICPE 2011-ECCE Asia , 543 (2011).

[29] J. Yang, J. E. Fletcher, and J. O'Reilly, *Short-Circuit and Ground Fault Analyses and Location in VSC-Based DC Network Cables,* Ieee Transactions on Industrial Electronics **59**, 3827 (2012).

[30] M. K. Bucher and C. M. Franck, *Comparison of Fault Currents in Multiterminal HVDC Grids with Different Grounding Schemes,* PES General Meeting | Conference & Exposition, 2014 IEEE , 1 (2014).

[31] M. Bucher and C. Franck, *Contribution of Fault Current Sources in Multiterminal HVDC Cable Networks,* Power Delivery, IEEE Transactions on **28**, 1796 (2013).

[32] N. R. Mahajan, *System Protection for Power Electronic Building Block Based DC Distribution Systems,* Ph.D. thesis (2004).

[33] L. T. L. Tang and B.-T. O. B.-T. Ooi, *Protection of VSC-multi-terminal HVDC against DC faults,* 2002 IEEE 33rd Annual IEEE Power Electronics Specialists Conference. Proceedings (Cat. No.02CH37289) **2**, 719 (2002).

[34] J. Candelaria and J. D. Park, *VSC-HVDC system protection: A review of current methods,* 2011 IEEE/PES Power Systems Conference and Exposition, PSCE 2011 , 1 (2011).

[35] J. Dorn, H. Huang, and D. Retzmann, *Novel Voltage-Sourced Converters for HVDC and FACTS Applications,* , 1 (2007).

[36] G. Ding, G. Tang, Z. He, and M. Ding, *New technologies of voltage source converter (VSC) for HVDC transmission system based on VSC,* 2008 IEEE Power and Energy Society General Meeting - Conversion and Delivery of Electrical Energy in the 21st Century , 1 (2008).

[37] K. A. Corzine and R. W. Ashton, *A New Z-Source DC Circuit Breaker,* **27**, 2796 (2012).

[38] K. Corzine, *Dc micro grid protection with the z-source breaker,* IECON Proceedings (Industrial Electronics Conference) , 2197 (2013).

[39] L. Tang and B. T. Ooi, *Locating and isolating DC faults in multi-terminal DC systems,* IEEE Transactions on Power Delivery **22**, 1877 (2007).

[40] A. A. S. Emhemed and G. M. Burt, *An Advanced Protection Scheme for Enabling an LVDC Last Mile Distribution Network,* IEEE Transactions on Smart Grid **5**, 2602 (2014).

[41] J. D. Park and J. Candelaria, *Fault detection and isolation in low-voltage dc-bus microgrid system,* IEEE Transactions on Power Delivery **28**, 779 (2013).

[42] S. D. a. Fletcher, P. J. Norman, S. J. Galloway, P. Crolla, and G. M. Burt, *Optimizing the roles of unit and non-unit protection methods within DC microgrids,* IEEE Transactions on Smart Grid **3**, 2079 (2012).

[43] S. D. A. Fletcher, P. J. Norman, K. Fong, S. J. Galloway, and G. M. Burt, *High-Speed Differential Protection for Smart DC Distribution Systems,* IEEE Transactions on Smart Grid **5**, 2610 (2014).

[44] D. Salomonsson, L. Soder, and A. Sannino, *Protection of Low-Voltage DC Microgrids,* IEEE Transactions on Power Delivery **24**, 1045 (2009).

[45] S. R. B. Vanteddu, A. Mohamed, and O. Mohammed, *Protection design and coordination of DC Distributed Power Systems Architectures,* Power and Energy Society General Meeting (PES), 2013 IEEE , 1 (2013).

[46] H. Li, W. Li, M. Luo, A. Monti, and F. Ponci, *Design of smart MVDC power grid protection,* IEEE Transactions on Instrumentation and Measurement **60**, 3035 (2011).

[47] D. K. B.V., *Draka cable specifications,* available at `http://www.draka.nl/product/124277?jointsView=False`.

[48] F. W. Grover, *Inductance Calculations* (2004) p. 197.

[49] S. S. Sivanagaraju S., *Electric Power Transmission and Distribution* (2008) p. 632.

[50] *ABB switchgear manual* (1993).

[51] H. H. U. R. Winston Revie, *Corrosion and Corrosion Control (4th edition)* (2008) pp. 206 – 212.